Linear Parameter Varying Approaches as Advanced Control Techniques: Application to Vehicle Dynamics

Marcelo Menezes Morato

DAS Departamento de Automação e Sistemas
CTC Centro Tecnológico
UFSC Universidade Federal de Santa Catarina

Linear Parameter Varying Approaches as Advanced Control Techniques: Application to Vehicle Dynamics

Report submitted to Universidade Federal de Santa Catarina

and also to Institut Nacional Polytechnique de Grenoble, École Nationale Supérieure de l'Energie, l'Eau et l'Environnement

as requirement for approval on the course:

DAS 5511: Projeto de Fim de Curso

(Final Study Project, Projet de fin d'Études)

Marcelo Menezes Morato

Grenoble, July of 2017

Linear Parameter Varying Approaches as Advanced Control Techniques: Application to Vehicle Dynamics

Marcelo Menezes Morato

This monograph was judged in the context of the course

DAS 5511: Projeto de Fim de Curso

and approved in its final form by

GIPSA-lab: Grenoble Images Parole Signal Automatique

and

Departamento de Automação e Sistemas

Prof. Dr. Olivier Sename

Prof. Dr. Julio Elias Normey-Rico

MENEZES MORATO, Marcelo

Linear Parameter Varying Approaches as Advanced Control Techniques: Application to Vehicle Dynamics / Marcelo Menezes Morato. – Grenoble, France, 2017.

166 p. : 30 cm.

Monograph (Curso de Engenharia de Controle e Automação) - Universidade Federal de Santa Catarina

Professor Advisor: Olivier Sename (GIPSA-lab)

Professor Co-Advisor: Julio Elias Normey-Rico (UFSC)

1. Fault Tolerant Control. 2. Linear Parameter Varying Systems. 2. Mechatronic Systems. I. Olivier Sename. II. Universidade Federal de Santa Catarina. III. Departamento de Automação e Sistemas. IV. Linear Parameter Varying Approaches as Advanced Control Techniques

Examination Board:

Prof. Dr. Olivier Sename
Professor Advisor

Prof. Dr. Julio Elias Normey-Rico
Professor Co-Advisor

Prof. Dr. Hector Bessa
Responsible for Course

Dr. Paulo Renato da Costa Mendes, Evaluator

Enga. Gislaine Hoffmann, Debater 1

Eng. Ricardo de Oliveira Gonzalez Aldeyturriaga, Debater 2

Acknowledgements

Eu gostaria de agradecer:

Primeiramente aos meus pais Débora e José Rubens, por todo o amor, carinho, incentivo e suporte em todos os momentos. Sou eternamente grato a vocês 2, vocês são demais!!! ♡

Também, aos meus avós Antônio e Dette, Gegênia e Tom (*in memoriam*), aos meus queridos padrinhos Emílio e Estera, à Tia Cleusa e à família amada de Floripa, Tanira, Gabriel, Thiago, Thaís e Guto, por todos os momentos juntos.

À minha namorada e melhor amiga, Lara, por todo amor, companheirismo, entusiasmo e apoio. Sou muito grato por teres entrado nessa aventura de vir pra Grenoble comigo! És a melhor! Também à toda a família da Lara pelo apoio e carinho, especialmente a: Alexandre, Denise, Flávia e Sunshine.

Aos meus amigos, amigas e colegas de graduação, principalmente ao Kaio Siqueira, ao João Vitor e ao Victor Petrassi, por terem me ajudado com os trabalhos feitos em conjunto durante os *PIBIC*s, as monitorias de Sistemas de Controle e Introdução ao Controle e durante toda a graduação. Também a todos os queridos amigos 13.1 que entraram comigo na *UFSC*. Aos meus amigos de longa data: Arthur Zand, Breno, Enzo, Henrique, Morena, Niterói, Rafinha, Victória, Teixeira e, especialmente, a Anamaria e ao Thaian, pelas risadas, ótimos filmes e parceria de todas as horas. Aos super-amigos que fiz na França: André, Argenis, Arthur, Bia, Dani, Deborah e Nomar, pela amizade sincera e quase instantânea!

Ao meu professor e orientador no Brasil, Julio, que me aceitou como bolsista *PIBIC*, mesmo já estando lotado de alunos a orientar, e sempre me guiou, ajudou e me acolheu, desde o primeiro dia, com muita confiança e competência. Obrigado pelos ensinamentos, conversas e todo o apoio ! ☺

Aos meus orientadores na França, Olivier e Luc, que me acolheram de forma excepcional no *gipsa-lab*, me instigaram à pesquisa e me proporcionaram várias oportunidades nesse sentido.

Aos colaboradores de pesquisa prof. Carlos Bordons e, principalmente, Paulo Renato, que me ajudaram muito nos trabalhos de pesquisa e nunca hesitaram em ajudar em todas as eventuais dúvidas, a todas as horas. Aos colegas do *gipsa* Manuel Molina e Alfonso Estrada, que me ajudaram muito com os trabalhos na plataforma experimental, e ao prof. Jomi que me deu a primeira oportunidade como bolsista *PIBIC* em 2013. Também ao prof. Jean-Marie, que me orientou quanto aos processos do *BRAFITEC* e me indicou a

seguir o caminho para um trabalho no *gipsa*.

Em termos de financiamento:

O autor reconhece a *CAPES* por financiar o projeto *BRAFITEC ECoSud* e o laboratório de excelência *LabEx PERSYVAL-Lab* por financiar o projeto *LPV4FTC*, através do programa francês *Investissements d'Avenir*, $ANR-11-LABX-0025-01$.

Abstract

Este Trabalho de Conclusão de Curso apresenta diversas técnicas de Modelagem, Identificação e Controle Avançado aplicadas ao estudo de Suspensões Semi-Ativas em Sistemas Veiculares. Este trabalho é divido em três eixos principais: *i)* Desenvolvimento e aplicação de técnicas LPV de Identificação de Falhas em amortecedores de sistemas de suspensão; *ii)* Desenvolvimento e implementação de um sistema de Controle Preditivo baseado em modelo aplicado em tempo-real para o controle de suspensões semi-ativas; *iii)* Desenvolvimento e aplicação de técnicas de reconfiguração LPV para o Controle Tolerante a Falhas de sistemas de suspensão. As técnicas e o desenvolvimento feito são analisados através de simulação e validação em uma plataforma mecatrônica experimental e demonstram-se satisfatórios.

Palavras-chave: Sistemas Automotivos; Sistemas Lineares a Parâmetros Variantes; Controle Preditivo baseado em Modelo; Detecção e Diagnóstico de Falhas; Controle Tolerante a Falhas

Abstract

This End-of-Studies Work presents a range of techniques of Modeling, Identification and Advanced Control applied to the study of Semi-Active Suspensions in Vehicular Systems. This work is divided into three main branches: *i)* development and application of LPV fault identification techniques on actuators of suspension systems; *ii)* development and implementation of a real-time model predictive control scheme applied the control of semi-active suspensions; *iii)* development and application of LPV reconfiguration techniques for fault tolerant control of suspension system. The developed control strategies are analysed through simulation and validation on a mechatronic test-bench and prove themselves satisfactory.

Keywords: Automotive Systems; Linear Parameter-Varying Systems; Model Predictive Control; Fault Detection and Diagnosis; Fault Tolerant Control.

Résumé

Ce travail de Fin-d'études présente plusieurs techniques de modélisation, identification et de la commande avancée appliqués a l'étude des systèmes de suspensions semi-actifs. Ce travail est divisé en trois domaines principaux: développement et l'application des techniques LPV pour l'identification des défauts sur les actionneurs dans les systèmes de suspension; développement et mise-en-œuvre d'un système de contrôle prédictif basé sur modèle appliqué en temps réel sur des suspensions semi-actifs; développement des techniques LPV de reconfiguration pour la commande tolerant aux défauts des systèmes de suspension. Les stratégies de commande développées sont analysées par simulation et validation et se montrent satisfaisantes.

Mots-clés: Systèmes Automobiles; Systèmes Linéaires à Paramètres-Variants; Contrôle Prédictif basé sur Modèle; Détection et Diagnostic de Défauts; Commande Tolérante aux Défauts.

List of Figures

List of Tables

List of abbreviations and acronyms

UFSC Universidade Federal de Santa Catarina

ENSE^3 École Nationale Supérieure de l'Energie, l'Eau et l'Environnement

INPG Institut National Polytechnique de Grenoble

GIPSA-lab Laboratoire Grenoble Image Paroles Signal Automatique

ODE Ordinary Differential Equation

MIMO Multi Inputs Multi Outputs

SISO Single Input Single Output

TF Transfer Function

CL Closed-Loop

OL Open-Loop

LHP Left Half-Plane

RHP Right Half-Plane

BIBO Bounded Input, Bounded Output

LTI Linear Time Invariant

MPC Model Predictive Control

LMI Linear Matrix Inequality

BMI Bilinear Matrix Inequality

DOF Degrees of Freedom

FD Fault Diagnosis

FDD Fault Diagnosis and Detection

FDI Fault Detection and Isolation

FTC Fault Tolerant Control

LPV Linear Parameter Varying

LQR Linear Quadratic Regulator

PWM Pulse-Width Modulation

COG Center of Gravity

List of symbols

$\mathbb{R}$	Real numbers set
$\mathbb{C}$	Complex numbers set
A^*	Conjugate of $A \in \mathbb{C}$
A^T	Transpose of $A \in \mathbb{R}$
$A = A^T$	Matrix A is symmetric
$\star$	Symmetric entry of a matrix

Contents

0 Monograph's Framework

This chapter introduces the author's work during the internship period at *gipsa-lab*, from February to end of June 2017. It is mostly important to remark that the work herein exposed was advised by professor *Olivier Sename*, whereas the project's responsables also include professor *Luc Dugard* (co-advisor) and others.

0.1 Collaborations

During this period at *gipsa-lab*, I had the opportunity to collaborate with professors *Olivier Sename*, *Luc Dugard* and *Simone Formentin* (*Politecnico de Milano*), with post-graduate students *Manh Quan Nguyen* and *Vu Tan Vu* and master students *Alfonso Estrada Vela*, *Manh-Hung Do* and *Manuel Alejandro Molina Villa*.

0.2 Monograph's Objectives

This monograph's main objectives are synthesized below:

- Present and compare Linear Parameter Varying approaches on Fault Estimation for loss of efficiency on **actuators** ;
- Test and develop viable ways for a *real-time* high-complexity Model Predictive Controller for the *Soben-Car* test-bench ;
- Present and justify new approaches for Fault Tolerant Control (of Multi-Input Multi-Output systems) in the case of **sensor** and **actuator** faults;
- Present the results of experimental validation of the *Soben-Car* test-bench.

0.3 Author's Activities

The author's activities during the internship period are summarized below:

- Preliminary literature review on dynamical systems, LPV systems, FTC, vehicle dynamics, vehicle suspensions and others ;
- Preliminary research on Fault Observers for Linear Systems and Closed-Loop Stabilizing Control for Faulty Systems ;

- Getting started with existing system models and *Automative Control* toolbox of *GIPSA-lab* tools ;
- Training on *MATLAB Robust Control Toolbox* and on *Linear Matrix Inequalities* ;
- Training on the *Soben-Car* test-bench ;
- Proposition, comparison and study of different approaches for Fault Estimation ;
- Study and developpement of viable high-complexity Model Predictive Controllers to be applied on real-time test-bench ;
- Proposition of Fault-Scheduling and Fault Tolerant Control structures ;
- Experimental validation on test-bench ;
- Result analysis and conclusions ;
- Documentation.

0.4 About this Document

The work done by the author is centered on the study and developpement of *Linear Parameter Varying Approaches as Advanced Control Techniques*, with application to Vehicle Dynamics. The rest of this document is organized in separate chapters, in the following sequence:

- Chapter 1 introduzes the this monograph's scope, preliminary concepts and the *LPV4FTC* project;
- Chapter 2 presents the literature review and key concepts to this work;
- Chapter 3 shows the study of different Linear Parameter Varying-based approaches for Fault Diagnosis and Identification for the case of actuator loss of effectiveness faults;
- Chapter 4 presents the results on the proposed implementation of a high-complexity Model Predictive Controller for the *Soben* test-bench;
- Chapter 5 presents the author's proposition of new approaches of LPV as FTC reconfiguration techniques, considering the control of a full vehicle model with actuator faults on each of its suspension systems;
- Finally, chapter 6 presents the conclusions to this work and themes for future studies;

- It is also important to enlighten that a prior report of a full semester period with a research course (*Parcours Recherche*) at $ENSE^3$ brought some background results used for this monograph; it is seen on [3].

1 Introduction

In the last decade, the *SLR* (Linear Systems and Robustness) Team of *Gipsa-lab* has developed several strategies for observation and control for vehicle dynamics [4], [5] in particular using the Linear Parameter Varying (LPV) approach.

The work herein presented is an end-of-studies monograph (*Projeto de Final de Curso*, *Projet de Fin d'Études*) supported by the project **PERSYVAL** *LPV4FTC – A Linear Parameter Varying approach for Fault Tolerant Control design*, in collaboration with *CRAN* Nancy and the Academy of sciences of Budapest (*MTA SZTAKI*). This document is required by *Universidade Federal de Santa Catarina* for approval on the course *DAS5511: Projeto de Final de Curso* and for the title of Automation and Control Engineer. This monograph also expresses the meaning of the exchange period, by the author, at Grenoble, funded by *CAPES*, on the means of the *BRAFITEC* project.

Theoretical background and literature review are found on chapter 2, please refer to this chapter whenever doubts appear on terms and technical knowledge. Each other chapter tries to express its goals and topics individually, in order to be able to be read detached from the whole document.

1.1 Project Scope

It is very important to, first of all, explicit the studied project's main goals and scope. The author's research and studies were set in the context of the **LPV4FTC** *PERSYVAL* project.

The *LPV4FTC* project's objective is to propose Linear Parameter Varying (LPV) approaches to develop an integrated Fault Detection and Diagnosis (FDD)/ Fault Tolerant Control (FTC) scheme for dynamical systems, topic for which very few studies and results have been obtained.

The control of LPV systems has attracted a great deal of attention in the last decade, since they have shown to be an interesting extension of the Robust Control theory applied to nonlinear system.

The LPV approach is today known and well-suited to handle system non-linearities by modelling them as varying parameters (or to settled the controller's performances as varying through gain-scheduling). This is further investigated and discussed on section 2.5 of this document.

Active FTC systems are today crucial for real applications, in order to always

maintain a controlled system operational whenever malfunctions and/or failures occur. The main issue of *FTC*, today, is an efficient integration of reconfiguration techniques to a *FDD* scheme. The background *FTC* systems and *FDD* schemes is seen on section 2.8 of this document.

The dynamical systems that are considered are vehicle systems, with plausible actuator/sensor faults. For this, the application of the proposed methodologies will be done on the Grenoble *INOVE* test-bench, *Soben-Car*. This will include objective assessment using direct measurement of achieved vehicle performance in case of faulty component (compared to the nominal case). The idea behind this project's goals is seen on figure 1, where we can see the combination of and *LPV FDD* scheme with an active *LPV FT* Controller.

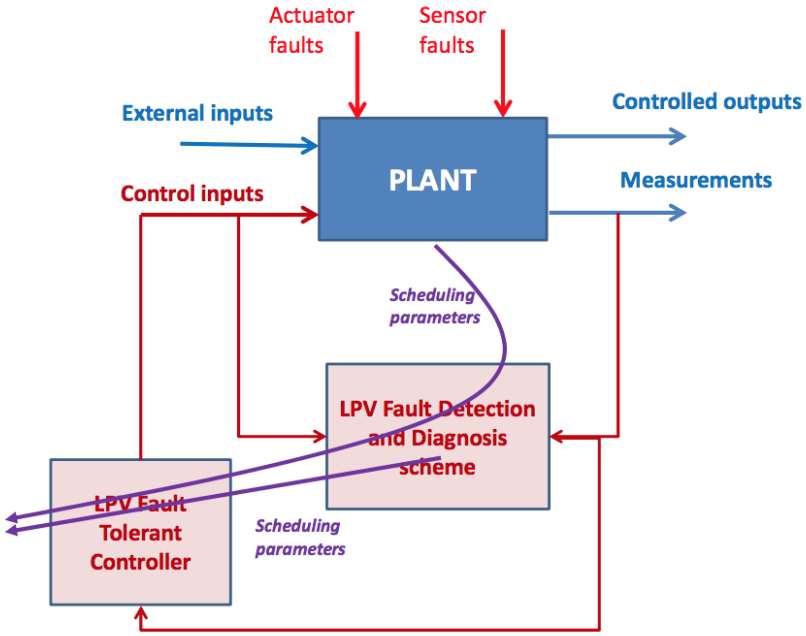

Figure 1 – Project : Methodology

In a more straightforward insight, the project's key goals are divided in three packets:

- *WP*1: Specifications ;
- *WP*2: Design Methods ;
- *WP*3: Tests and Validation attained on Mechatronic testbed.

1.1.1 *WP*1: Specifications

This packet, the backbone of the project, includes definition of functional requirements, study of potential use cases realizable on the considered testbed and the definition of an internation benchmark (for the application of *FTC* methods on a mechatronic testbed).

1.1.2 *WP*2: Design Methods

For the second packet, the methodological core of the project, theoretical developments will be carried out, following by the proposition of generic *LPV* tools able to ensure stability and improve performances of *FTC* systems (under specification form *WP*1). In terms of tasks, these can be put as:

i) Design *LPV* for *FDD/FTC* for single-actuator case;

ii) Design *LPV* automatic control reconfiguration approached for multiple component failures/faults.

1.1.3 *WP*3: Tests and Validation on Mechatronic testbed

The final packet, comprises the campaign of tests and results analysis on the Mechatronic testbed. This work is to be carried out into three main tasks:

i) Application and tests of *LPV4FTC* to a quarter-car system with a faulty damper;

ii) Application and tests of *LPV4FTC* to a full car case with four dampers;

iii) Implementation and tests for the proposed benchmark (*WP*1).

1.2 On the Mechatronic Testbed

The Test-Bench that was used for this work was the *Soben-Car*, an experimental platform that allows dealing with several configurations and use cases (from single input to multi input systems). Figure 2 shows a picture of this test-bench. This testbed has been built in 2012, partially supported by the *ANR* funds of the *ANR BLAN* 0308 *INOVE* project, that is focused on the observation and control of vehicle dynamics using methods for estimation and observation, *LPV* approaches for observation and robust control and Fault-Tolerant control techniques; see [6].

Figure 2 – *Soben-Car* Test-Bench

This testbed is composed of three main parts, as it is put in figure 3. Let us remark that:

- The **Host PC** represents the computer where the control interface is hosted. This interface is developed using *MATLAB* and *SimuLink*, [7];
- The **Target PC** runs a *RT* operating system [8]. In this computer, the control algorithm is compiled and executed at a sampling rate of $f_s = 200\,\text{Hz}$;
- The **Process** represents sensors, actuators and the scaled vehicle. The main component here is the 1/5-scaled racing car, which represents a full vehicle, including wheels, engine, steering, breaking system and a semi-active suspension system as a key element. It is important to remark that this scaled vehicle is most importantly dedicated to the study of vertical behaviour and, for this, neither the steering nor the breaking system will be in use.

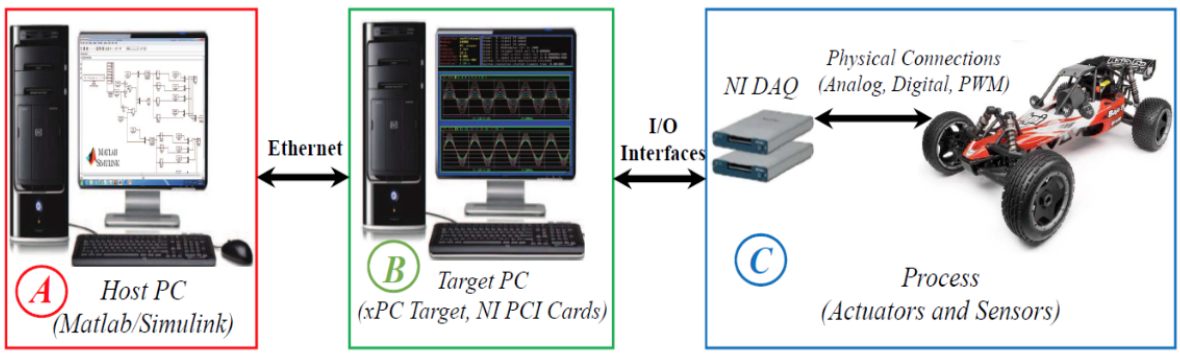

Figure 3 – Schematic of the *INOVE* Experimental Platform

The Semi-Active suspension system involves four Electro-Rheological (*ER*) dampers wich have a force range of $\pm\,50\,\mathrm{N}$. These dampers are adjusted using a controlled voltage inside the range of $[0\,,\,5]\,\mathrm{kV}$, generated by amplifier modules. The control input for these modules are *PWM* signals at $25\,\mathrm{kHz}$. These amplifier proportionally transform the duty-cycle of the received *PWM* signal into voltage.

Linear servomotors mimics the desired road profile below each wheel. These servomotors have a bandwidth of $0\,-\,20\,\mathrm{Hz}$ with a maximum velocity of $1.5\,\frac{\mathrm{m}}{\mathrm{s}}$. Each motor has its own servo-driver and is operated from the **Host PC**, by sending the desired road profile through a Data Acquisition Card.

On terms of capturing the vehicle's behaviour, this test-bench is equipped with a wide variety of sensors. To measure the vertical accelerations of the nsprung masses ($\ddot{z_{us}}$), four capacitive accelerometers are used. The deflection of the suspensions (z_{def}) are measured using four resistive linear displacement sensors and other four sensors are used to measure the road profile (z_r). Four draw-wire displacement sensors are also used to measure the unsprung masses displacement (z_{us}). To analyse the force variations upon the *ER* dampers, four force sensores are available for use. Also, other four sensors are used to measure tyre forces.

The main goal of this platform is to evaluate the dynamical behaviour of the full vehicle. For this, the system is equipped with a *MEMS*-based Attitude and Heading Reference System (*AHRS*) which measures the movement of the sprung mass on three accelerations and on three angular velocities: longitudinal acceleration ($\ddot{x}$), lateral acceleration ($\ddot{y}$), vertical acceleration ($\ddot{z}$), pitch rate ($\dot{\phi}$), roll rate ($\dot{\theta}$) and yaw rate ($\dot{\psi}$).

It is important to remark that the data acquisition and signal outputs for all sensors and actuators are done through two *National Instruments* Data Acquisitions Cards (*NI DAQs*) [9].

The closed-loop scheme that represents the controlled test-bench is put on figure 4.

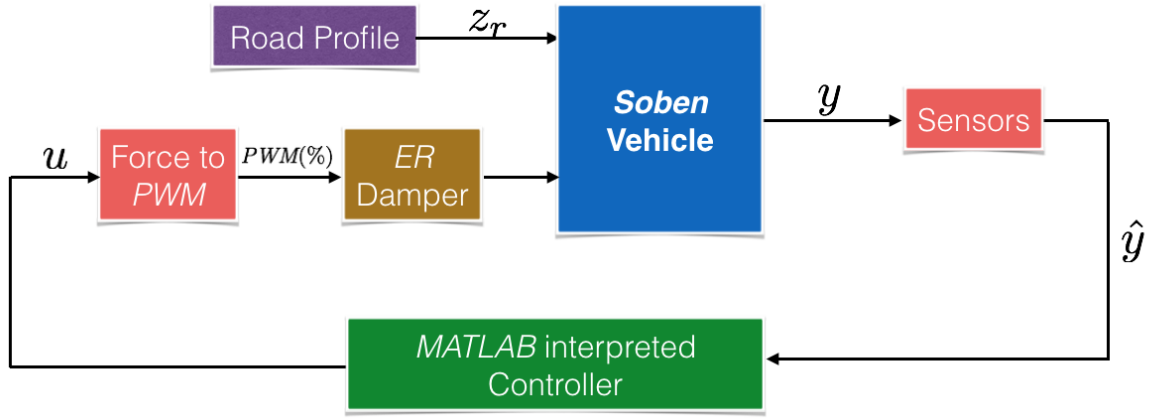

Figure 4 – Closed-Loop of *Soben-Car* Test-Bench

1.2.1 Some Operational Remarks for the Test-Bench

As this system is specially designed to evaluate the vertical dynamics of a vehicle controlled by the semi-active suspension system, some operational remarks have to be taken into account:

- The only external input of the system is the movement of the linear servomotors (that impose the road profile, z_r, for each wheel) ;
- The operation of the semi-active dampers considers that the control input should be the percentage of the duty cycle for the PWM command signal. These signals can vary in the range of 0.1 to 0.8, although some results show that when the PWM signals are higher than 0.35, the damper forces have the same behaviours (see [5]) ;
- Due to the physical characteristics of the system, only the vertical dynamics, pitch, roll and vertical bounce can be inferred from the system evolution. Even if the sensors detect other dynamics (lateral or longitudinal), these should be neglected ;
- The limitations on the type of controllers to be implemented are **none**, for the computation resides on the operation directly coming from the *MATLAB* interface.

2 Theoretical Background

This chapter presents a review on the availible literature on key concepts, theorems and propositions to this work.

2.1 On Automotive Suspension Systems

First of all, it is very important to provide the key concepts behind automotive suspensions.

An automative suspension comprises, basically, two components: a spring and a damping (shock absorbing) structure, as it can be seen on figure 50. These components have to work together to maintain the tyre's contact with the ground. The goal of the damping structure is to reduce the effect of travelling upon a rough road by absorbing shock and helping with driving performance, ensuring a smoother and safer drive. In a automative suspension without an efficient damping system, the vehicle is able to absorb damps, but continues to bounce, may causing the tyres to leave the road.

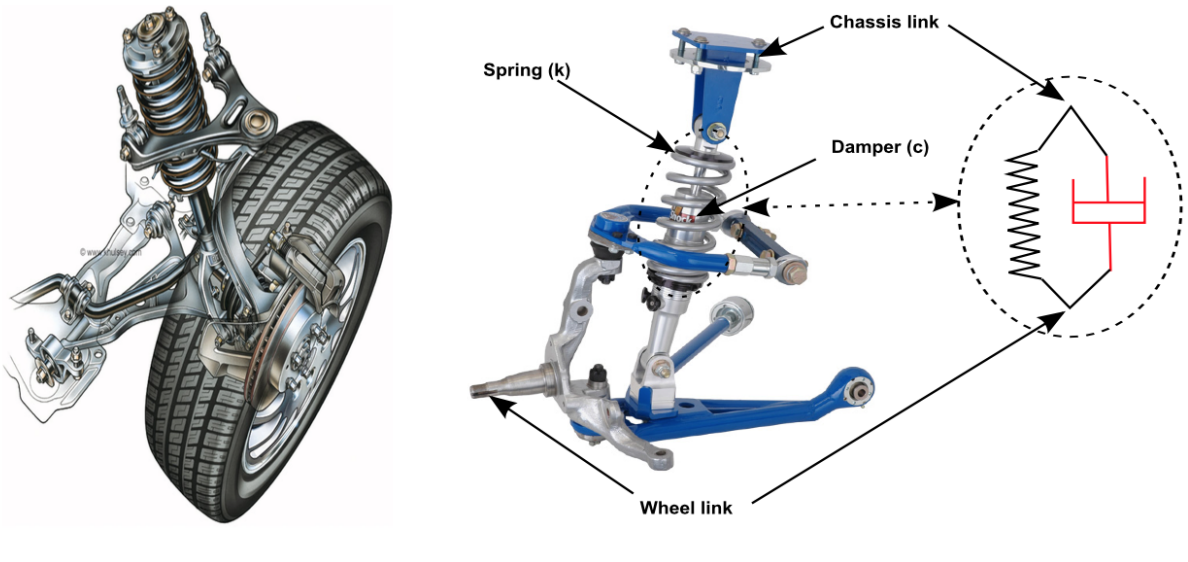

Figure 5 – Outline of Studied Suspension System

Automative suspension systems can be classified in two main groups: Passive Suspension Systems and Controllable Suspension Systems (Active and Semi-Active Suspensions). This is throughly exploited on [10] and [11].

2.1.1 On Passive Automative Suspension Systems

An automative suspension system is considered as passive if the characteristics of its components (spring and damper) are fixed. This is so described on [11] and [12]. These characteristics are determined by the designer of the suspension according to the intended application. A passive suspension system is only able to dissipate the energy which is defined by the *Speed Effort Rule* (*SER*) between the suspension deflection speed (given by difference between chassis speed and wheel speed) and the damping force of the passive suspension. Notice that a passive damper is only able to dissipate energy!

Figure 6 gives the *SER* diagram of a passive Electro-Rheological damper of the *SOBEN* Car for a fixed level duty cycle (see section 1.2 and [5]).

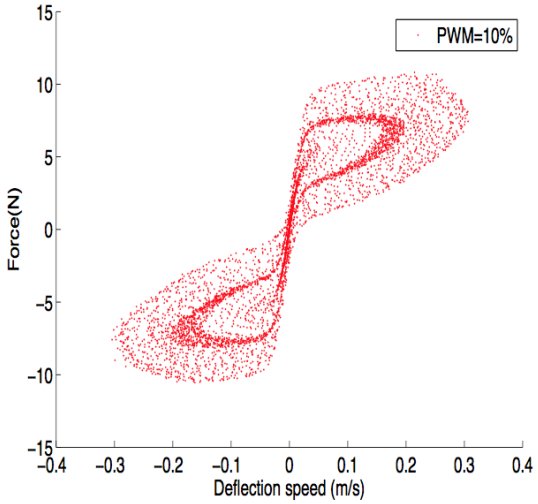

Figure 6 – Force over Speed deflection characteristics of a Passive Damper

2.1.2 On Controllable Automative Suspension Systems

Controllable Automative Suspension Systems can be divided into Active and Semi-Active Suspension Systems.

2.1.2.1 Active Suspension

An automative suspension system is considered as active if the passive damper (or the passive damper and the spring) are replaced by a force actuator. This actuator should be able to both generate and dissipate energy for (from) the system, as it is represented on figure 7.

In an active suspension, the actuator can apply force independent of the relative displacement across the suspension. Given a sensible control strategy, an active suspension can present better results in respect to ride confort and vehicle stability, as seen on [13] and [12].

The disadvantages of active suspension systems reside on the fact that the actuator of these systems usually have large power requirements, so that these types of suspensions are mostly found in more expensive passenger vehicles. The power demands of active suspensions in luxury and (or) heavy vehicles is much greater than standard vehicular supplies.

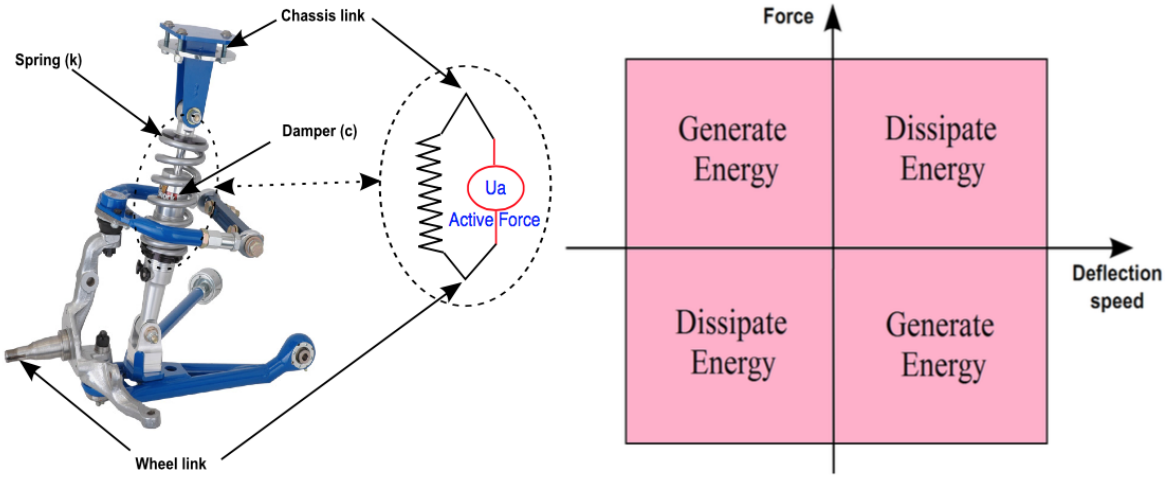

Figure 7 – Force over Speed deflection characteristics of an Active Damper

2.1.2.2 Semi-Active Suspension

An automative suspension system is considered semi-active when the conventional spring component is retained, but the damper is replaced by a controlled damper structure. Semi-active suspension systems have gained much attention by car manufacturers during the last decades, for they do not require great amounts of external energy sources to power actuators as active suspension systems. The power used by semi-active suspensions is only to adjust the damping levels and operate an embedded controller and a set of sensors. This embedded controller is adjusted to determine the level of damping, based on the used control strategy. Likewise as the passive suspension systems, semi-active systems can only dissipate energy, although the damping capacity (practically, the damping coefficient) can be modified online to meet the tradeoff between passanger confort and driving (vehicle) safety. The characteristic set that represents a semi-active damper by the Force over Speed graph is seen on figure 8.

Further details on semi-active suspension systems are throughly discussed on [14], [13] and [12].

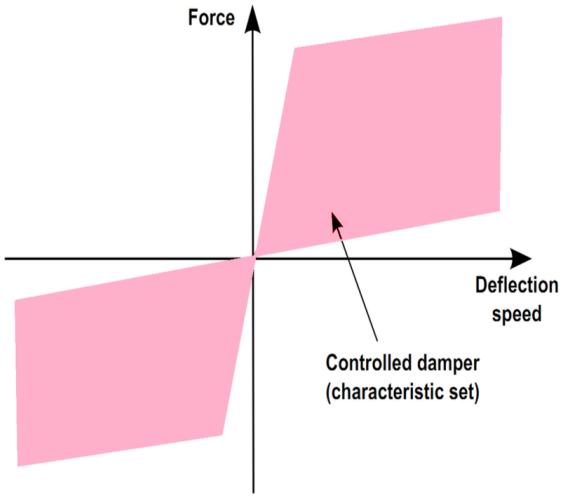

Figure 8 – Force over Speed deflection characteristics of a Semi-Active Damper

2.2 Vehicle Modeling

Vehicles can be placed as a part of complex dynamical systems. Vehicular systems are composed of many components: engine, gearbox, clutch, wheels, suspensions, shock absorbers, brakes and many other subsystems. As of this, dynamical models of these systems are *highly* nonlinear and very complex, as their behaviours change frequently due to each driving situation.

Enhancing vehicle dynamics and performances using advanced control techniques and smart systems has become, nowadays, a key requirement for the automotive industry. For this, the undestandment of vehicle behaviour and a good, *consistent* physical model is of uttermost importance to control design. Vehicle modelling is not an easy task, but has been throughly discussed on [15], [16] and [17]. Figure 9 represents the idea behind the modelling of a vehicular system.

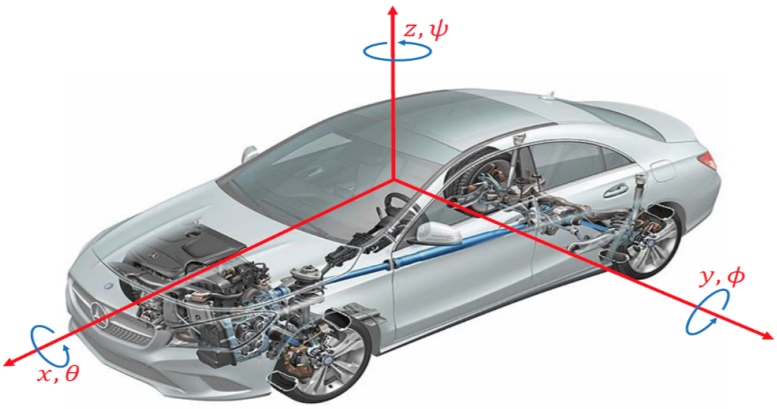

Figure 9 – Modelling of Vehicular Systems

Throughout literature, some well-established models are dedicated to specific

studies (for example, the vertical dynamics, including suspensions). This section shall present three very interesting models for the study of suspensions systems and vertical vehicular dynamics. These models are: the vertical quarter-car model, the full vertical vehicle model and the full vehicle nonlinear model. These models will be referred to and used for validation and control design throughout this work. On background and auxiliary literature, see [18], [19] and [20].

2.3 Linear Matrix Inequalities

Let us remark some of the important topics on linear matrix inequalities, crucial for many of the solutions presented throughout this work. A thorough review of the application of *LMI*s in control theory can be found on [21]. The references [22] and [23] also present well this subject.

2.3.1 Convex Optimization

First of all, a brief on optimisation is necessary. Let us define:

Definition 2.1. A function $f : \mathbb{R}^m \to \mathbb{R}$ is said to be convex if and only if for all $x, y \in \mathbb{R}^m$ and $\lambda \in [0\,,\,1]$, it is true that $f(\lambda x + (1-\lambda)y) \leq \lambda f(x) + (1-\lambda)f(y)$. Equivalently, f is convex if and only if its epigraph is convex.

Remark 1. The epigraph (or supergraph) of a function $f : \mathbb{R}^n \to \mathbb{R}$ is defined as the set of point lying on or above its graph. This is:

$$\text{epi}(f) \quad = \quad \{(x,y) : x \in \mathbb{R}^n\,,\, y \in \mathbb{R} \,|\, f(x) \leq y\} \tag{2.1}$$

From this, we can define the concept of a Linear Matrix Inequality.

Definition 2.2. An *LMI* constraint on a vector $x \in \mathbb{R}^m$ is defined as $F(x)$, for $F(x) = F_0 + \sum_{i=1}^{m} F_i.x_i \succeq 0\,(\succ 0)$, where $F_0 = F_0^T$ and $F_i = F_i^T \in \mathbb{R}^{n\times m}$.

There are two kinds of problems to be handled by the use of *LMI*s:

- The **feasibility** problem: the answer (feasible or not) to the question whether or not there exists elements $x \in X$ so that $F(x) < 0$.
- The **optimization** problem: given an objective function $J : S \to R$ where $S = \{x \,|\, F(x) < 0\}$, this problem is to determine $V_{opt} = inf_{x\in S}\, J(x)$.

2.4 Dynamical Systems

The study (literature review) of dynamical system is important for this work. The books [24] and [25] should certainly be remarked, for they present the key topics on dynamical (linear and nonlinear) systems, including observability, controllability, linear and nonlinear control, flatness and others. [26] is also a good and strong reference.

2.4.1 *LTI* System Control

It is important to present some key concepts for *LTI* systems, as well as for general dynamical systems.

Given the generical *LTI* system put in (2.2), we can deduce characteristics. Note that, as usual, $x(t)$ represents a vector of system states, $u(t)$ represents a vector of system inputs and $y(t)$ represents a vector of outputs. $\dot{x(t)}$ represents $\frac{dx(t)}{dt}$. The system (2.2) has n states, m inputs and p outputs.

$$\begin{aligned} \dot{x(t)} &= A.x(t) + B.u(t) \\ y(t) &= C.x(t) + D.u(t) \end{aligned} \tag{2.2}$$

From this, we can define:

Definition 2.3. A system is said controllable when, given inicial condition $x_0 \in \mathbb{R}^n$ and each final state $x_T \in \mathbb{R}^n$, there exists an input $u : [0,T] \to \mathbb{R}^m$ so that the solution to (2.2), $x : [0,T] \to \mathbb{R}^n$, for the initial condition $x(0) = x_0$ satisfies $x(T) = x_T$, for a generic $T > 0$. This means that that system (2.2) can be driven from a inicial state to an arbitrary final state in a finite time, given the adequate input. A system is said to be uncontrollable when it is not controllable.

Definition 2.4. A system is said to be observable when, for every unknown inicial state $x(0) \in \mathbb{R}^n$, there exists $T > 0$ so that the knowledge of the system input $u(t) \in \mathbb{R}^n$ and the system output $y(t) \in \mathbb{R}^p$ through the time intervale $[0,T]$ is sufficient to determine, by a single way, the inicial state $x(0)$. A system is said to be unobservable when it is not observable.

Given, now, the following matrices:

- Controllability Matrix, $\mathcal{C} = [B\, AB\, A^2B\, \ldots\, A^{n-1}B]_{n \times nm}$;
- Observability Matrix, $\mathcal{O} = ([C\, CA\, CA^2\, \ldots\, CA^{n-1}]_{n \times np})^T$.

Theorem 2.5. *Given the* LTI *system (2.2):*

- *The system is controllable* ***if and only if*** $rank(\mathcal{C}) = n$ *(complete line rank). In this case, we can say, simply, that the pair* (A, B) *is controllable, for the controllability matrix* $\mathcal{C}$ *depends on matrices* A *and* B*;*
- *The system is observable* ***if and only if*** $rank(\mathcal{O}) = n$ *(complete column rank). In this case, we can say, simply, that the pair* (A, C) *is observable, for the observability matrix* $\mathcal{O}$ *depends on matrices* A *and* C*;*
- *The pair* (A, C) *is observable* ***if and only if*** *the pair* (A^T, C^T) *is controllable;*
- *When (2.2) is* SISO *(*$m = p = 1$*), the system is controllable* ***if and only if*** $det(\mathcal{C}) \neq 0$*. And, for* $p = 1$ *(one output), the system is observable* ***if and only if*** $det(\mathcal{O}) \neq 0$*.*

2.4.2 Closed-Loop Pole Placement

It is important to depict, given the previous theorem and definitions, how to stabilize, in closed-loop, an unstable (or stable) open-loop system. For this, consider the system put in (2.3), without direct transfer between entrance $u(t)$ and $y(t)$.

$$\begin{aligned} \dot{x(t)} &= A.x(t) + B.u(t) \\ y(t) &= C.x(t) \end{aligned} \tag{2.3}$$

Consider the following system input: $u(t) = r(t) - K.x(t)$, given $r(t)$ a new auxiliary entrance ($r(t) \in \mathbb{R}^m$) and $K = (k_{ij})$ a constant gain matrix ($K \in \mathbb{R}^{m \times n}$). K is often described as a feedback matrix. In closed-loop, the system (2.3) results in the system (2.4).

$$\begin{aligned} \dot{x(t)} &= (A - BK).x(t) + B.r(t) \\ y(t) &= C.x(t) \end{aligned} \tag{2.4}$$

So, the closed-loop transfer function of (2.4) is $G_{CL}(s) = C(sI - (A - BK))^{-1}B$, for $Y(s) = G_{CL}(s)R(s)$. From this, it can be neatly seen that the poles (eigenvalues) of $(A - BK)$ define the CL system's behaviour.

Definition 2.6. The **Stabilization Problem by State Feedback with Pole Placement** is so that a matrix $K \in \mathbb{R}^{m \times n}$ has to be found so that the CL poles of the system as arbitrarily placed on the complex plane, when $u(t) = r(t) - K.x(t)$ is said a state feedback. Particularly, if all poles of $(A - BK)$ are placed on the LHP, it is assured that $x^e = 0$ is a globally asymptotically stable equilibrium point of the CL system and that the transfer matrix $G_{CL}(s)$ is $BIBO$ stable.

Theorem 2.7. *The pair* (A, B) *is controllable* ***if and only if*** *the pair* $(A - BK, B)$ *is controllable, where* $K \in \mathbb{R}^{m \times n}$ *is a constant matrix.*

Theorem 2.8. *The poles (eigenvalues) of the* CL *matrix* $(A - BK)$ *can be arbitrarily placed on the complex plane by and adequate choice of* $K \in \mathbb{R}^{m \times n}$ ***if and only if*** *the pair* (A, B) *is controllable.*

2.4.3 System Observer

It is also important to put, due to this chapter's study, the concept of system observer. Let it be suposed that the (2.3) system states $x(t) \in \mathbb{R}^n$ cannot be measured, but are of importance. The only available measurements are those of $y(t) \in \mathbb{R}^p$.

A system observer will be herein defined as:

$$\dot{\hat{x}}(t) = A.\hat{x}(t) + B.u(t) + L[y(t) - C.\hat{x}(t)] \tag{2.5}$$

where $\hat{x}(t)$ represents the estimated system states.

For the sake of the argument, let us consider the dynamics of the error $e(t) = x(t) - \hat{x}(t)$:

$$\dot{e}(t) = \dot{x}(t) - \dot{\hat{x}}(t) = (A - LC).e(t) \tag{2.6}$$

For this, given the analysis of (2.6), it can be easily seen that dynamics of the estimation error $e(t) = x(t) - \hat{x}(t)$, by the proposed system observer (2.5), depend on the placement of the eigenvalues of the matrix $(A - LC)$. If these poles are placed on the *LHP*, it is assured by the proposed **asymptotical state observer** that, given any inicial condition $e(0) = x(0) - \hat{x}(0) \in \mathbb{R}^n$, it is true that:

$$\lim_{t \to \infty} e(t) = \lim_{t \to \infty} [x(t) - \hat{x}(t)] = 0 \tag{2.7}$$

Theorem 2.9. *All eigenvalues of the matrix* $(A - LC)$ *can be arbitrarily placed on the complex plane by an adequate choice of* $L \in \mathbb{R}^{p \times n}$ ***if and only if*** *the pair* (A, C) *is observable.*

Note: a state observer can be used, for example, for a stabilizing state feedback input, on the estimated states, as so: $u(t) = r(t) - K.\hat{x}(t)$. Practically, the poles of $(A - L.C)$ are placed on the complex plane to be **faster** than the poles of $(A - B.K)$.

2.4.4 The Linear Quadratic Regulator

Let it be remarked, also, the *Linear Quadratic Regulator* control approach. Let us, then, show the solution to the **Stabilization Problem by State Feedback** by finding a matrix $K \in \mathbb{R}^{m \times n}$ so that the quadratic cost function $J(x(t), u(t))$ is minimized.

Considering $\phi(x(t_f)$ as a terminal cost for the states $x(t)$ at $t = t_f$, we can write the cost function $J(x(t), u(t))$ as:

$$J(x(t), u(t)) = \phi(x(t_f) + \int_{t_0}^{t_f} [\frac{1}{2}x^T(t).Q.x(t) + \frac{1}{2}u^T(t).R.u(t) + x^T(t).N.u(t)]dt \quad (2.8)$$

Considering t_0 the initial time and $\phi(x(t_f) = 0$ we have a full LQR formulation.

The solution of the minimization problem is given by:

$$u(t) = -K.x(t) \quad (2.9)$$

$$K = R^{-1}.B^T.P \quad (2.10)$$

where P is the solution of the continuous time algebraic Ricatti [1] equation seen below:

$$A^T.P + P.A - (P.B + N).R^{-1}(B^T.P + N^T) + Q = 0 \quad (2.11)$$

.

In sum, we can weigh the matrices Q and R depending on the system CL response we expect.

This is control design is further investigated on [28] and [29].

2.5 Linear Parameter Varying Systems

Let us present the basic concepts of a Linear Parameter Varying (LPV) System. These can be revisited on the references [30], [31] and [32].

Definition 2.10. A LPV system can be defined as in equation (2.12), where, as usual, $x(t)$ represents a vector of system states, $u(t)$ represents a vector of system inputs, $w(t)$ represents a vector of disturbances, $y(t)$ represents a vector of measured outputs and $z(t)$ represents a vector of controlled outputs. $\dot{x(t)}$ represents $\frac{dx(t)}{dt}$. The system (2.12) has n states, m inputs, d disturbances, p measured outputs and p_z controlled outputs. $\rho = (\rho_1(t), \rho_2(t), \ldots, \rho_N(t)) \in \Omega$ is a vector of time-varying parameters, assumed to be **known** for all t, where Ω is a convex set. $\rho(\cdot)$ varies in the set of continuously differentiable parameter curves $\rho : [0, +\infty) \to \mathbb{R}^N$. The **scheduling** parameters ρ are assumed to be **bounded**: $\rho \in \mathcal{U}_\rho \subset \mathbb{R}^N$ and $\mathcal{U}_\rho$ is compact, defined by the minimal $\underline{\rho_i}$ and maximal $\overline{\rho_i}$ values of $\rho_i(t)$: $\rho_i(t) \in [\underline{\rho_i}, \overline{\rho_i}]$, $\forall i$. The matrices $A(\cdot)$ to $D_{22}(\cdot)$ are continuous on $\mathcal{U}_\rho$.

$$\sum(\rho) := \left\{ \left[\begin{array}{c} \dot{x}(t) \\ \hline z(t) \\ y(t) \end{array}\right] = \left[\begin{array}{c|cc} A(\rho) & B_1(\rho) & B_2(\rho) \\ \hline C_1(\rho) & D_{11}(\rho) & D_{12}(\rho) \\ C_2(\rho) & D_{21}(\rho) & D_{22}(\rho) \end{array}\right] \left[\begin{array}{c} x(t) \\ \hline w(t) \\ u(t) \end{array}\right] \right\} \quad (2.12)$$

[1] see [27]

The LPV system representation can be understood as something in between the classical duo of nonlinear and LTI systems. Theoretical analysis of the LPV system properties (stability, observability, controllability) often falls into the framework of linear time-varying systems or of nonlinear systems, which usually presents more difficulty compared to the classical LTI framework.

The scheduling parameters can be exogenous if they are external variables (non stationary systems), or endogenous if they are a function of the state variables (quasi-LPV system).

2.6 On Norms

First of all, two definitions are important:

Definition 2.11. The inferior limit of a function can be defined as the inferior bound of a function $f : \mathbb{R} \to \mathbb{R}$. This is:

$$\inf(f(x)) \quad = \quad \{\min(y) \,|\, y = f(x)\} \tag{2.13}$$

Definition 2.12. The superior limit of a function can be defined as the upper bound of a function $f : \mathbb{R} \to \mathbb{R}$. This is:

$$\sup(f(x)) \quad = \quad \{\max(y) \,|\, y = f(x)\} \tag{2.14}$$

The book [33] is essential to this study, where all the following definitions are given.

Definition 2.13. Let V be a finite dimension space, then $\forall \rho \geq 1$, the application $\|\cdot\|_\rho$ is a norm, defined formally as $\|v\|_\rho = (\sum_i |v_i|^\rho)^{\frac{1}{\rho}}$. Let V be a vector space over $\mathbb{C}$ and let $\|\cdot\|$ be a norm define on V: then V is a normed space.

2.6.1 Signal Norms

The 1-Norm of a function is defined as:

$$\|x(t)\|_1 = \int_0^{+\infty} |x(t)| dt \tag{2.15}$$

The 2-Norm of a function is defined as:

$$\|x(t)\|_2 = \sqrt{\int_0^{+\infty} x^*(t).x(t) dt} = \sqrt{\frac{1}{2\pi} \int_{-\infty}^{+\infty} X^*(jw).X(jw) dw} \tag{2.16}$$

The ∞-Norm of a function is defined as:

$$\|x(t)\|_\infty = sup_t |x(t)| \tag{2.17}$$

2.6.2 System Norms

Let us consider *SISO* system. Let $g(t)$ be the impulse response of this system. Then, the H_2 norm of $G(s)$ is defined as:

$$||G||_2 = ||g(t)||_2 \tag{2.18}$$

Let us consider *MIMO* systems with n_u inputs and n_y outputs. The H_∞-norm of this system $G(s)$ is defined as:

$$||G||_\infty = sup_{u(t)\text{s.t.}||u(t)||_2 \neq 0} \frac{||G(s).u(s)||_2}{||u(t)||_2} \tag{2.19}$$

This quantity represents the largest possible 2-norm gain provided by the system.

2.7 On Stability

Let us remark briefly the concepts on system stability, as explored in details on [34] and [35]. Can also be found on [24] and [25].

2.7.1 *BIBO* Stability

An arbitrary system G is said to be *BIBO* stable for whichever limited system entry $u(t)$ ($||u(t)||_\infty < \infty$) there is a resulting (mapped) limited output $y(t)$ ($||y(t)||_\infty < \infty$). If this is not true, the system is said to be *BIBO* unstable. The system is *BIBO* stable if and only if the inequality 2.20 holds, where $h(t)$ is the time impulse response of the system G.

$$M_h = \int_{-\infty}^{+\infty} |h(\tau)|d\tau < \infty \tag{2.20}$$

Remark: *BIBO* Stability is often referred to as **external** stability.

2.7.2 Lyapunov Stability

Also referred to as **internal** ($\mathcal{L}_2$ or *asymptotical*) stability. In respect to this criterion, we can define:

Definition 2.14.

- A system is said to be asymptotically stable when, for whichever initial condition $x_0 \neq 0$, it is true that $\lim_{t\to\infty} y(t) = 0$.
- A system is said to be asymptotically unstable when, for whichever initial condition $x_0 \neq 0$, $y(t)$ is unbounded.

- A system is said to be *marginally* stable if we desire to obtain $y(t)$, $t \in \mathbb{R}$, limited and arbitrarily close to the origin (0), it is only needed that the initial condition x_0 is sufficiently close to zero.

2.7.3 *LTI* Systems Stability Analysis

A system G is $\mathcal{L}_2$ stable if $\|u(t)\|_2 < \infty$ implies $\|y(t)\|_2 < \infty$. The quantification of the signal amplification (gain) is evaluated as $\gamma = sup_{0<\|u\|_2<\infty} \frac{\|y\|_2}{\|u\|_2}$.

2.7.4 *LPV* Systems Stability Analysis

The $\mathcal{L}_2$ stability of *LPV* systems is seen on [36]. Given a parametrically dependent stable *LPV* system as in equation (2.12), for zero initial conditions x_0, the induced $\mathcal{L}_2$ norm is defined as:

$$\| \sum_{\rho} \|_{i,2} = sup_{\rho(t)\in\Omega} \; sup_{w(t)\neq 0 \in \mathcal{L}_2} \frac{\|y\|_2}{\|u\|_2} \tag{2.21}$$

Theorem 2.15. *A sufficient condition for the $\mathcal{L}_2$ of the system $\sum_\rho$ is the generalized bounded real lemma using parameter dependent Lyapunov functions, assuming $|\dot{\rho}_i| < \nu_i \; \forall i$. If there existis $P(\rho) > 0 \;\; \forall \rho$ such that the* LMI *(2.22) holds, then it is true that $\| \sum_\rho \|_{i,2} \leq \gamma$.*

$$\begin{bmatrix} (A^T(\rho)P(\rho) + P(\rho)A(\rho) + \sum_{i=1}^{N} \nu_i \frac{\partial P(\rho)}{\partial \rho_i}) & P(\rho)B(\rho) & C^T(\rho) \\ \star & -\gamma\mathbb{I} & D^T(\rho) \\ \star & \star & -\gamma\mathbb{I} \end{bmatrix} < 0 \,, \; \forall i \tag{2.22}$$

2.8 Fault Tolerant Control

A holistic and interesting approach on the concept behind Fault Tolerant Control (*FTC*) is of uttermost importance to this work, and can be found on the article [37]. A comparative study between active and passive *FTC* approaches is seen on [1], where there se a debate of the use and application results of each of these two methods. Last but not least, on the article [38] we can find a tutorial introduction on reconfigurable *FTC*.

Let us remark the main idea of Active *FTC*, theme of this work: any controlled system is *always* subject to faults and failures - these can be upon components, signal processing or even a total system crash. A classical feedback control system usually comprises actuators and sensors coupled to the real plant (system). Let us admit, then, that there are faults (measurable or not) each of these three subsystems. An active *FTC* scheme is comprised of two parts: a Fault Detection and Diagnosis (*FDD*) structure and

a reconfigurable controller. The *FTC* controller, thus, has an intrinsic reconfiguration mechanism for the faults upon the system that are well detected by the *FDD* scheme. This is clear on figure 10.

A notable article about an implementation of a *FDD* scheme using parity space is seen on [39]. The study of different linear reconfiguration mechanisms is studied by the author on [3].

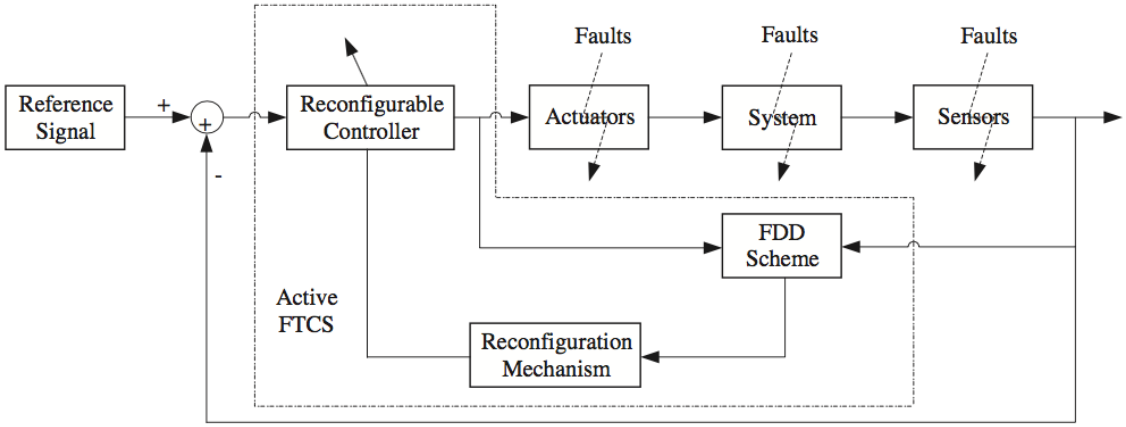

Figure 10 – The Active *FTC* Strategy, as seen on [1]

2.9 Conclusions

This chapter presented some key literature review for what is presented on the following chapters of this work.

3 A Survey of *LPV FDI* Schemes: Loss of Effectiveness on Actuators

3.1 About Chapter

The previous chapters were introductory to this work. Now, this chapter presents approaches for Fault Estimation for Semi-Active Suspension Systems. The idea herein proposed is an extension of what was firstly studied at research course at $ENSE^3$, exposed on [3].

The main problem herein exposed is how to identify faults on actuators by only measuring outputs of the system, considering vehicular semi-active suspension systems.

This chapter is focused on comparing different methods for actuator fault identification considering the use of *LPV* approaches and a *quarter-car* model.

3.1.1 Abstract

This chapter presents and compares three different *LPV* methods for actuator fault detection and diagnosis (*FDD*) on automotive systems with semi-active suspensions, considering a *Quarter of a Vehicle* model. A first *polytopic LPV* approach is detailed, followed by a Mode-Dependent *Dwell-Time* Constrained *Switched LPV* approach, with stronger detectability guarantees, and a final *LPV sliding-mode* approach. The faults are considered as *loss of effectiveness* upon actuators and are, thus, identified. Through simulation, the efficiency of each presented method is discussed and results show the behaviour operation of each *FDD* method.

Keywords: Fault Detection and Diagnosis; *LPV* Systems; Switched Systems; *Sliding-Mode* Observers; Vehicle Systems; Semi-Active Suspensions.

3.2 Introduction

Advanced technological processes present evermore an increase on complexity and become more vulnerable to faults on instrumentation. For this, highlights have been given to Fault Tolerant Control (*FTC*) schemes, that offer increased process availability, avoiding process breakdowns from simple faults, as described in [37]. Reconfiguration mechanisms of compensation represent a common way of how to accomodate faults, see [40].

Considering **active** Fault Tolerant Control, there is a need of an accurate *online* Fault Detection and Isolation (*FDI*) strategy in order to compute an efficient reconfig-

uration mechanism, as show [41] and [1]. A solid Fault Detection and Diagnosis (FDD) structure is, thus, important for FTC as to provide timely information on the condition, location, type of failure that occurs on the controlled plant. This chapter shall compare and conclude on three LPV-based fault estimation schemes specially on their use as to estimate **Loss of Effectiveness** situation on actuators.

Although there exist nonlinear model-based approaches for FDI, as presented on [42], [43] and [39], most methods suppose linear time-invariance (LTI) system characteristics and work with parity space approaches, as seen on [44], [45] and [46]. These classical LTI FDD designs usually face problems when dealing with changes on the observed plant's operational point. Whenever these changes occur, there should not appear (false) fault alarms or the necessity for further observer reconfiguration, which is not always true with these design methods.

Some approaches to overcome these problems reside on gain-scheduling to extend the scope of the linear FDI methods to nonlinear systems. A much more natural approach is to consider the extension of LTI to Linear Parameter Varying (LPV) systems based methods, as it is exploited on [47], [48], [49] and [50].

LPV systems can be understood as a gamma of nonlinear systems to be well suited for the control of dynamical systems with parameter variations. These systems can be represented as an extension of LTI systems, assuming the classical state-space representation matrix are dependent on known **bounded** scheduling parameter ρ. Briefly, these scheduling parameters must abide to $\{\rho \in \Omega \,|\, \rho_{\min} \leq \rho \leq \rho_{\max}\}$. Sometimes, bounds are also needed on the scheduling parameters' variations, $\dot{\rho}$.

An LPV-based fault estimation is able to autonomously adjust and schedule observer or detection filter gains. This is a suitable trade-off between full scaled nonlinear designs and LTI methods based on a fixed operating condition, since LPV-based FDI methods provides most of the conveniences of LTI design and still guarantees good performance and stability conditions over a wider operating set.

In recent years, literature is evermore rich on LPV control design (as seen in [51], [52] and [53]), although the literature on LPV-based FDI is still limited, up to the author's knowledge. For this, this chapter shall discuss the use of some key LPV-based FDI methods to faults on actuators, considering the application to vehicle suspension systems.

Three LPV FDI techniques shall be herein presented and analyzed: a first *polytopic* LPV approach, similar to what is discussed in [49]; a continuation to a *switched* approach, with stability guarantees under mode-dependent dwell-time constraints; and, finally, a *sliding-mode* approach extended to the LPV paradigma, extending what is presented in literature on [54].

3.2.1 The Studied System

In this study, we shall consider the study case of a vehicle's suspension system that is subject to faults.

A good trade-off between a vehicle's road handling performance and ride confort is strictly related to the vehicle's suspension system. Evermore present in the automotive industry, the *Semi-active* suspension systems are to be highlighted, being efficient and, at the same time, less energy-consuming and less expensive than purely active suspensions. The use of semi-active suspension systems seems to provide a good balance between costs and performance requirements. This type of suspension is present on new *state-of-the-art top*-cars and a good deal of academic and industrial research is focused on this topic, as seen on [55], [56] and others. Further details on semi-active suspension systems are throughly discussed on [14], [13] and [12].

A semi-active suspension comprises, basically, a spring and a controlled damper. In terms of system modelling, we shall herein consider the suspension system of a *Quarter of a Vehicle* (QoV) model as our study-case. A QoV model with a semi-active suspension is ruled by the dynamical equations (3.1) and can be represented as on figure 11, where the vehicle's tyre is modelled as a linear spring, with k_t coefficient. In this representation, k_s represents the suspensions spring coefficient, m_s and m_{us} the sprung and unsprung masses, respectively, z_r the road profile disturbance, and z_s and z_{us} the displacements of the sprung and unsprung masses, respectively.

$$\begin{aligned} m_s.\ddot{z_s}(t) &= -k_s(z_s(t) - z_{us}(t)) + F_{ER}(t) \\ m_{us}.\ddot{z_{us}}(t) &= k_s(z_s(t) - z_{us}(t)) - F_{ER}(t) - k_t(z_{us}(t) - z_r(t)) \end{aligned} \tag{3.1}$$

Considering an Electro-Rheological (ER) damper, the semi-active damper's force is given by equation (3.2), and can be re-written as (3.3) considering a nominal (uncontrolled, fixed) and controlled force, where $u(t)$ represents the control input to the semi-active suspension system.

$$F_{ER}(t) = c(\cdot).(\dot{z_s}(t) - \dot{z_{us}}(t)) \tag{3.2}$$

$$F_{ER}(t) = \underbrace{c_0(\dot{z_s}(t) - \dot{z_{us}}(t))}_{\text{nominal}} + \underbrace{u(t)}_{\text{controlled}} \tag{3.3}$$

Remark: c_0 stands herein for the minimal damping coefficient, even for faulty situations. This can be adjusted according to each simulation scenario.

This chapter shall detail and compare different LPV FDI methods and their results on a QoV model with semi-active damper. This chapter is organized as follows:

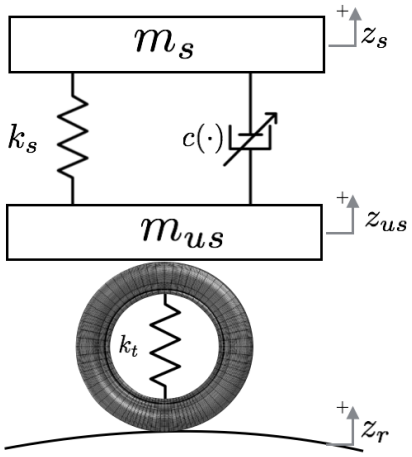

Figure 11 – Control-Oriented Semi-Active Suspension of Quarter-Vehicle with *ER* Damper

the modelling of actuator faults, for the studied suspension system is seen on section 3.3; the *polytopic LPV* fault identification scheme is presented on section 3.4; on section 3.5, the *switched LPV* fault identification scheme is detailed; on section 3.6, the *Sliding-Mode FDD* scheme is designed and discussed; on section 3.7, these approaches to actuator fault identification are compared and discussed; conclusions are drawn on section 3.8.

3.3 Problem Statement: Fault Representation and Modelling

This chapter is focused on the identification of faults on the Semi-Active Damper structure of the described vehicle suspension system. This can later on be used as information for a Fault Tolerant Control Strategy.

We shall assume that a fault occurs upon the controlled part of the actuation of the semi-active *ER* damper. This fault can represent anything that leads to a loss in the effectiveness of the damper, for instance, an oil leakage.

Thus, the fault will be represented by a **loss of effectiveness factor** α, such that:

$$F_{ER}(t) = -c_0.(\dot{z_s}(t) - \dot{z_{us}}(t)) + \alpha.u(t) \tag{3.4}$$

In a faultless situation, we shall have $\alpha = 1$ and, in the worst of scenarios (where the damper is no longer controlled, thus passive), we shall have $\alpha = 0$. For this, $\alpha \in [0\,,\,1]$.

Let us now consider a state-space representation of this semi-active suspension of a *QoV* model with an *ER* damper subject to faults. By using equations (3.1) and (3.4), considering system states as $x(t) = \begin{bmatrix} z_s(t) & \dot{z_s}(t) & z_{us}(t) & \dot{z_{us}}(t) \end{bmatrix}^T$, the disturbance input $w(t) = z_r(t)$ and the measured outputs $y(t) = \begin{bmatrix} z_{def}(t) & \dot{z_{def}}(t) & \ddot{z_s}(t) \end{bmatrix}^T$, we are cast into the following *state-space* representation of our studied system. These measurements are, in a certain way, common on vehicular suspension systems. They can be acquired using

accelerometers (for $\ddot{z_s}(t)$), relative displacement sensors (for the suspension deflection, $z_{def}(t) = z_s(t) - z_{us}(t)$). The deflection velocity ($\dot{z_{def}}(t)$) and unsprung mass velocity ($\dot{z_{us}}(t)$) can be used with certain carefullness, as they arise from derivative filters; this will be further discussed on results section. Finally, this leads us to:

$$\dot{x}(t) = \overbrace{\begin{bmatrix} 0 & 1 & 0 & 0 \\ \frac{-k_s}{m_s} & \frac{-c}{m_s} & \frac{k_s}{m_s} & \frac{c}{m_s} \\ 0 & 0 & 0 & 1 \\ \frac{k_s}{m_{us}} & \frac{c}{m_{us}} & -\frac{(k_t+k_s)}{m_{us}} & \frac{-c}{m_{us}} \end{bmatrix}}^{A}.x(t) + \overbrace{\begin{bmatrix} 0 \\ 0 \\ 0 \\ \frac{k_t}{m_{us}} \end{bmatrix}}^{B_1}.w(t) + \overbrace{\begin{bmatrix} 0 \\ \frac{1}{m_s} \\ 0 \\ -\frac{1}{m_{us}} \end{bmatrix}}^{B_2}.\alpha.u(t) \tag{3.5}$$

$$y(t) = \underbrace{\begin{bmatrix} 1 & 0 & -1 & 0 \\ 0 & 1 & 0 & -1 \\ \frac{-k_s}{m_s} & \frac{-c}{m_s} & \frac{k_s}{m_s} & \frac{c}{m_s} \end{bmatrix}}_{C}.x(t) + \underbrace{\begin{bmatrix} 0 \\ 0 \\ 0 \end{bmatrix}}_{D_1}.w(t) + \underbrace{\begin{bmatrix} 0 \\ 0 \\ \frac{1}{m_s} \end{bmatrix}}_{D_2}.\alpha.u(t)$$

The problem herein studied is, finally, to estimate, identify and diagnose the value of this fault factor α only through the measurements of the system outputs $y(t)$.

To facilitate further development, let us re-write the faulty damper QoV system with an augmented *space-state* representation considering $x_a(t) = \begin{bmatrix} x^T(t) & \alpha & w(t) \end{bmatrix}^T$. We also assume that the fault factor α is constant, so $\dot{\alpha} = 0$. As of this, we have:

$$\sum_{\text{Aug. Sys.}} := \left\{ \begin{array}{rcl} \overbrace{\begin{bmatrix} \dot{x}(t) \\ \dot{\alpha} \\ \dot{w}(t) \end{bmatrix}}^{\dot{x_a}(t)} & = & \overbrace{\begin{bmatrix} A & \underbrace{B_2.u(t)}_{B_\alpha} & B_1 \\ 0 & 0 & 0 \\ 0 & 0 & A_{mw} \end{bmatrix}}^{A_a}.x_a(t) \\ y(t) & = & \underbrace{\begin{bmatrix} C & \overbrace{D_2.u(t)}^{D_\alpha} & D_1 \end{bmatrix}}_{C_a}.x_a(t) \end{array} \right\}$$

where we assume to have information on the type of road profile disturbance. On this basis, we have a model of the disturbance: $\dot{w}(t) = A_{mw}.w(t)$. This information may come from an external adaptive road profile estimator, as proposed in [57]. Remark that different road profiles may have greater *state-space* models with more than one state (say n_w states), which leads to the growth of matrices B_1 and D_1 with $(n_w - 1)$ *null* columns - for example, a sinusoidal road profile has, at least, $n_w = 2$ states.

Notice that the matrices A_a and C_a are affine on $u(t)$, due to the terms (respectively) B_α and D_α. This will be treated with the studied LPV representations, in next sections.

Finally, we can design an asymptotical state observer to estimate the value of the fault factor α given by:

$$\sum_{\text{Fault Obs.}} := \left\{ \begin{array}{rcl} \dot{\hat{x}_a}(t) & = & A_a.\hat{x_a}(t) \quad + \quad L(\cdot).[y(t) - C_a.\hat{x}_a(t)] \\ \hat{\alpha} & = & \underbrace{\left[\begin{array}{ccc} 0_{\text{size}(x)} & \mathbb{I}_{\text{size}(\alpha)} & 0_{\text{size}(w)} \end{array} \right]}_{M}.\hat{x_a}(t) \end{array} \right\} \quad (3.6)$$

The dynamics of the estimation error are given in equation (3.7). Then, we shall compare three different approaches on how to compute the gain matrix $L(\cdot)$. This observer matrix gain will be computed so that $(A_a - L(\cdot).C_a)$ is Lyapunov-sense stable.

$$\dot{e}(t) = \dot{x_a}(t) - \dot{\hat{x}_a}(t) = [A_a - L(\cdot).C_a].e(t) \quad (3.7)$$

A representation of the complete problem structure is given in figure 12. Notice that the controller is not a subject of this study, but it will be considered in further works on a complete *FTC-FDI* scheme.

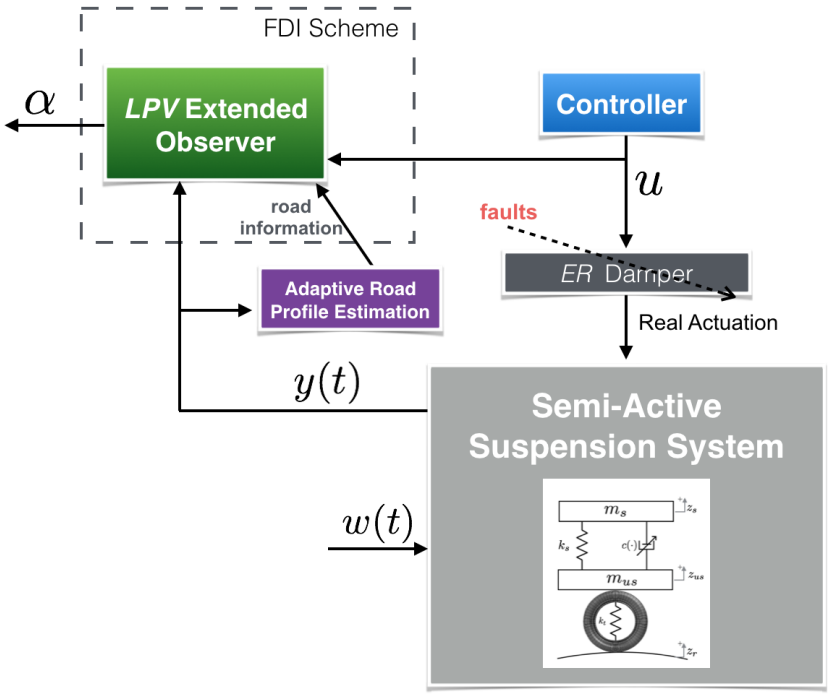

Figure 12 – Proposed *FDI* Scheme

3.4 Polytopic *LPV* State Observer

Let us, firstly, consider a simpler *LPV* approach to compute the gain matrix $L(\cdot)$. Let us remark that the control signal $u(t)$ is *perfectly known*, and **bounded** (due to saturation constraints of the semi-active damper) inside the convex set $\mathcal{U}_{\text{sat}}$, delimited by the minimal and maximal values of $u(t)$, $\underline{u}$ and $\overline{u}$, respectively.

Thus, we can assume $u(t)$ as the scheduling parameter $\rho(t)$, as it satisfies $0 < \rho_{min} \leq \rho \leq \rho_{max}$. From this, we arrive at $B_\alpha = B_2.\rho$ and $A_a = A_a(\rho)$ and, similarly, $D_\alpha = D_2.\rho$ and $C_a = C_a(\rho)$. Thus, the augmented system (3.6) becomes *LPV*.

A *Polytopic* representation of the extended state observer (3.6) is, then:

$$\sum_{\text{Fault Obs.}}(\rho) = \sum_{k=1}^{2} \beta_k(\rho) \left[\begin{array}{c|c} (A_a^k - L^k.C_a^k) & L^k \\ \hline M & 0 \end{array}\right], \text{ with } \sum_{k=1}^{2} \beta_k(\rho) = 1\,,\ \beta_k(\rho) > 0 \tag{3.8}$$

where each $\left[\begin{array}{c|c} (A_a^k - L^k.C_a^k) & L^k \\ \hline M & 0 \end{array}\right]$ is an individual *LTI* system *frozen* at the vertex k of a polytope $\mathcal{P}$ defined by the boundaries of $\mathcal{U}_{\text{sat}}$.

To compute the matrix gain $L(\cdot)$ of the proposed extended observer which guarantees the stability of (3.7), we can use a H_2 (noise filtering) criteria, as seen in [23], considering the measurement noise as an input to the estimation error system. This is an appropriate method to design the observer, for the H_2 norm of a system, from a stochastic point-of-view, is equal to the square root of the asymptotic variance of the output when the input is a white noise (see proof in [22]), which means that the measurement noise effect will be diminished when estimating the loss of effectiveness fault factor α.

3.4.0.1 H_2 Observer: Problem Definition

The H_2 observer problem definition resides, then, on minimizing the following objective function:

$$J = ||T_{e\nu}(s)||_2 \quad \text{under} \quad e(t)|_{t=0} = 0 \tag{3.9}$$

under the two following conditions (exponential stability of $T_{e\nu}(s)$ and *closed-loop* observation error dynamics):

$$\lim_{t\to\infty} e(t) \to 0 \quad \text{for} \quad \nu \equiv \overrightarrow{0} \tag{3.10}$$

$$\dot{e}(t) = (A_a(\cdot) - L(\cdot).C_a(\cdot)).e(t) - L(\cdot).D_\nu\nu(t) \tag{3.11}$$

where $T_{e\nu}(s)$ represents the *Laplace*-domain transfer function between the estimation error $e(t)$ and an additive measurement noise $\nu(t)$ on each component of $y(t)$. Notice, also, that the matrix D_ν represents the influence of the measurement noise on the system measured outputs.

3.4.0.2 Problem Solution

This problem's solution is, then, obtained by minimizing the scalar γ in:

$$\text{Trace}(N) \leq \gamma \tag{3.12}$$

and solving the following *LMI*s, given in equations (3.13)-(3.15), taking $Q = P.L(\cdot)$, with P and N being two positive definite matrices.

Remark: the maximal variance of the estimation error, with this solution, is given by Trace(N).

$$\begin{bmatrix} A_a^T(\rho).P + P.A_a(\rho) - C_a^T(\rho).Q^T - Q.C_a(\rho) & -Q \\ \star & -\mathbb{I} \end{bmatrix} < 0 \quad (3.13)$$

$$2\beta.P + A_a^T(\rho).P + P.A_a(\rho) - C_a^T(\rho).Q^T - Q.C_a(\rho) < 0 \quad (3.14)$$

$$\begin{bmatrix} N & -D_\nu^T.Q^T \\ \star & P \end{bmatrix} > 0 \quad (3.15)$$

Notice that β, in the *LMI* (3.14), is a *root-locus* condition imposed on the eigenvalues of $(A_a(\rho) - L(\rho).C_a(\rho))$: these must be greater, in module, than β (chosen due to settling time restrictions of each application), inside region $\mathcal{R}_p$ of complex plane $\mathbb{C}$, as described by figure 13.

It is also worth remarking that a weighting function can be introduced to specify the frequency range on which sensor noises should be attenuated. Besides, (obviously) sensor noise is considered as a high frequency signal.

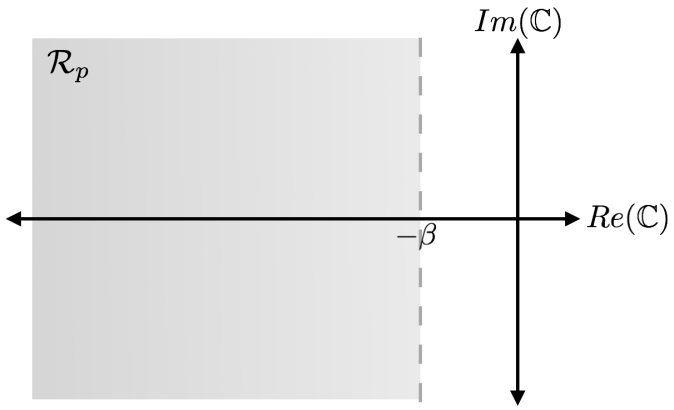

Figure 13 – Pole Placement Region

The interest of the polytopic *LPV* approach is that the *LMI*s (3.13)-(3.15) are computed *offline* at each vertex of $\mathcal{P}$, minimizing the H_2 criterion.

As we have only one scheduling parameter ρ, we shall solve (3.13)-(3.15) at $\rho = \underline{u}$, finding $\underline{L}$, and at $\rho = \overline{u}$, finding $\overline{L}$. Finally, the gain matrix $L(\cdot)$ is given by:

$$L(\rho) = \left(\frac{\rho_{max} - \rho}{\rho_{max} - \rho_{min}}\right).\underline{L} + \left(\frac{\rho - \rho_{min}}{\rho_{max} - \rho_{min}}\right).\overline{L} \quad (3.16)$$

Simulation and validation results with this Polytopic *LPV* approach can be found on section 3.7.

3.5 Switched *LPV* State Observer

This previous Polytopic approach might present some Structural Observability (understood as in the sense presented on [58]) problems whenever $u(t) = 0$, for the rank conditions of the structural observability matrix $\mathcal{O}(\rho) = \begin{pmatrix} C_a(\rho) & C_a(\rho).A_a(\rho) & \dots \end{pmatrix}^T$ might not be guaranteed. This is easier to grasp if one takes a look at $A_a(\rho)|_{\rho=0}$, which presents an empty column. Let us now, thus, consider a more robust approach to overcome this possible problems; this topic is discussed on [59] and [60].

We shall suppose, now, that our systems switched between two types of subsystems: one of fully observable modes (or, at least, detectable) and one that is not structurally observable.

From this, we can designed a switched *LPV* extended observer in order to guarantee closed-loop continuous observability under dwell-time constraints; *dwell-time* being, herein, the time period for which the systems is set to its structurally undetectable mode.

3.5.1 Switched Systems

Before presenting this second *LPV FDI* approach, let us touch some topics on switched systems. As presented on [61] and [62], switched systems represent a class of hybrid dynamical systems consisting on a family of subsystems and a rule that implies a commutation between them.

This systems can be represented, for instance in discrete-time, as in equation (3.17). Herein, $x[k] \in \mathbb{R}^n$ represents the state vector, $u[k] \in \mathbb{R}^m$ the control input vector and $y[k] \in \mathbb{R}^p$ the system output vector. $\sigma[k] : \mathbb{N} \to \mathcal{J}$ represents the discrete **switching rule**, with $\mathcal{J} = \{1, \dots, N\}$, which means the triplet of matrices $(A_{\sigma[k]}, B_{\sigma[k]}, C_{\sigma[k]})$ are defined, at each arbitrary step k, within the finite set $\{(A_1, B_1, C_1), \dots, (A_N, B_N, C_N)\}$.

$$\begin{aligned} x[k+1] &= A_{\sigma[k]}.x[k] + B_{\sigma[k]}.u[k] \\ y[k] &= C_{\sigma[k]}.x[k] \end{aligned} \tag{3.17}$$

Some assumptions shall be considered for further analysis:

- The matrix $C_{\sigma[k]}$ is full (row) rank ;
- The switching rule $\sigma[k]$ is assumed to be known (available) at each instant k.

3.5.2 Stability Condition for Switched *LPV* Systems

One has, still, to look closely at (Lyapunov-sense) stability conditions for switched *LPV* systems. It is important to notice that, for instant, the system (3.17) might be stable

for every triplet $(A_{\sigma[k]}, B_{\sigma[k]}, C_{\sigma[k]})$, but Lyapunov-sense unstable due to the switching phenomenon.

Let us consider a simple continuos system $\dot{x}(t) = A_\sigma(\rho).x(t)$, with $x(0) = x_0$ and A_σ switching according to the switching rule $\sigma(t)$ and, thus, $A_\sigma \in \{A_1(\rho), \ldots, A_N(\rho)\}$ for $A_i \in \mathbb{R}^{n\times n}$ and $i = 1, \ldots, N$.

The guarantees of (asymptotical) stability to this system reside on: if all subsystems A_i are stable and the Lyapunov function $V(x(t))$ is **non-increasing** at the switching instants, the system is stable. This is:

$$\begin{aligned} A_i(\rho)^T.P_\sigma + P_\sigma.A_i(\rho) + \dot{P}_\sigma < 0,\ \forall i = 1, \ldots, M \\ V(x(\tau_k)) \leq V(x(\tau_k^-)),\ \tau_k \text{ is the switching instant} \end{aligned} \tag{3.18}$$

3.5.3 New *LPV* Representation

Herein, to facilitate a LPV representation of this system, we shall explicit the controlled force as $u(t) = |u(t)|.sign(u(t))$, settling a scheduling parameter $\rho(t) = |u(t)|$. Remark: once again, ρ is assumed to satisfy $0 < \rho_{min} \leq \rho \leq \rho_{max}$, which is true for our studied system, for $u(t)$ is bounded inside the convex set $\mathcal{U}_{\text{sat}}$.

From this, we arrive at $B_\alpha = B_2.\rho.\text{sign}(u(t))$ and $A_a = A_a(\rho)$, and, similarly, $D_\alpha = D_2.\rho.\text{sign}(u(t))$ and $C_a = C_a(\rho)$. Thus, once again, our augmented system (3.6) becomes LPV.

We shall, then, take our switching rule as the discontinuous function $\sigma(t) = \text{sign}(u(t))$, considering:

$$\text{sign}(u(t)) := \left\{ \begin{array}{lll} +1\,, & \text{if } u(t) & > 0 \\ 0\,, & \text{if } u(t) & = 0 \\ -1\,, & \text{otherwise} & \end{array} \right\} \tag{3.19}$$

It is important to remark that the matrix $B_\alpha(\rho) \in [-B_2.\rho\,,\, B_2.\rho]$ and, thus, $A_a(\rho)$ switches among the **three** subsystems put on equation (3.20). This similarly occurs to the matrix $C_a(\rho)$, that switches according to the same rule among the three subsystems seen on (3.21). On figure 14, we can see a representation of the system $(\sum_{\text{Fault Obs.}})$ switching between its modes due to the switching law $\sigma(t)$, considering the discontinuous function $\text{sign}(\cdot)$ as explained on (3.19).

$$A_a(\rho) = \mathrm{col}\left\{\begin{bmatrix} A & -B_2.\rho & B_1 \\ 0 & 0 & 0 \\ 0 & 0 & A_{mw} \end{bmatrix}, \begin{bmatrix} A & 0 & B_1 \\ 0 & 0 & 0 \\ 0 & 0 & A_{mw} \end{bmatrix}, \begin{bmatrix} A & B_2.\rho & B_1 \\ 0 & 0 & 0 \\ 0 & 0 & A_{mw} \end{bmatrix}\right\} \tag{3.20}$$

$$C_a(\rho) = \mathrm{col}\left\{\begin{bmatrix} C & -D_2.\rho & D_1 \end{bmatrix}, \begin{bmatrix} C & 0 & D_1 \end{bmatrix}, \begin{bmatrix} C & D_2.\rho & D_1 \end{bmatrix}\right\} \tag{3.21}$$

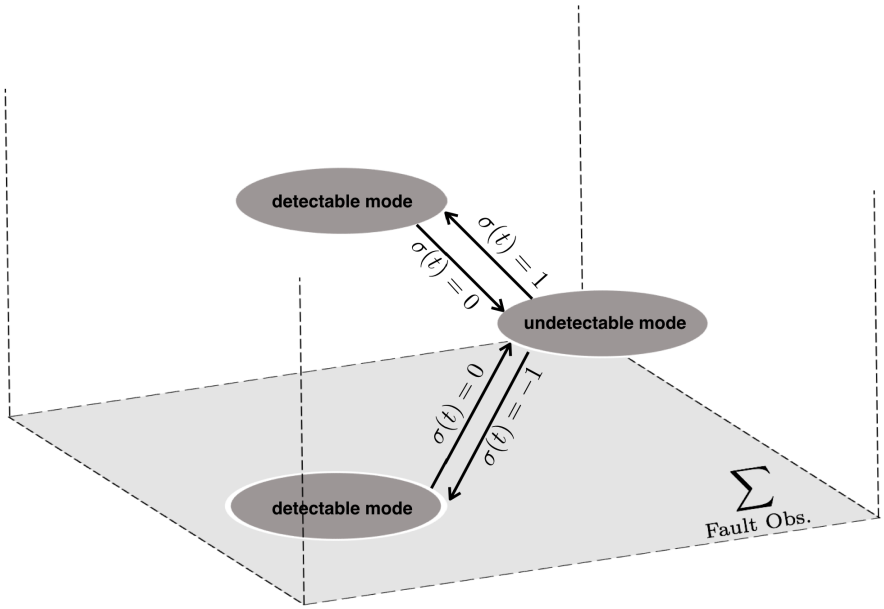

Figure 14 – Switched System and All Switching Modes

Our problem, now, resides on finding $L(\cdot)$ for the switched system (3.6), considering the switching rule $\sigma(t)$, under dwell-time conditions.

3.5.4 Theoretical Background on Minimal Dwell-Time

Let us recall what is presented on [60], on some theoretical background results that are welcome to this present study. Considering the generic (continuous-time) switched system

$$\begin{cases} \dot{x}(t) &= A_{\sigma(t)}.x(t) \\ x(t_0) &= x_0 \\ \sigma(t_0) &= \sigma_0 \end{cases} \tag{3.22}$$

we can scrutinize:

Lemma 3.1. The following statements are equivalent and when one of them holds, the switched system (3.22) is (Lyapunov-sense) asymptotically stable for any and all sequence of switching instants. These statements are:

(i) The quadratic map $V(x(t),\sigma(t)) = x^T(t).P_{\sigma(t)}.x(t)$ with each P_j being a positive definite matrix with $j = 1, \ldots, N$, is a Lyapunov function for system (3.22) with

$$\dot{V}(x(t),j) \leq -\mu\|x(t)\|_2^2, t \in (\tau_k, \tau_{k+1}),\ j = 1, \ldots, N \tag{3.23}$$

and

$$V(x(\tau_{k+1}),\sigma(\tau_{k+1})) - V(x(\tau_k),\sigma(\tau_k)) \leq -\xi\|x(\tau_k)\|_2^2 \tag{3.24}$$

hold for some $\mu, \xi > 0$, all $x(\tau), x(\tau_k) \in \mathbb{R}^n$ and any sequence of switching instants $\{\tau_k\}_{k\in\mathbb{N}}$.

(ii) There exists a positive definite matrix P_j with $j = 1, \ldots, N$, such that the *LMI*s (3.25) and (3.26) hold for all $j,k = 1, \ldots, N$, $j \neq k$ and all $\phi \geq \hat{T}$.

$$A_j^T.P_j + P_j.A_j \prec 0 \tag{3.25}$$
$$e^{A_j^T.\phi}.P_j.e^{A_j.\phi} - P_m \prec 0 \tag{3.26}$$

(iii) There exists some positive definite matrix P_j with $j = 1, \ldots, N$, such that the *LMI*s (3.27) and (3.28) hold for all $j,k = 1, \ldots, N$ and $j \neq k$.

$$A_j^T.P_j + P_j.A_j \prec 0 \tag{3.27}$$
$$e^{A_j^T.\hat{T}}.P_j.e^{A_j.\hat{T}} - P_m \prec 0 \tag{3.28}$$

Proof. Proof of $(i) \Leftrightarrow (ii)$. Assuming that (3.23) holds, this would imply that equation (3.29) is true for all $x(t) \in \mathbb{R}^n$, $t \neq \tau_k$, $k \in \mathbb{N}$. This is equivalent to stating that (3.25) holds. The proof that (3.24) implies (3.26) follows the same reasoning. With reverse argumentation, the proof that $(ii) \Rightarrow (i)$ follows.

$$x^T(t).[A_j.P_j + P_j.A_j].x(t) \leq -\mu\|x(t)\|_2^2 \tag{3.29}$$

The proof of $(ii) \Rightarrow (iii)$ is immediate. Let us consider that (3.27) and (3.28) hold. From this, one can consider a Taylor expansion of the term $\mathcal{T}(\phi) = e^{A_j^T.\phi}.P_j.e^{A_j.\phi}$ around $\phi = \phi_0 \geq \hat{T}$. This yields:

$$\mathcal{T}(\phi_0 + \delta) = e^{A_j^T.\phi_0}.P_j.e^{A_j.\phi_0} + \sigma e^{A_j^T.\phi_0}.[A_j^T.P_j + P_j^T.A_j].e^{A_j.\phi_0} + o(\sigma) \tag{3.30}$$

where $o(\cdot)$ represents a Landau small-o notation. Hence, we arrive at:

$$\mathcal{T}(\phi_0 + \delta) - \mathcal{T}(\phi_0) = \sigma e^{A_j^T.\phi_0}.[A_j^T.P_j + P_j^T.A_j].e^{A_j.\phi_0} + o(\sigma) \tag{3.31}$$

Since (3.27) holds, the right-hand side is negative definite for all $\phi_0 \geq \hat{T}$ and, therefore, we have that:

$$e^{A_j^T(\hat{T}+\delta)}.P_j.e^{A_j(\hat{T}+\delta)} \leq e^{A_j^T.\hat{T}}.P_j.e^{A_j.\hat{T}} \tag{3.32}$$

for all $\delta \geq 0$ and, thus:

$$e^{A_j^T.\phi}.P_j.e^{A_j.\phi} - P_m \preceq e^{A_j^T.\hat{T}}.P_j.e^{A_j.\hat{T}} - P_m \prec 0 \tag{3.33}$$

hold for all $\delta \geq \hat{T}$. The proof, then, is complete. □

Finally, let us state:

Theorem 3.2. *The following statements are equivalent and when one of them holds, the switched system (3.22) is (Lyapunov-sense) asymptotically stable for any and all sequence of switching instants. These statements are:*

(i) There exists some positive definite matrices P_j with $j = 1, \ldots, N$ such that the LMI*s (3.34) to (3.35) hold for all $j, k = 1, \ldots, N$ and $j \neq k$.*

$$A_j^T.P_j + P_j.A_j \prec 0 \tag{3.34}$$
$$e^{A_j^T.\hat{T}}.P_j.e^{A_j.\hat{T}} - P_m \prec 0 \tag{3.35}$$

(ii) There exists matrix maps $R_j : [0, \hat{T}] \to \mathbb{S}^n$, being $\mathbb{S}^n$ the set of symmetric matrices, with $j = 1, \ldots, N$, with $R_j(0)$ being positive definite, and a scalar $\xi > 0$ such that the LMI*s (3.36) to (3.37) hold for all $j, k = 1, \ldots, N$, $j \neq k$ and $\tau \in [0, \hat{T}]$.*

$$A_j^T.R_j(0) + R_j(0).A_j \prec 0 A_j^T.R_J(\tau) + R_j(\tau).A_j - \dot{R}_j(\tau) \preceq 0 \tag{3.36}$$
$$R_j(\hat{T}) - R_m(0) \preceq -\xi.\mathbb{I} \tag{3.37}$$

(iii) There exists matrix maps $S_j : [0, \hat{T}] \to \mathbb{S}^n$, being $\mathbb{S}^n$ the set of symmetric matrices, with $j = 1, \ldots, N$, with $S_j(\hat{T})$ being positive definite, and a scalar $\xi > 0$ such that the LMI*s (3.38) to (3.40) hold for all $j, k = 1, \ldots, N$, $j \neq k$ and $\tau \in [0, \hat{T}]$.*

$$A_j^T.S_j(\hat{T}) + S_j(\hat{T}).A_j \prec 0 \tag{3.38}$$
$$A_j^T.S_J(\tau) + S_j(\tau).A_j - \dot{S}_j(\tau) \preceq 0 \tag{3.39}$$
$$-S_m(0) + S_j(\hat{T}) \preceq -\xi.\mathbb{I} \tag{3.40}$$

Proof. Proof follows from Lemma 3.1 and what is presented as *Stability with Periodic Switching Times* theorem on [60]. □

Notice that the notion of maximal dwell-time was herein represented by $\hat{T}$. The preliminary results brought by lemma 3.1 and theorem 3.2 can be extended considering a dwell-time condition for each of the systems modes, this is $\hat{T}_j$.

3.5.5 Detectability of *LPV* Switched Systems Under Mode-Dependent Dwell-Time

Now, we can formally investigate the issue of **guaranteed detectability** of a *LPV* switched system, with mode-dependent dwell-time constraints. Let us highlight that the notion of mode-dependent dwell-time is understood in the sense of [63].

From what is presented on Lemma 3.1 and Theorem 3.2, and considering the convex conditions Lemma presented on the following (as on [64]), we can consider that our *LPV* system (3.6) has dwell-time conditions for each of its modes (refer to figure 14).

Lemma 3.3. Consider the generic switched system $\dot{x}(t) = A.x(t)$. Assume that for some interval $t \in [t_0\,,\, t_f]$ and $\delta_t = t_f - t_0$, there exists two positive definite symmetric matrices P_1 and P_2 of appropriate dimensions that satisfy the following conditions:

$$\begin{aligned} \frac{P_2 - P_1}{\delta_t} + P_1.A + A^T.P_1 < 0 \\ \frac{P_2 - P_1}{\delta_t} + P_2.A + A^T.P_2 < 0 \end{aligned} \tag{3.41}$$

Then, for this system, there is stability when considering Lyapunov function $V(t) = x^T(t).P(t).x(t)$, with $P(t) = P_1 + (P_2 - P_1).(\frac{t-t_0}{\delta_t})$, which is strictly decreasing over the time interval $t \in [t_0\,,\, t_f]$.

Proof. Proof is detailed on [64]. □

Assuming that upper and lower bounds for the dwell-time for each mode are those seen on (3.42), for $j = 2$ as the undetectable mode (taken into by the switching rule $\text{sign}(u(t))|_{u(t)=0} = 0$). Then, as explained, the dwell-time constraints are $T^j_{max} \geq (\tau^j_{s+1} - \tau^j_s) \geq T^j_{min}$ for all $s \in \mathbb{N}$, considering τ^j_s a switching instant onto (or from) mode j.

$$\mathcal{DT} := [T^1_{min}, T^1_{max}] \times \cdots \times [T^N_{min}, T^N_{max}] = [T^1_{min}, +\infty) \times [T^2_{min}, T^2_{max}] \times [T^3_{min}, +\infty) \tag{3.42}$$

Remark: When $T^j_{max} = +\infty$, for some index j, it is then necessary that the respectful subsystem j is (Lyapunov sense) stable (likewise, detectable); in our study case, then, the pairs $(A^1_a(\rho), C^1_a(\rho))$ and $(A^3_a(\rho), C^3_a(\rho))$ should be detectable, which is true.

From this, we can cast our analysis to the following theorem for the observability of switched systems under mode-dependent dwell-time constraints, considering the classical asymptotical observer design, as in (3.6) and its error dynamics. Remark that the controllability and observability are *dual* problems!

Thus, let us now propose Theorem 3.4 so that there is **guaranteed continuous detection** of α, under the given constrained mode-dependent dwell-time conditions, for our studied *LPV* system.

Theorem 3.4. ***Guaranteed Continuity of Detection of* LPV *Switched Systems under Mode-Dependent Dwell-Time Constraints***

Firstly, let us remark that, herein, guaranteed continuity of detection is understood in the sense that a continuous-time asymptotical observer can be designed and a matrix gain $L(\cdot)$ can be found so that the observation error $e(t)$ converges asymptotically to $(0,0)$ in finite time.

It is also, herein, assumed that $T^1_{min} \geq T^3_{min} > T^2_{max}$. This might be to conservative, but its goal is to guarantee the time-wise stabilization of the tracking error e (after possible instabilities at mode $j = 2$).

Consider the switched LPV *system (3.6) with bounded scheduling parameters ρ that abide to $\{\rho \in \Omega \,|\, \rho_{min} \leq \rho \leq \rho_{max}\}$. Consider τ_s as the switching instants to (or from) mode 2 (structurally undetectable), with $s \in \mathbb{N}$ and $T^2_{min} \leq (\tau_{s+1} - \tau_s) \leq T^2_{max}$, in respect to the bound presented on (3.42).*

If the following statements are true, then there is guaranteed detectability of (3.6) for any $\rho \in \Omega$ (and for any control input $u(t)$) and for all t if the dwell-time within each mode respect the proposed bounded conditions:

(i) There exists positive definite matrices K_j with $j = 1, \ldots, N$ so that the LMI*s (3.43) hold for all $T_j \in [T^j_{min}, T^j_{max}]$ and $j, k = 1, \ldots, N$ for $j \neq k$ where it is implied that (3.44) is necessary, considering $\Psi_j(0) = \mathbb{I}$ and $s \geq 0$.*

$$\Psi_j(T^j).K_j.\Psi_j(T^j)^T - K_k \prec 0 \tag{3.43}$$

$$\frac{\Psi_j}{ds}(s) = [A_a(\rho) - L_i(\rho).C_a(\rho)](s).\Psi_j(s) \tag{3.44}$$

(ii) There exists a collection of N positive definite matrices P_j and Y_j for all $j = 0, \ldots, N$ such that the LMI*s (3.45) to (3.47) hold, where each $P_j(\rho)$ is polytopic within each bounded variations of ρ within each of the systems modes. It is important to remark that: i_0 represents the initial mode for the initial switching rule, this is $\sigma(t)|_{t=0}$ - it most importantly assumed that $i_0 \neq 2$; τ_δ is a prescribed time period to guarantee the piecewise continuity of $P_\sigma(\rho, t)$ and $Y_\sigma(\rho, t)$. The notation on these equations is simplified: A represents $A_a(\rho)$ and C represents $C_a(\rho)$, whereas P_j and Y_j are $P_j(\rho)$ and $Y_j(\rho)$. Remark: the matrices $P_{j\to 2}$ and $Y_{j\to 2}$ represents the matices whiting witch the continuous $P_\sigma(\rho, t)$ and $Y_\sigma(\rho, t)$ were, respectively, when occurred the switching transition $\tau^{2\to m}_{s+1}$, inside the time interval $t \in [\tau_s, \tau_s + T^2_{max})||[\tau_s, \tau_s + T^2_{min})$.*

$$\frac{(P_{j+1}-P_j)}{T_{max}^2}+A_j^T.P_j-C_j^T.Y_j^T+P_j.A_j-Y_j.C_j<0, \tag{3.45}$$

$$A_j^TP_j-C_j^T.Y_j^T+P_j.A_j-Y_j.C_j<0 \tag{3.46}$$

$$P_{j+1}-P_j\geq 0\,\forall j=1,\ldots,(N-1) \tag{3.47}$$

$$P_\sigma(\rho,t):=\begin{cases} P_{i_0}(\rho) & & & & if & t\in[0\,,\,\tau_1)\\ P_j(\rho) & + & (P_2(\rho)-P_j(\rho)).\left(\frac{t-\tau_s}{T_{max}^2}\right) & if & t\in[\tau_s\,,\,\tau_s+T_{max}^2)\|[\tau_s\,,\,\tau_s+T_{min}^2)\\ P_{j\to 2}(\rho) & + & (P_m(\rho)-P_{j\to 2}(\rho)).\left(\frac{t-\tau_{s+1}}{\tau_\delta}\right) & if & t\in[\tau_{s+1}^{2\to m}\,,\,\tau_{s+1}^{2\to m}+\tau_\delta)\\ P_m(\rho) & & & if & t\in[\tau_{s+1}+\tau_\delta\,,\,\tau_{s+2}) \end{cases} \tag{3.48}$$

$$Y_\sigma(\rho,t):=\begin{cases} Y_{i_0}(\rho) & & & & if & t\in[0\,,\,\tau_1)\\ Y_j(\rho) & + & (Y_2(\rho)-Y_j(\rho)).\left(\frac{t-\tau_s}{T_{max}^2}\right) & if & t\in[\tau_s\,,\,\tau_s+T_{max}^2)\|[\tau_s\,,\,\tau_s+T_{min}^2)\\ Y_{j\to 2}(\rho) & + & (Y_m(\rho)-Y_{j\to 2}(\rho)).\left(\frac{t-\tau_{s+1}}{\tau_\delta}\right) & if & t\in[\tau_{s+1}^{2\to m}\,,\,\tau_{s+1}^{2\to m}+\tau_\delta)\\ Y_m(\rho) & & & if & t\in[\tau_{s+1}+\tau_\delta\,,\,\tau_{s+2}) \end{cases} \tag{3.49}$$

(iii) Moreover, if one takes in consideration the observer error dynamics, as on (3.7), these will be (Lyapunov-sense) asymptotically stable for all switching instants in $\mathcal{I}_\tau$ and the states of the system (3.6) are continuously reconstructable only if one takes the proper choice of matrix function $L_\sigma(\cdot)$ as on (3.51).

$$\mathcal{I}_\tau=col\{\tau_1\,,\,\tau_2\,,\,\ldots\} \tag{3.50}$$

$$L_\sigma(\rho,t)=P_\sigma^{-1}(\rho,t).Y_\sigma(\rho,t) \tag{3.51}$$

Proof. Proof of *(i)*: The goal is to show that this statement is a necessary and sufficient condition for the existence of a feedback gain $L_\sigma(\cdot)$ for the system (3.52) where $m(t)=-C_a.e(t)$.

$$\dot{e}(t)=A_a.e(t)+L_\sigma(\cdot).m(t) \tag{3.52}$$

Then, the idea is to use Lemma 3.1 and Theorem 3.2 to prove stability (equivalent problem to observability) of a closed-loop system subject to a minimum dwell-time, as presented on [60]. Noting that for all $\phi\geq\hat{T}$ and $L_\sigma(\cdot)|_{t=\phi}=L_\sigma(\cdot)|_{t=\hat{T}}$ and following the same argumentation as on the proof of Lemma 3.1, we find that condition (3.27) exactly becomes a classical algebraic Ricatti stabilization condition for our system and condition (3.28) is cast into (3.43), which proves the exactness of *(i)*.

Proof of *(ii)*: Let us reduce our analysis to the generic switched system (3.22). Let us recall that this system is (Lyapunov-sense) asymptotically stable if:

$$\dot{V}(x(t)) = x^T(t).(A_j(\rho).P_\sigma(\rho,t) + P_\sigma(\rho,t).A_j(\rho) + \dot{P}_\sigma(\rho,t)).x(t) < 0 \qquad (3.53)$$
$$V(x(\tau_k)) \leq V(x(\tau_k^-))\,,\ \tau_k \text{ as switching instant}$$

It is assumed, then, that at the switching instant τ_k, the system switched from $A_j(\rho)$ to $A_m(\rho)$. Thus, we can write the Lyapunov function at instant τ_k as:

$$V(x(\tau_k^-)) = x^T(\tau_k).P_m.x(\tau_k)\,,\ \ V(x(\tau_k)) = x^T(\tau_k).P_j.x(\tau_k) \qquad (3.54)$$

Then the non-increasing Lyapunov function condition $V(x(\tau_k)) \leq V(x(\tau_k^-))$ holds if $P_m - P_j \geq 0$, which is actually (3.47). Now, we can apply Lemma 3.3 for each switching instant τ_s. Indeed, during dwell-time, considering the bounded time interval $[\tau_s^{n\to j}\,,\ \tau_{s+1}^{j\to m}]$ the Lyapunov matrix $P_\sigma(\rho,t)$ changes linearly from P_j to P_m. Then, from Lemma 3.3 with δ_t (bounded at the maximal time interval T^2_{max}) the *LMI* (3.53) is true if (3.45) holds. After the dwell time and before the next switching instant the Lyapunov matrix $P_\sigma(\rho,t)$ becomes the time independent $P_m(\rho)$, then, once again (3.53) hold if $A_m^T(\rho).P_m(\rho) + P_m(\rho).A_m(\rho) < 0$, which is equivalent to (3.46), given the polytopic approach for the *LPV* system.

Proof of *(iii)* follows from *(i)* using a change of variables $Y_j = -M_j.K_j.L_j$ and continuing with the solution of the *LMI*s on *(ii)*. Notice that the condition implied by *(i)* is solved by the proposition on *(ii)*. □

3.5.6 Method Synthesis

The main idea with this method is to guarantee the observer's asymptotical stability (considering error dynamics) for all t, considering there is a restriction on the system's maximal *dwell-time* on each of its modes. With the first *polytopic* approach, for this study, there was no guarantees of continuous detection of α (or stability on $\dot{e}(t)$) if the system passed through its undetectable mode (for $u(t) = 0$).

Simulation and validation results with this Switched *LPV* approach can be found on section 3.7.

3.6 Sliding Mode *LPV* State Observer

Let us now consider the use of a *Sliding Mode LPV* State Observer to determine the value of the loss of effectiveness on actuator α. This method is adapted from what is throughly discussed on [54], where both actuator and sensor faults are considered, to a feasible application to our studied system (*QoV* model).

For this method, we shall consider that the system states can be separated into two main parts: those state that are unsensible to faults ($x_1(t)$) and those which suffer influence

of faults ($x_2(t)$). For the QoV system, we shall consider a new state-space representation for this kind of separation. This is:

$$\dot{x_1}(t) = \mathcal{A}_{11}.x_1(t) + \mathcal{A}_{12}.x_2(t) \tag{3.55}$$

$$\dot{x_2}(t) = \mathcal{A}_{11}.x_1(t) + \mathcal{A}_{12}.x_2(t) + \mathcal{B}_{1_2}.w(t) + \mathcal{B}_{2_2}.u(t) + \mathcal{D}_2(\rho).f_i(t) \tag{3.56}$$

$$y_{new}(t) = x_2(t) \tag{3.57}$$

$$\tag{3.58}$$

where $\mathcal{A} \in \mathbb{R}^{n\times n}$ is a linear transformation on states $x_{new}(t) = T_x.x(t)$, this is $\mathcal{A} = T_x.A.T_x^{-1}$, $\mathcal{B}_1 \in \mathbb{R}^{n\times w}$ comes from $T_x.B_1$, likewise for $\mathcal{B}_2 = T_x.B_2 \in \mathbb{R}^{n\times m}$; finally, $\mathcal{D}(\rho) \in \mathbb{R}^{n\times q}$ represents the fault distribution matrix. Notice that, with this formulation, the road disturbance $w(t)$ and control signal $u(t)$ only influences $x_2(t)$.

Notice that, for this *FDI* approach, other measured outputs are considered. These are the deflection velocity, the unsprung mass velocity; the suspension deflection is also considered as an auxiliary output. This is $y(t) = \left[\underbrace{\dot{z_{def}}(t)}_{y^1_{new}(t)} \quad \underbrace{\dot{z_{us}}(t)}_{y^2_{new}(t)} \quad \underbrace{z_{def}(t)}_{y_{aux}(t)} \right]$, where $y_{new}(t) = x_2(t)$ and $x_1(t) = \left[\; z_s(t) \quad z_{us}(t) \; \right]$. The use of the auxiliary output shall be described soon.

It is assumed that $\mathcal{D}(\rho)$ can always be decomposed into fixed and a varying component, $\mathcal{D}(\rho) = D.E(\rho)$, for $D \in \mathbb{R}^{n\times q}$ and $E(\rho) \in \mathbb{R}^{q\times q}$. It is important to remark that $r_1(\rho)$ and $\psi : \mathbb{R}_+ \times \mathbb{R}^p \times \mathbb{R}^d \to \mathbb{R}_+$ are known well-defined functions. Taking our scheduling parameter as $\rho = u(t)$, with known bounded conditions (explained in the two previous approaches), we shall arrive, with this formulation, at the point where detected faults $f_i(t)$ will, numerically, represent $(\alpha - 1)$. From this, we can write $D = \mathcal{B}_2$ and $E(\rho) = \rho.\mathbb{I}_q$. Then, let us consider a function $f_v(t,\rho) : \mathbb{R}_+ \times \mathbb{R}^d \to \mathbb{R}^q$ to represent *"virtual faults"* upon the actuators, in order to incorporate the LPV variations. Then, it is assumed that (3.59) is always guaranteed.

$$\|f_v(t,\rho)\| < r_1(\rho).\|u(t)\| + \psi(t,y,\rho) \tag{3.59}$$

The determinant $\det(E(\rho))$ will be considered as $det(E(\rho)) \neq 0$ and, for this, the actual fault factor α will be able to be retrieved from the estimative $f_v(t,\rho)$. The functions $r_1(\rho)$ and $\psi(t,y,\rho)$ are defined so to constitute the upper bound on the worst of a loss of effectiveness fault on the system dynamics (this is, for $\alpha = 0$), as shows equation (3.59). The scenario for which $\det(E(\rho)) = 0$ will be treated as an exception and discussed afterwards.

Then, the fault observer for this approach will little modify what is presented on

(3.6) to a different structure for observing the fault-free states x_1 and the fault-prone states x_2. This is presented on the following structure:

$$\dot{\hat{x}_1}(t) = \mathcal{A}_{11}.\hat{x_1}(t) + \mathcal{A}_{12}.\hat{x_2}(t) - G_{L_1}.e_y(t) - G_{N_1}.\nu_1(t) \tag{3.60}$$

$$\dot{\hat{x}_2}(t) = \mathcal{A}_{21}.\hat{x_1}(t) + \mathcal{A}_{22}.\hat{x_2}(t) - G_{L_2}.e_y(t) - G_{N_2}.\nu_2(t) + \mathcal{B}_{1_2}.\hat{w}(t) + \mathcal{B}_{2_2}.u(t) \tag{3.61}$$

$$e_y(t) = y_{new}(t) - \hat{y_{new}}(t) \tag{3.62}$$

$$\hat{y_{new}}(t) = \hat{x_2}(t) = \underbrace{\begin{bmatrix} 0_{x_1} & \mathbb{I}_{x_2} \end{bmatrix}}_{C_{new}} . \begin{bmatrix} \hat{x_1}(t) \\ \hat{x_2}(t) \end{bmatrix} \tag{3.63}$$

where, instead of defining the gain matrix $L(\cdot)$, one has to define the gain matrices G_L and G_N and the auxiliary input $\nu(t)$. These are so that a sliding motion is induced and the output estimation error $e_y(t)$ (see equation (3.62)) goes to zero in finite time. Once this is true, a first order sliding mode is said to have been obtained on the surface $\mathcal{S}$ (see book [65]), for:

$$\mathcal{S} = \{e \in \mathbb{R}^n : C_{new}.e = 0\} \tag{3.64}$$

Remark that the observer on equations (3.60)-(3.61) is purely a state observer and does not consider the augmented states as in the previous approaches. The information on the disturbance $\hat{w}(t)$ shall be generated by a parallel estimator, detailed further on this section. The state estimation error ($e_j = x_j(t) - \hat{x_j}(t)$) dynamics will be, thus, given by what is presented on equations (3.65)-(3.66), considering $\hat{w}(t) = w(t)$, for simplicity.

$$\dot{e_1}(t) = \mathcal{A}_{11}.e_1(t) + \mathcal{A}_{12}.e_2(t) + G_{L_1}.e_y(t) + G_{N_1}.\nu_1(t) \tag{3.65}$$

$$\dot{e_2}(t) = \mathcal{A}_{21}.e_1(t) + \mathcal{A}_{22}.e_2(t) + G_{L_2}.e_y(t) + G_{N_2}.\nu_2(t) + D_2.f_v(t,\rho) \tag{3.66}$$

As once proposed on [66], we can, from this point, start with design tools so that the sliding mode is attained on the surface $\mathcal{S}$, given by (3.64).

It is important to remark that, with this representation we have $\mathcal{A}_{11} = 0_{2\times2}$. From this, considering an adequate *fast* stabilization of (3.65), we can take, for instance:

$$G_{L_1} = -\mathcal{A}_{12} \tag{3.67}$$

$$G_{N_1} = \mathcal{L} = \begin{bmatrix} -\lambda_1 & 0 \\ 0 & -\lambda_2 \end{bmatrix} \tag{3.68}$$

$$\lambda_1 \geq \lambda_2 > 0 \tag{3.69}$$

$$\nu_1(t) = \breve{e_1}(t) \tag{3.70}$$

which means $\mathcal{L}$ is chosen with fast-enough eigenvalues λ_j and $\breve{e_1}(t)$ represents an (open-loop) estimative of the prediction error e_1. Taking, for simplicity, $\breve{e_1}(t) = e_1(t)$, we arrive at:

$$\dot{e_1}(t) = \mathcal{L}.e_1(t) \tag{3.71}$$

which is (Lyapunov sense) stable and converges to zero in finite time. The estimation $\breve{e_1}(t)$ is retrieved with the used of the measured (and auxiliary) outputs. This is:

$$\breve{e_1}(t) = \overbrace{\begin{bmatrix} \breve{z_s}(t) \\ \breve{z_{us}}(t) \end{bmatrix}}^{\breve{x_1}(t)} - \hat{x_1}(t) \tag{3.72}$$

$$\breve{z_{us}}(t) = \int_{-\infty}^{t} y_{new}^2(\tau) d\tau \tag{3.73}$$

$$\breve{z_s}(t) = y_{aux}(t) + \breve{z_{us}}(t) \tag{3.74}$$

Notice that, as our system (QoV model) has physical bounded limits, every state has bounded conditions: for example $\underline{z_s} \leq z_s(t) \leq \overline{z_s}$. This means that there are (known) bounds on the maximal estimation of $e_1(t)$. The error between the estimation ($\breve{e_1}(t)$) and the real error $e_1(t)$ are given by the initial conditions of the integral on (3.73). Notice that, then:

$$e_1(t) - \breve{e_1}(t) \leq \epsilon \tag{3.75}$$

which means that, on the worst case scenario, we shall have:

$$\dot{e_1}(t) = \mathcal{L}.e_1(t) + \mathcal{L}\epsilon \tag{3.76}$$

$$e_1(t) \to \epsilon_e$$

Now, let us analyse how to choose the degrees-of-freedom on the other error dynamics ($\dot{e_2}(t)$). This is, let us expand (3.66), considering that:

$$w(t) - \hat{w}(t) \to \epsilon_w \tag{3.77}$$

$$e_1(t) \to \epsilon_e \tag{3.78}$$

$$G_{L_2} = (\mathcal{A}_{22}^{\text{stab}} - \mathcal{A}_{22}) \tag{3.79}$$

$$\nu_2(t) = \mu.\|D_2\|.\text{sign}(e_y(t)) \tag{3.80}$$

wherein $\nu_2(t)$ is a sliding-mode injection term, that μ is an appropriate scalar so that $\|\mathcal{B}_{1_2}\epsilon_w\| + \|\mathcal{A}_{12}.\epsilon_e\| + \|f_v(t,\rho)\| < \mu$ and that G_{N_2} is a *Lyapunov* matrix for $\mathcal{A}_{22}^{\text{stab}}$, we shall arrive at:

$$G_{N_2}.\mathcal{A}_{22}^{\text{stab}} + (\mathcal{A}_{22}^{\text{stab}})^T.G_{N_2} = \mathbb{I}_2 \tag{3.81}$$

$$\dot{e_2}(t) = \mathcal{A}_{22}^{\text{stab}}.e_2(t) + \underbrace{G_{N_2}.\nu_2(t)}_{\text{Sliding-Mode Term}} + D_2.f_v(t,\rho) + \underbrace{(\mathcal{A}_{12}.\epsilon_e + \mathcal{B}_{1_2}.\epsilon_w)}_{\text{ideally=0}} \tag{3.82}$$

3.6.1 The Sliding-Mode Injection Term

A complete analysis on the Sliding-Mode injection term $\nu_2(t)$ is exposed on [67], with results on stability and proofs that the output error will converge to zero in finite time, considering the suitable choice of G_{N_2}.

3.6.2 Retrieving Fault Information

Let it be assumed that the sliding-mode observer has been well designed and that the sliding motion on the surface $\mathcal{S}$ has been established. Then, during the sliding motion, we know it is true that $e_y(t) = 0$ and $\frac{de_y(t)}{dt} = 0$, considering the assumptions presented beforehand. From this, we know:

$$\dot{e_2}(t) = \underbrace{[\mathcal{A}_{21}.e_1(t) + \mathcal{B}_{1_2}(\hat{w}(t) - w(t))]}_{\text{stable convergence}} + \mathcal{A}_{22}^{\text{stab}}.e_2(t) + G_{N_2}.\nu_2(t) + D_2.f_v(t,\rho) \tag{3.83}$$

$$G_{N_2}.\nu_2^{\text{sliding}}(t) \to -D_2.f_v(t,\rho) \tag{3.84}$$

The function $\nu_2(t)$ is discontinuous, but can replaced by a continuous approximation, considering a suitable (small enough) choice of σ. This is, for every component k of $\nu_2(t)$, we can take:

$$(\nu_2^{\text{sliding}})_k(t) \approx \mu.\|D_2\|.\frac{e_{y_k}(t)}{\|e_{y_k}(t)\| + \sigma} \tag{3.85}$$

Finally, one can retrieve the fault information and the fault factor α by following the steps:

- Computing the approximate $\nu_2^{\text{sliding}}(t) = \text{col}\{(\nu_2^{\text{sliding}})_k(t)\}$;
- Retrieving $\hat{f}_v(t,\rho) = -\breve{\mathcal{D}}_2^{\star}.(G_{N_2}.\nu_2^{\text{sliding}})$, for $\breve{\mathcal{D}}_2^{\star}$ being the pseudo-inverse of $\breve{\mathcal{D}}_2$;
- Reconstructing $f_i(t)$ as of $\hat{f}_i(t) = E^{-1}(\rho).\hat{f}_v(t,\rho)$;
- Computing the loss of effectiveness factor α as $\hat{\alpha} = 1 + \hat{f}_i$.

Let us consider, for this method, that the changes upon α are extremely low-frequency. This is, we are not interested in transitory behaviour of α, but mostly on steady-state information on the loss of effectiveness of the actuator. Then, after the procedure detailed above, one should consider the use of (small band) low-pass a filter with a time constant sufficiently small to pass the slow component of the fault, but large enough to eliminate the high frequency components (noise and other nonlinearities).

3.6.2.1 Zero-Determinant: Problem Solution

Let us emphasize the solution added to this method to overcome the problems when reconstruction faults $\hat{f}_i(t)$ for $\rho(t) = 0$. Notice that, when this is true, $\det(E(\rho)) = 0$ and, thus, there is no inverse $E^{-1}(\rho)$. In this situation, a feedback of past values of the loss of effectiveness is used to maintain the signal $\alpha(t)$ continuous. This is, on a discrete-time sense, when $\rho = 0$, $\alpha[k]$ is taken as $z^{-1}\alpha[k]$.

3.6.3 Disturbance Estimation

As, for this study, it is assumed that there is a known model on the type of road profile disturbance, a reduced-order state observer can be designed as on:

$$\left\{ \begin{array}{rcl} \dot{\hat{x}}(t) &=& A.\hat{x}(t) + B_1.\hat{w}(t) + B_2.u(t).\hat{\alpha} + M_x \\ \dot{\hat{w}}(t) &=& A_{mw}.\hat{w}(t) + M_w \end{array} \right\} \tag{3.86}$$

$$\left[\begin{array}{c} M_x \\ M_w \end{array} \right] = L_w.y(t) - L_w.\left[\begin{array}{cc} C & 0_{n_w} \end{array} \right].\hat{x}(t)$$

where $\hat{\alpha}$ comes from the output of the sliding-mode *FDI* scheme and L_w is an appropriate gain matrix.

Finally, we can see on figure 15 a full representation of this *LPV Sliding-Mode* Fault Estimation Observer, with details to every sub-block.

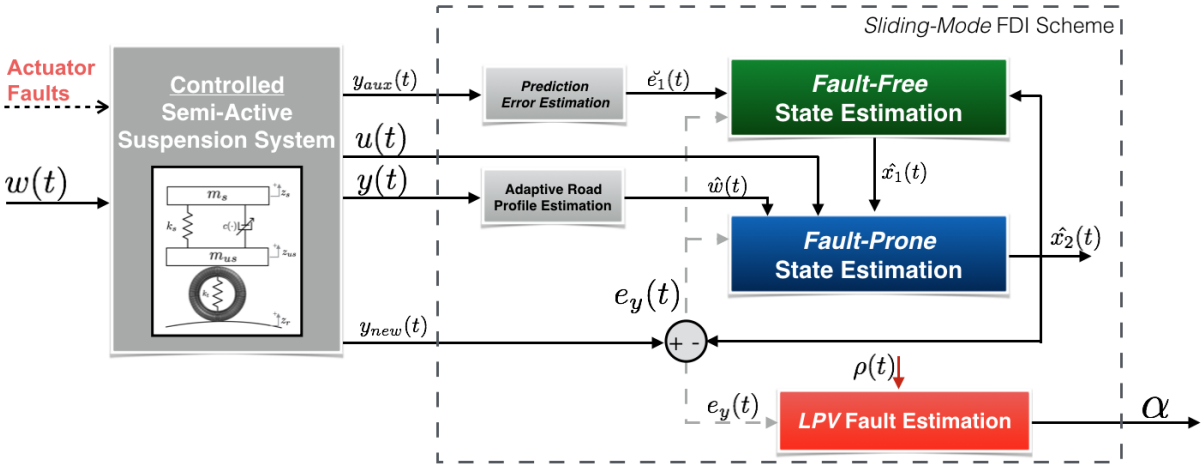

Figure 15 – *LPV* Sliding-Mode *FDI* Scheme

3.7 Simulation and Final Discussion

In this section, we will present some simulation results considering the problem of estimating actuator (loss of effectiveness) faults on a semi-active suspension system of a *Quarter of a Vehicle*, with *ER* dampers.

This simulation scenario (given road profile and control signal) is show in figure 16. The system is initially considered at the origin $x(0) = x_0 = \begin{bmatrix} 0 & 0 & 0 & 0 \end{bmatrix}^T$.

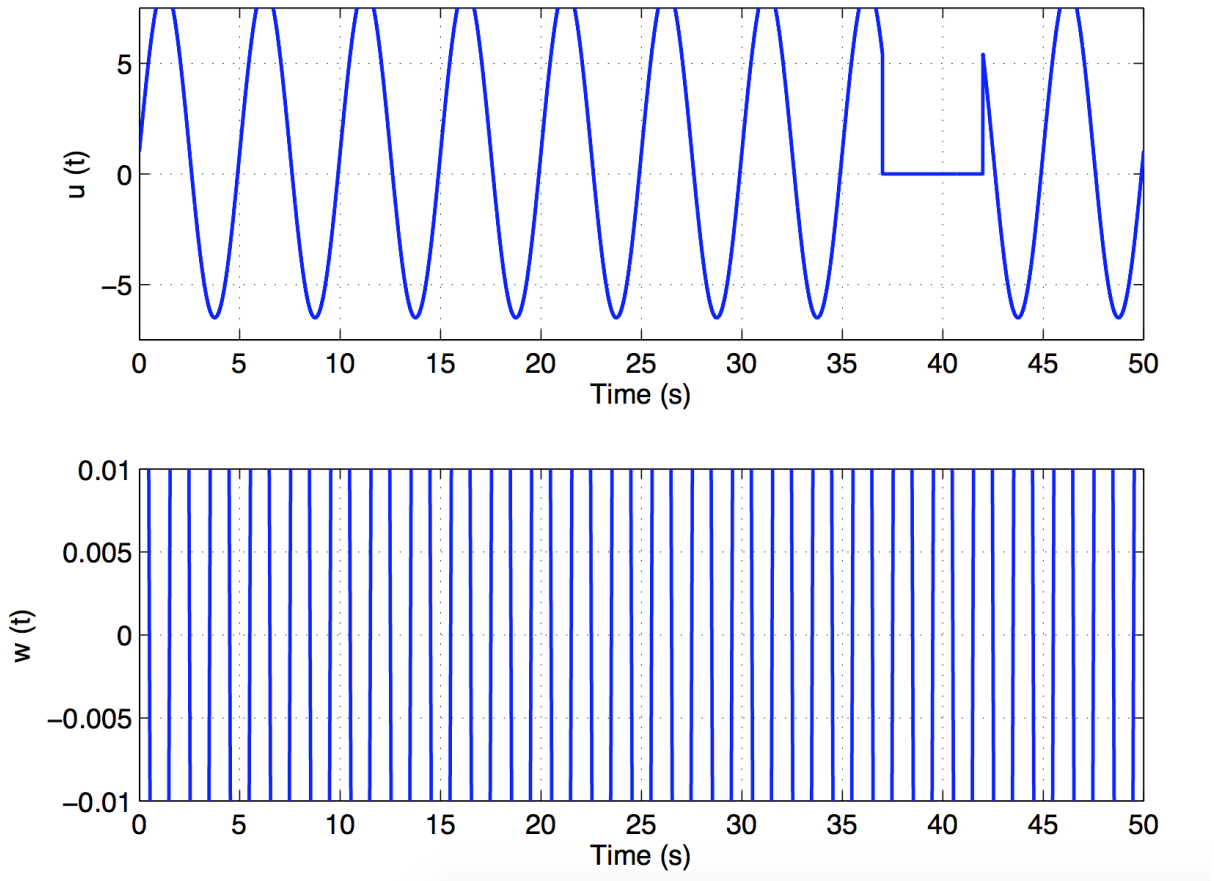

Figure 16 – Simulation Scenario

Notice that $u(t)$ is set to zero inside the time interval $t \in [37\,,\,42]$s, meaning that the *ER* damper is uncontrolled inside this interval. This allows us to analyse the switching behaviour of the studied system and observability conditions of the augmented *LPV* system (3.6).

As explained, the information used on the dynamics of the road profile disturbance $w(t)$ is considered to be provided by a road identification scheme, prior to the *FDI* structure.

In figures 17 and 18 we can find, respectively, the obtained simulation results considering each of the following fault estimation approaches: *Polytopic* and *Sliding-Mode*.

The considered loss of effectiveness factor α varies from 1 to 0.753 at $t = 13\,\text{s}$ and, then, to 0.357 at $t = 25\,\text{s}$ - which means that the effectiveness of actuator is successively lost. At $t = 37\,\text{s}$, the fault factor α returns to 1, which is, obviously, hypothetical.

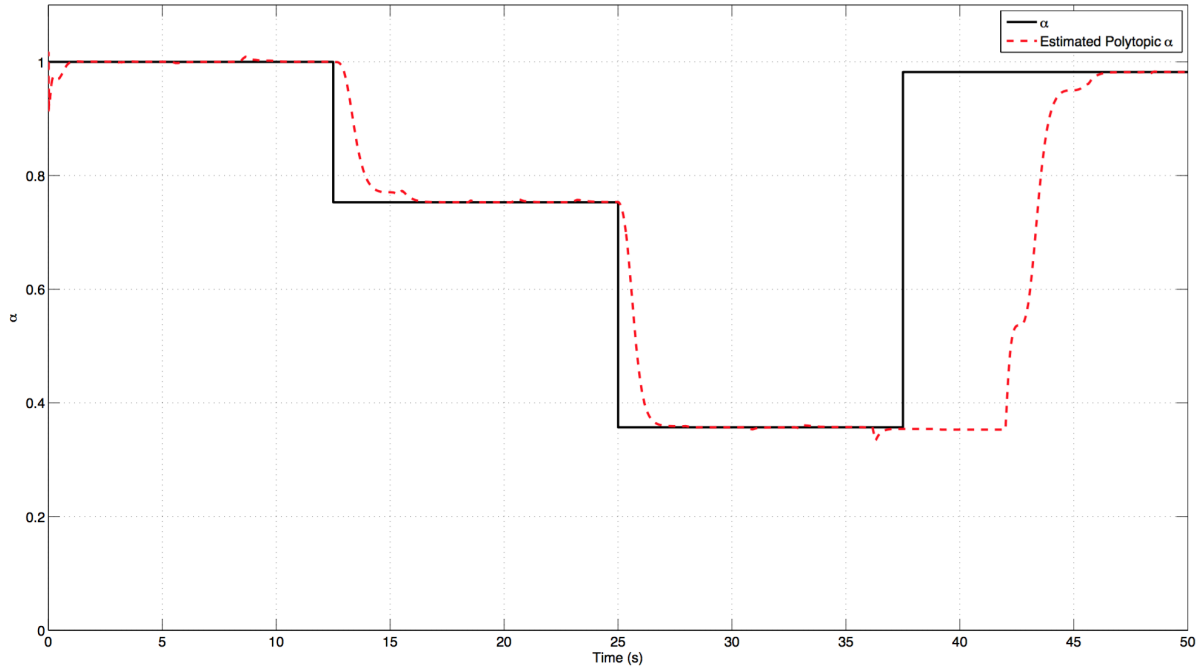

Figure 17 – Fault Estimation: *Polytopic LPV* Observer Approach

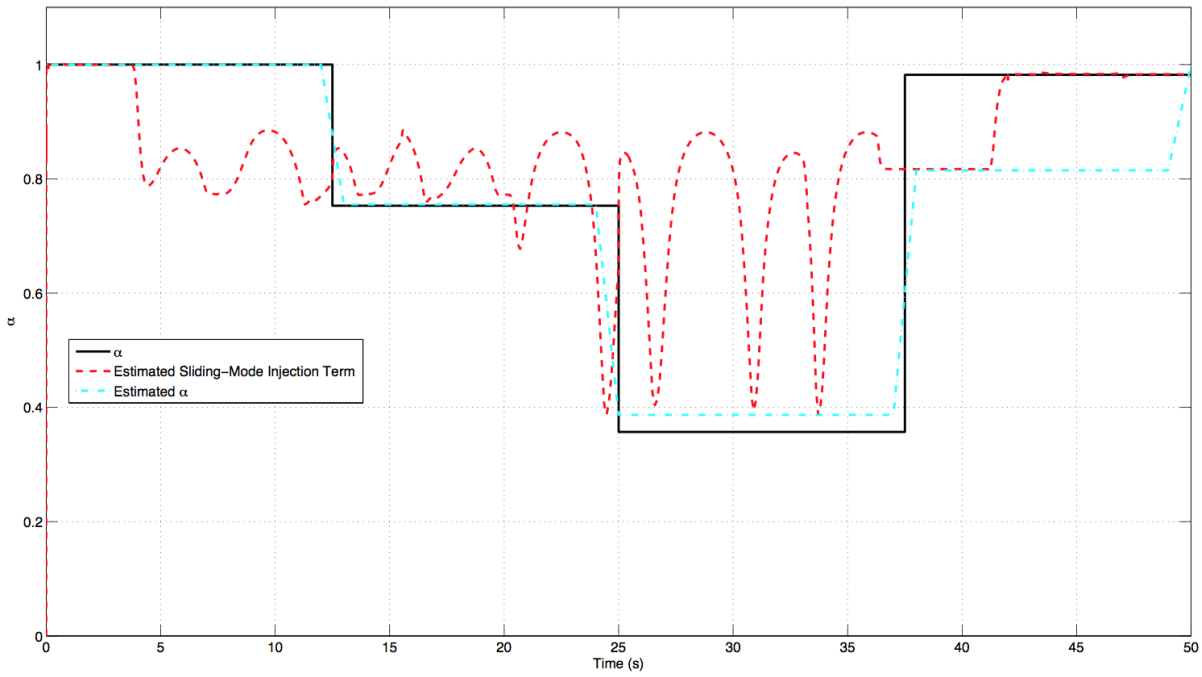

Figure 18 – Fault Estimation: *Sliding-Mode LPV* Observer Approach

Figure 17 shows that the proposed polytopic approach accurately estimates the faults (loss of effectiveness) on the semi-active suspension actuators (dampers) for whenever $u(t) \neq 0$. Likewise, in figure 18, we see that the sliding-mode approach gives an estimated $\hat{\alpha}$ that follows the main trend of $\alpha(t)$, but its estimation error $(\alpha - \hat{\alpha})$ is much bigger than with the polytopic approach.

3.7.1 Second Simulation Scenario

For goals of illustrations, we shall consider a second simulation scenario as well. For this scenario, we will use small sinusoidal road profile $w(t)$, that could represent a series of bumps for a vehicle running on a dry road at constant speed.

In terms of the expected damper force, which is computed with the use of equation (3.87), where $d_c(t)$ represents a manipulated PWM signal, which is taken as a series of steps to simulate changes upon the damping coefficient $c(\cdot)$. In these following simulations, the control signal (damper force) never stays at $u(t) = 0$ for any t.

$$F_{ER}(t) = \overbrace{f_c.d_c(t).\tanh(a_1.\dot{z}_{def}(t) + a_2.z_{def}(t))}^{\text{controlled}} + \underbrace{b_1.\dot{z}_{def}(t) + b_2.z_{def}(t)}_{\text{passive}} \tag{3.87}$$

It important, also, to show the values used for the damper's parameters, as of equation (3.87), seen in table 1.

Table 1 – Semi-Active *ER* Damper Parameters

Parameter	Value	Unit
f_c	6.5137	N
a_1	27.7154	s/m^2
a_2	1.3297	1/m
b_1	-19.8951	$N.s/m^2$
b_2	37.2670	N/m

The simulated vehicular suspension system is initially considered close to its origin (this is, $x(0) \neq 0$), and the initial conditions on $w(t)$ are also non-null. The suspension damper is initially fault-less ($\alpha = 1$). An additive (high-frequency) measurement noise is added on each measured output $y(t)$, in order to better represent a real situation.

As explained, the information used on the dynamics of each road profile disturbance $w(t)$ is considered to be provided by a road identification scheme, prior to the proposed Fault Detection and Identification structure. For the following simulation results, the disturbance model A_{mw} is different than the disturbance's dynamic behaviour, to induce a modelling error and to check if this error is overlapped by the robustness of the H_2 extended observer approach. This modelling error is detailed on equation (3.88).

$$\begin{aligned} A_{mw}^{\text{real}} &= \begin{bmatrix} 0 & -2.4674 \\ 4 & 0 \end{bmatrix} \\ A_{mw}^{\text{used}} &= \begin{bmatrix} 0 & -2.5 \\ 3 & 0 \end{bmatrix} \end{aligned} \tag{3.88}$$

For the these simulation results, we consider a sequence of steps as the loss of effectiveness fault. This can represent, for instance, a successive oil leakage scenario. At $t = 13\,\text{s}$, α decreases to 0.735. This is done once again at $t = 25\,\text{s}$, when the loss of effectiveness fault α decreases to 0.375. Finally, at $t = 37\,\text{s}$, α decreases to 0.275. The estimation $\hat{\alpha}$ is seen in figure 19, in comparison with the actual value of α.

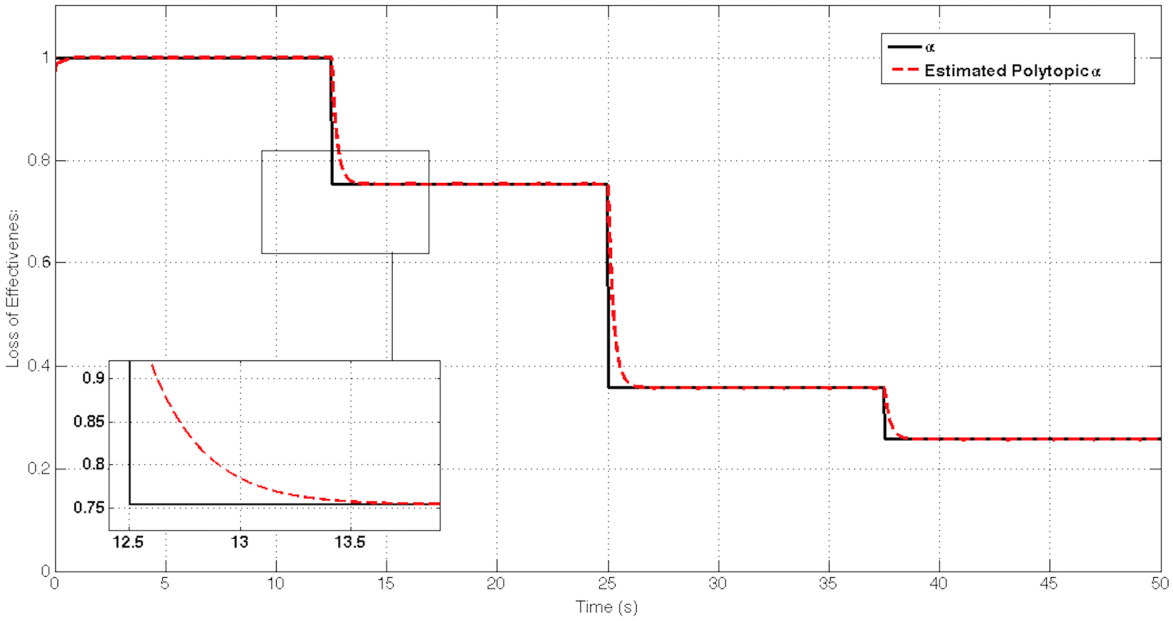

Figure 19 – Simulation of Fault Estimation: Sequence of Steps

In figure 20, we see the used data for road profile, PWM signal and expected (fault-less) damper force $u(t) = F_{ER}(t)$, according to the measured outputs $y(t)$.

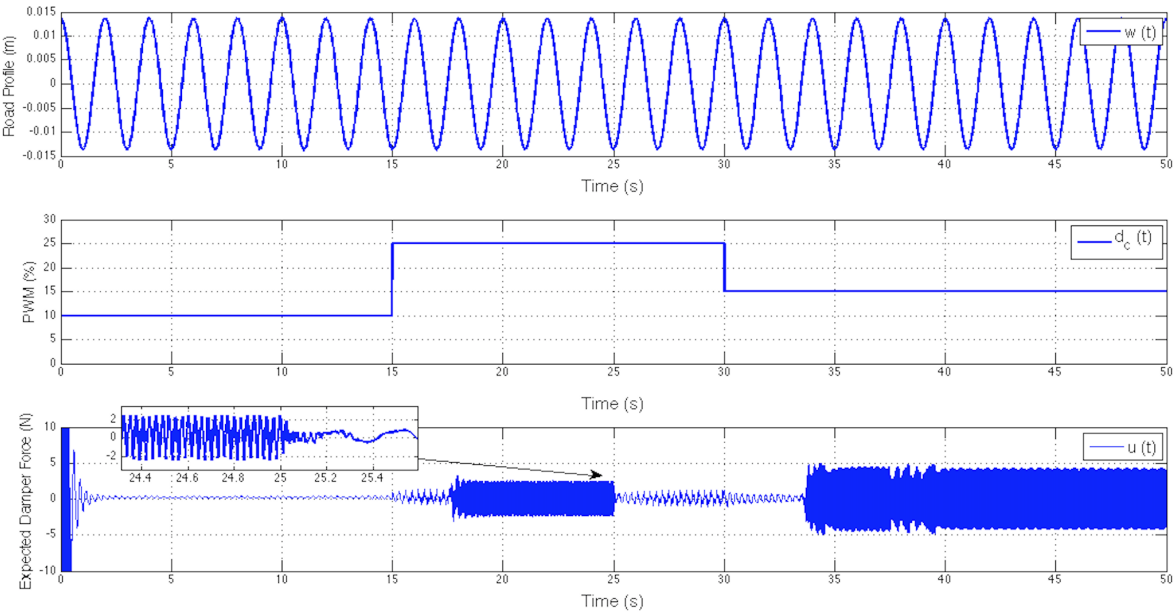

Figure 20 – Simulation Scenario

For another simulation result, we shall consider that the loss of effectiveness fault upon the damper's actuation is constantly decreasing, as a ramp. This can represent that the electro-rheological fluid inside the damper chamber is continuously loss. At $t = 17\,\mathrm{s}$, α

starts to slowly decrease to 0.5. The estimation of $\hat{\alpha}$ is seen in figure 21, in comparison with the actual value of α. The same road profile and *PWM* signal are used for this simulation.

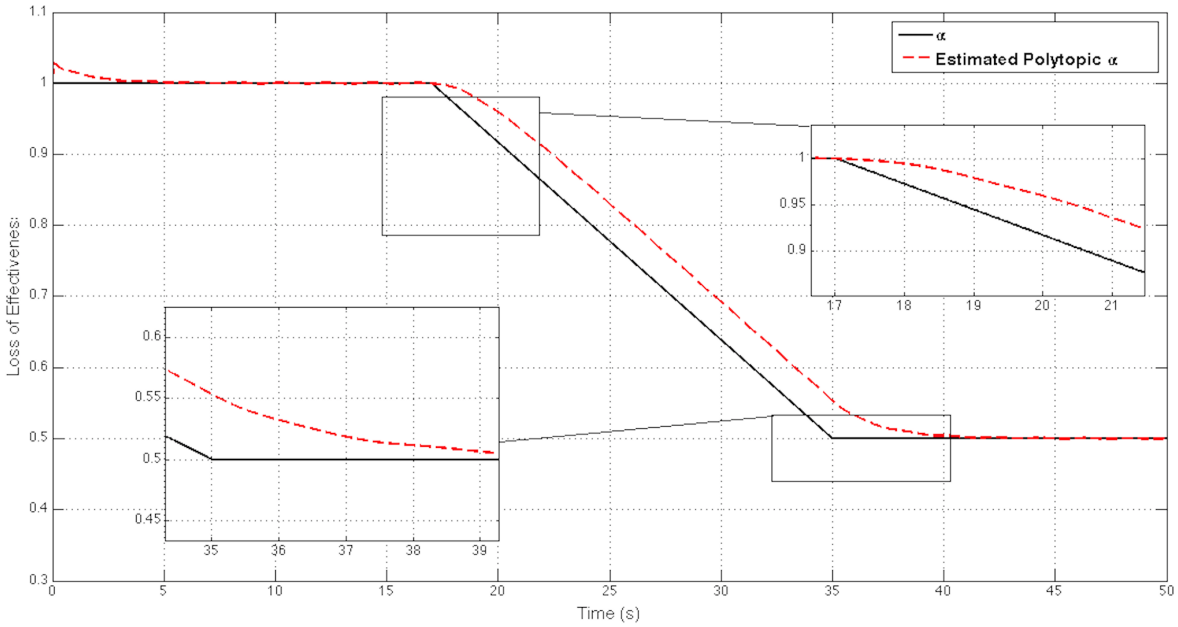

Figure 21 – Simulation of Fault Estimation: Ramp

Finally, we shall herein compare the proposed *polytopic LPV FDD* scheme to a Sliding-Mode fault reconstruction approach, as proposed by [68].

For this, we shall take a simple single-step scenario, wherein the loss of effectiveness fault α decreases at $t = 25\,\mathrm{s}$ to 0.85. The estimation of $\hat{\alpha}$ by both approaches is seen in figure 22, in comparison with the actual value of α.

Remark 2. In real applications, a fault would not be so harsh (step), but actually a decreasing exponential curve. Nonetheless, simulations with step-like faults are sufficient to prove accuracy of estimation.

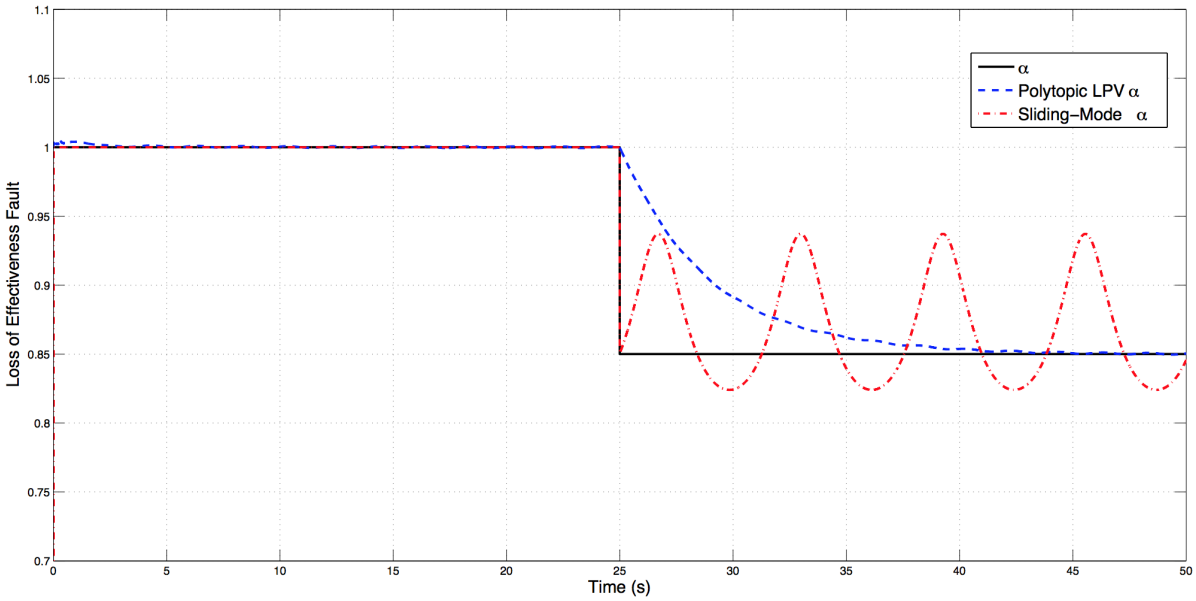

Figure 22 – Simulation of Fault Estimation: Comparison to *Sliding-Mode* Approach

As seen in the presented simulation results, the proposed *Polytopic LPV* approach presents some accurate and smooth results on estimating damper loss of effectiveness faults.

In comparison with the discussed *sliding-mode* fault reconstruction approach, which is very common in literature, as seen in [54], [69] and [70], the proposed *Polytopic LPV* scheme presented more efficient and accurate results.

In terms of simulation, this is very satisfactory, for the accurateness of the approach proposed by this article is very strong and it is, also, much simpler and less complex than a sliding-mode approach (or even a parity-space residue analysis approach).

3.7.2 Experimental Validation

Now, in order to throughly validate the proposed approach for damper fault identification, we shall present some experimental testing. This is of most importance as it is a proof of the efficiency, reliability and feasibility of the proposed fault detection method.

For this, a real test-bench is used for the application of this method. This testbed is the *INOVE Soben-Car* experimental platform that allows dealing with several configurations and use cases (see full details on [6]). Figure 23 shows the outline of this test-bench.

Figure 23 – *INOVE Soben-Car* Test-Bench

On this plant, the Semi-Active suspension system involves four Electro-Rheological (ER) dampers which have a force range of $\pm 50\,\mathrm{N}$. These dampers are adjusted using a controlled voltage inside the range of $[0\,,\,5]\,\mathrm{kV}$, generated by amplifier modules. The control input for these modules are PWM signals at $25\,\mathrm{kHz}$. On terms of capturing the vehicle's behaviour, this testbed is equipped with a wide variety of sensors, like the available measured outputs (y). Once again, remark that the deflection velocity measurement is computed thanks to the use of a derivative-filter, as explained beforehand.

On table 2, we see the numerical values for each of the parameters of this vehicle testbed, where the indexes ij represent the vehicle's front/rear - left/right corners ($i = (f, r)$ and $j = (l, r)$).

Let us, then, describe the considered experimental validation scenario:

The used road profile (considering a full vehicle plant and its four suspension systems) is the scenario of a vehicle running at $120\,\mathrm{km/h}$ in a straight line on a dry road, when it encounters a sequence of $10\,\mathrm{mm}$ sinusoidal bumps. This road profile, considering the front-left corner, is seen on figure 24. The information on this disturbance model A_{mw} is considered accurate, although there exists some modelling error because, at this testbed, the actual road profile is slightly different than the desired road due to an internal motor control system.

The measured system outputs for this validation scenario are seen in figure 25. Real measurements are $z_{def}(t)$ and $\ddot{z}_s(t)$, whereas $\dot{z}_{def}(t)$ was computed numerically. Obviously, measurement noises are already present, due to (physical) instrumentation constraints of the used test-bench.

For the detailed validation purposes, the loss of effectiveness faults were virtually set upon the actuators. To mimic a loss of effectiveness fault on the dampers of this

Table 2 – Vehicle Model Parameters: *INOVE Soben-car*

Parameter	Value	Unit
total m_s	9.08	kg
$m_{us_{fl}}$	0.32	kg
$m_{us_{fr}}$	0.32	kg
$m_{us_{rl}}$	0.485	kg
$m_{us_{rr}}$	0.485	kg
$k_{t_{fl}}$	18097.60	N/m
$k_{t_{fr}}$	18097.60	N/m
$k_{t_{rl}}$	20819.40	N/m
$k_{t_{rr}}$	20819.40	N/m
k_{fl}	1396	N/m
k_{fr}	1396	N/m
k_{rl}	1396	N/m
k_{rr}	1396	N/m
$c_{nom_{fl}}$	71.3645	N.s/m
$c_{nom_{fr}}$	71.3645	N.s/m
$c_{nom_{rl}}$	71.3645	N.s/m
$c_{nom_{rr}}$	71.3645	N.s/m

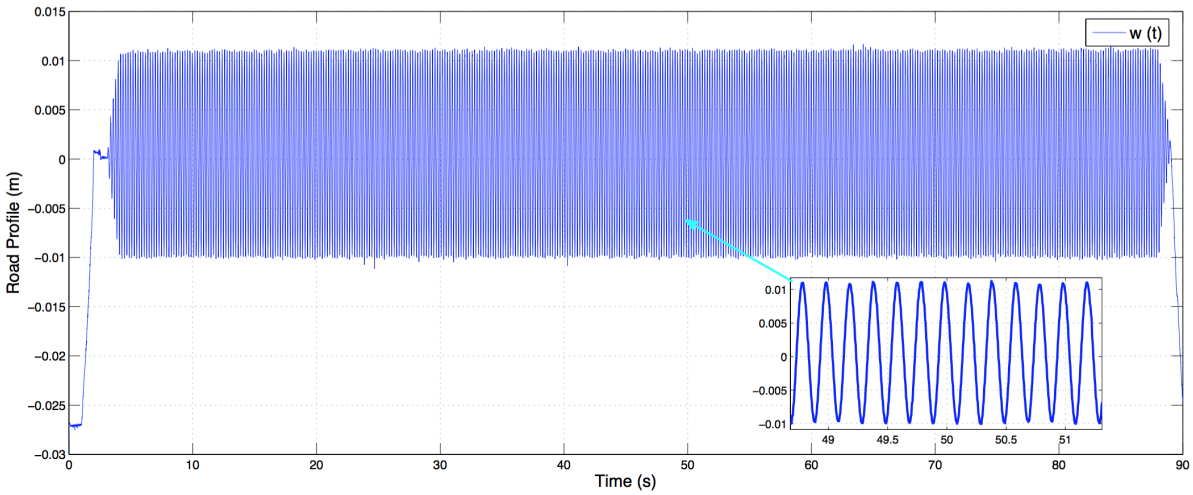

Figure 24 – Experimental Validation Scenario: Road Profile

experimental testbed, the *PWM* signal is multiplied by $\kappa(t)$, so that the actual damper force is given by $\alpha.u(t)$. The variation of the *PWM* signal is seen in figure 26. In terms of the desired (mimicked) loss of effectiveness fault α, it is considered as a single decreasing step at $t = 45\,\text{s}$, decreasing to 0.5.

As well in figure in figure 26, we can see the expected (faultless) damper force compared with the real (faulty) damper fault. The expected damper force is computed with the use of equation (3.87) taking a constant *PWM* signal at 30 %, whereas the actual damper force comes from a force sensor present on the used vehicle test-bench.

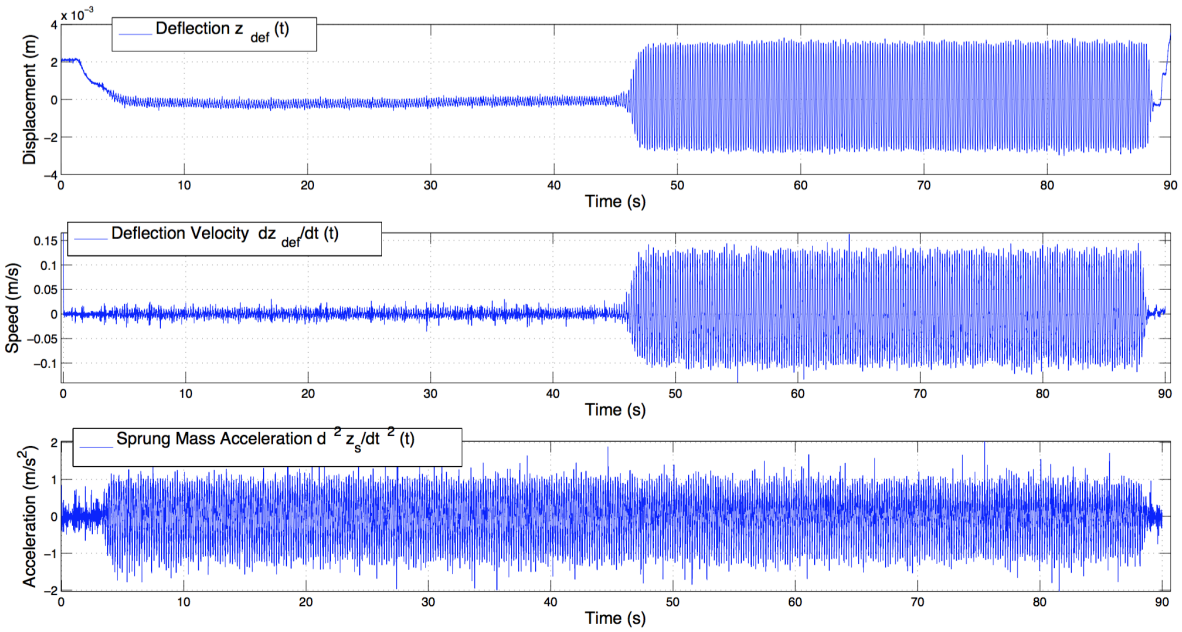

Figure 25 – Experimental Validation Scenario: Measured Outputs

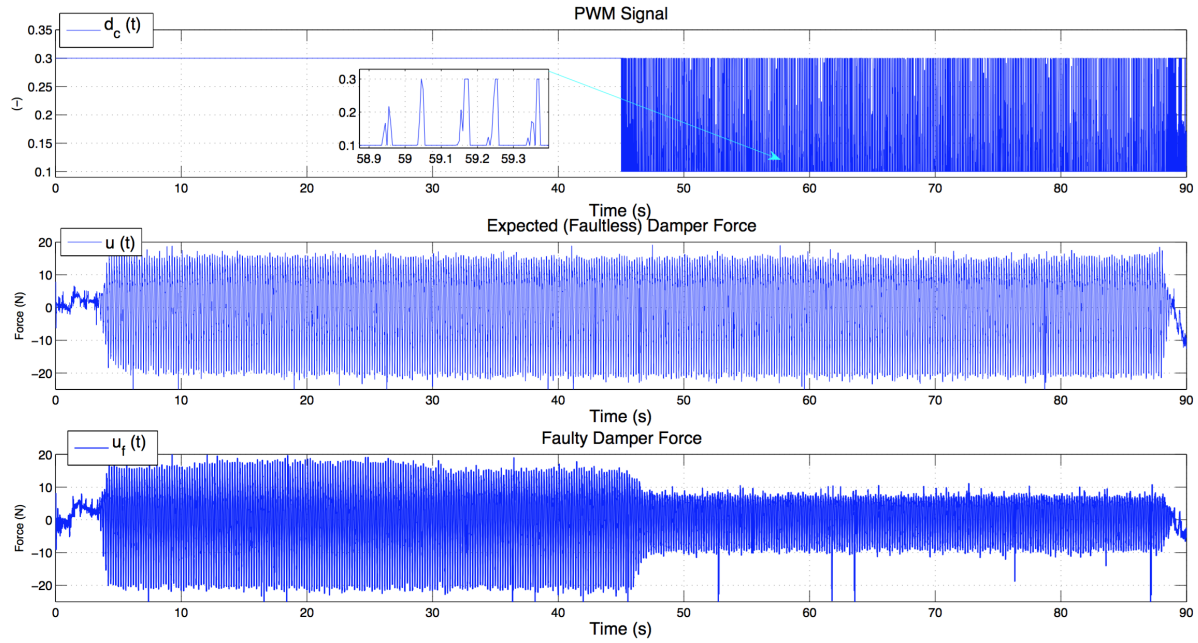

Figure 26 – Experimental Validation Scenario: *PWM* Signal

Finally and most importantly, in figure 27, we see the detection of the loss of effectiveness fault factor α and its respectively (virtually set) real value. This proofs the worthiness of the *FDI* approach proposed in this paper and how it can be efficiently used for the identification of faults on real dampers of automotive suspension systems. The accurateness on experimental validation is, obviously, not as strong as on simulation, due

to physical instrumentation constraints, nonlinearities and noise. On the other hand, the approach is **sufficient** and **strong** to detect faults on dampers, which is the goal of this article.

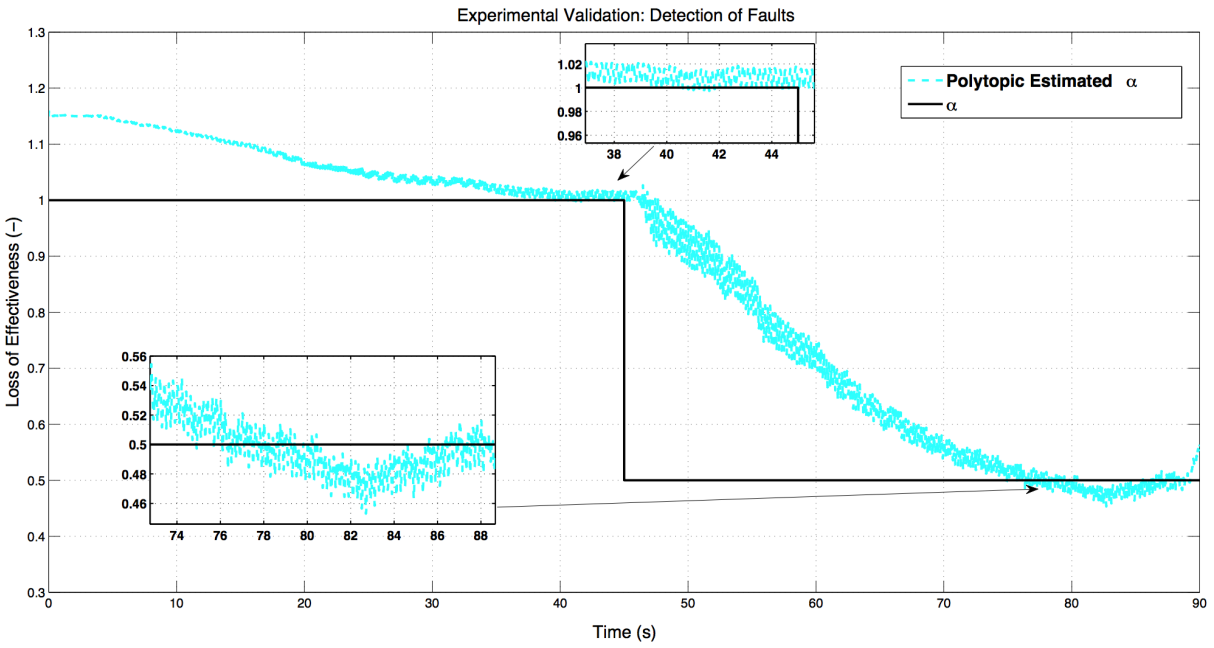

Figure 27 – Experimental Validation: Damper Loss of Effectiveness Detection

3.7.3 Analysis and Discussion

As we could see all these two approaches were able to partially detect the loss of effectiveness on the damper actuator (α), although a discussion should be made on when each approach is more appropriate.

3.7.3.1 Uncontrolled Damper Situation

Both *sliding-mode* and *polytopic LPV FDI* approaches give an inaccurate estimation of $\hat{\alpha}$ whenever $u = 0$. The *switched LPV* approach, on the other hand, might prove itself to better compute $\hat{\alpha}$ for this kind of situation.

This is no necessarily a problem on detection the loss of effectiveness, for it is not logical to detect the loss of effectiveness of an actuator when there is no actuation. This means that the Electro-Rheological damper of the suspension system is uncontrolled (thus, passive). In a purely mathematical sense, not taking into account the actual system (QoV), the *switched LPV* should be considered.

The switched approach is not yet shown herein, for its goals is mostly to provide tools to guarantee an overall continuity of detection. This approach will be dealt with in

future works, depicting the proposed theorem and its application to a range of numerical examples.

3.7.3.2 Complexity of Observers

In terms of implementation complexity, it is important to remark that the *sliding-mode* approach is far more complex than the other two: it consists of several steps of filtering and relies on the use of the sliding-mode term, which is highly nonlinear and must be implemented with a certain amount of precision so that the results converge to what is expected. In terms of simulation, this approach need an overly small relative tolerance error on integrating solvers.

It is also important to remark that this approach need information $\dot{z_{def}}(t)$ and $\dot{z_{us}}(t)$. This signals are not usually measured on vehicle systems and have to be retrieved through the use of filtered derivatives upon $z_{def}(t)$ and $z_{us}(t)$, which might increase noisy behaviour and worsten results on the estimation of α.

Regarding the polytopic approach, it only needs the *offline* computation of the $L(\cdot)$ matrix and, so, requires small implementation complexity.

3.7.3.3 On the use of Derivative-Filters

Not of least importance, one has still to remark that this studied consider the use of two measurements ($\dot{z_{def}}(t)$ and $\dot{z_{us}}(t)$). These signals are acquired through the use of derivative-filters, in order to estimate the derivative and reject high-frequency noise. As the average bandwidth of these signals are known, these derivative filter could be designed as exposes the (*Laplace*-domain) equation (3.89), for each variable z_j with bandwidth w_{z_j}.

$$F_{z_j}(s) = \frac{s}{(\frac{3}{1.3w_{z_j}}.s + 1)^3} \tag{3.89}$$

3.7.3.4 Overall Analysis

Finally, after a carefull inspection of the results presented on figures 17 to 18, we can claim that, for the studied problem and purpose (considering the QoV model, the sliding-mode observer approach, as proposed in [54], is not as efficient as purely LPV approaches.

The extended version of *polytopic* LPV observer design proved itself a much more natural and straightforward extension of almost-LTI control tools to the nonlinear observation problem, as in [47] and [49]. The proposed *switched* LPV approach presented tools of analysis to guarantee detectability of α, assuming that the control signal stays null for a given maximal period.

The choice between these two approaches should be made considering each studied application. For this study, for instance, the simpler *polytopic LPV FDI* is already sufficient, given the discussion uncontrolled damper situation, for $u(t) = 0$.

3.8 Conclusions

This chapter presented the issue of detecting and identifying actuator faults with three different LPV strategies. As showed by some simulation results, these strategies are able to collect information on actuator faults, considering the problem of a *Quarter of Vehicle* model with a semi-active suspension system and a faulty ER damper. A discussion is made on which approach should be taken for different situations.

4 Design of a *Real-Time* Model Predictive Control Scheme for Semi-Active Suspension Control of a Full Vehicle

4.1 About Chapter

The previous chapter dealt with *Fault Detection* problems on *actuators*. Now, in this chapter, let us consider the problem of controlling the semi-active dampers.

The main problem here is to handle the dissipativity constraints of this semi-active dampers. These constraints can be cast as actuator saturation conditions. From this, our control design problem is resumed by handling actuator and state contraints with fast computation.

This chapter is focused on solving the *Real-Time* application of an *MPC* controller scheme for the control of a full car model with semi-active suspension system, with possibility of implementation on the *Soben* testbed.

This is a continuation of the theoretical formulation presented in [5] and referenced as future works in [71].

4.1.1 Abstract

This chapter presents a control structure, based on Model Predictive Control, for the **Real-Time** control of a semi-active suspension system of a full vehicle, equipped with four Electro-Rheological dampers. This control scheme considers a full linear vehicle model of 14 states and a state-plus-disturbance estimator based on a H_2 filtering approach. The proposed control algorithm should provide a suitable trade-off between comfort and handling performances of the vehicle in a very short sampling period ($T_s = 5\,\text{ms}$), for the implementation in a real vehicle test-bench. The control structure is tested and compared to other standard fast control approaches. Results show the overall good behaviour of this control scheme.

Keywords: Model Predictive Control; *LPV* Control; Real Time Control; Sub-optimal Optimization; Vehicle System; Semi-Active Suspensions.

4.2 Introduction

In order to enhance a vehicle's driving performance in terms of road handling and ride comfort, one should take special care with the vehicle's suspension system. Evermore present in the automotive industry, *Semi-Active* suspension systems are to be highlighted, being efficient and, at the same time, less energy-consuming and less expensive than purely active suspensions.

The use of semi-active suspension systems seems to provide a good trade-off between costs and performance requirements. This type of suspension is present on new *state-of-the-art top*-cars and a good deal of academic and industrial research is focused on this topic, as seen in [55], [56] and others. Further details on semi-active suspension systems are throughly discussed in [14], [13] and [12].

The main challenge faced by semi-active suspension control problems is how to handle the dissipativity constraints of these dampers. Several control design problems have been worked on with a range of different approaches. In [72], and more recently in [73] and [74], we can find an extensive review of semi-active suspension control approaches. Some of the most recent and modern control techniques have been applied for this kind of problem. In [75], it is proposed an LQ-based clipped optimal control; a H_2 control approach is presented in [76]; LPV control approaches, dealing with the dissipativity constraints of these suspension systems, are given in [53], [77] and [78].

Nevertheless, the most natural approach towards optimal control of processes subject to constraints is Model Predictive Control (MPC), as throughly detailed in [79]. MPC allows to explicitly consider the effect of input and state constraints in the control design process. As the studied system does have an actuator saturation problem, MPC presents itself as a plausible and elegant control solution.

Some works have employed a MPC approach for semi-active suspension systems, although most of these studies only consider a simpler *quarter-car* vehicle model. In [80], a *fast MPC* scheme is designed for a *half-car* vehicle, where the controller is tuned based on a *quarter-car* suspension model and does not take into account the effect of future disturbances. In [81], a methodology is proposed for optimal semi-active suspension control, based on MPC, considering a *quarter-car* vehicle model and previously-measured road disturbances. However, the *quarter-car* model is not sufficient to describe the dynamics of a full vehicle with four semi-active dampers. The idea of solving the control problem at each corner of the car (four separate controllers) might seem persuading and simple enough, but the effects of coupling and load transfer distribution between corners may not be handled, which should lead to degraded performance, as seen on [71].

Throughout literature, only a few studies have considered multivariable MPC semi-active control techniques considering the full car dynamics. On [82], a nonlinear

programming solution approach to this problem is proposed, considering an approximate description of constraints. A practical implementation of this approach might be not be suitable.

On the other hand, in [71], a full vehicle semi-active suspension *MPC* control is formulated and solved using Mixed Integer constraints and optimization, where simulation results show the interest of this control approach. The same author presents a more detailed version on [5], where we can see that **practical implementation** on a vehicle testbed is not yet satisfied, since the computational time of the *MPC* is greater than the nominal sampling periods. It is a known fact that the computation requirements of predictive controllers (*MPC*) is usually high, due to an optimization problem which has to be solved **online**, at every sampling period.

Thus, in this work, a **practical implementation** of a semi-active suspension *MPC* controller for a full vehicle testbed with 4 semi-active dampers is proposed. The designed control scheme includes a feedback *LPV* **Fast** *MPC* controller with an H_2 extended state observer for system states and future road disturbances. This chapter contains several contributions:

- A H_2 noise-attenuation extended state observer solution is presented as to estimate system states and predict future road disturbances. Notice that the performance of *MPC* controllers are improved with the use of accurate future disturbance information (as seen in a class of applications, in [83] and [84]);
- A Clipped Analytical *MPC* suspension controller is presented, obtained by the analytical solution of quadratic function;
- A Feedback *LPV MPC* suspension control is presented by solving a quadratic minimization problem with polyhedral constraints, with explicit mathematical methods, in a sufficient computational time (for a possible *real-time* application);
- Theoretical formulation, simulation results and observer validation are presented with details, showing the interest of the proposed control approach. Comparisons are made with other simpler control approaches.

The structure of this chapter is given as follows: section 4.3 describes the full vertical vehicle model with 4 semi-active suspensions and the problem to be solved; section 4.4 shows the first theoretical results with the computation of an extended H_2 state observer to estimate future disturbances and system states; section 4.5 presents the *MPC* controller for the semi-active suspension problem; in section 4.6, the practical implementation, on a vehicle testbed, of this *LPV MPC* approach is described; finally, results are presented and discussed in section 4.7 and conclusions are drawn in section 4.8.

4.3 Full Car Model

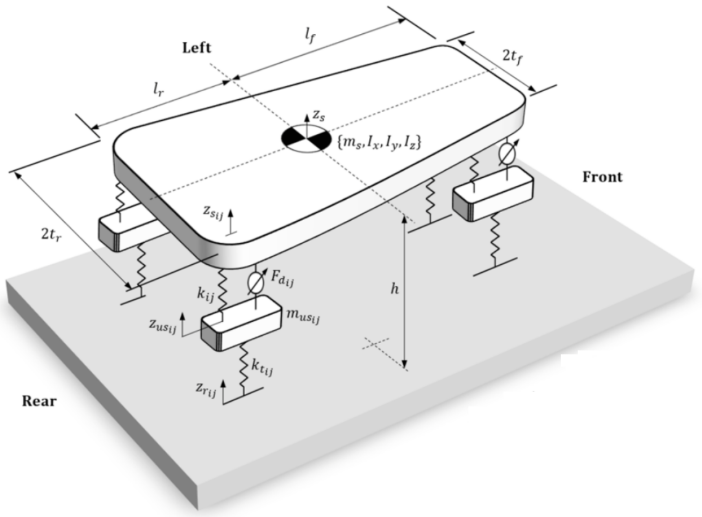

Figure 28 – Full Vehicle Model with 4 Semi-Active Suspensions

Let us, firstly, present the dynamical model of a vehicle's vertical behaviour. This is a classic 7 degrees of freedom suspension model, as seen in figure 28 and referred to in [85], and will be used for analysis and control purposes. This model involves the chassis dynamics (vertical displacement (z_s), roll angle (θ) and pitch angle (ϕ)) and the vertical displacements of the wheels ($z_{us_{ij}}$) at the front/rear - left/right corners ($i = (f, r)$ and $j = (l, r)$). This described $7 - DOF$ model is governed by the following equations:

$$\begin{aligned} m_s.\ddot{z}_s &= -F_{sfl} - F_{sfr} - F_{srl} - F_{srr} \\ I_x.\ddot{\theta} &= (-F_{sfr} + F_{sfl}).t_f + (F_{srl} - F_{srr}).t_r \\ I_y.\ddot{\phi} &= (F_{srr} + F_{srl}).l_r - (F_{sfr} + F_{sfl}).l_f \\ m_{us_{ij}}.\ddot{z}_{us_{ij}} &= F_{s_{ij}} - F_{tz_{ij}} \end{aligned} \tag{4.1}$$

where I_x and I_y represent the moments of inertia of the sprung mass around the longitudinal and lateral axis, respectively, h represents the height of the center of gravity (COG). l_f,l_r,t_f and t_r are the COG-front, rear, left and right distances, respectively.

In terms of the forces, $F_{tz_{ij}}$ depicts the vertical tire forces, given by:

$$F_{tz_{ij}} = k_{t_{ij}}.(z_{us_{ij}} - z_{r_{ij}}) \tag{4.2}$$

where $k_{t_{ij}}$ represent the stiffness coefficients of the tires and $z_{r_{ij}}$ are the road profile disturbances that the vehicle is subject to.

Each vertical suspension forces (for each of the 4 corners of the vehicle) is represented by $F_{s_{ij}}$ and, in this study, will be modeled by a spring and a damper with linear and

nonlinear characteristics, respectively. This is:

$$F_{s_{ij}} = k_{ij}.(z_{s_{ij}} - z_{us_{ij}}) + F_{d_{ij}} \tag{4.3}$$

where k_{ij} representes the nominal spring stiffness coefficient and $F_{d_{ij}}$ the semi-active controlled damper force. This damper force is given by (4.4), where $c_{ij}(\cdot)$ represents controlled damping coefficient. The dissipativity constraints of each semi-active damper are given in (4.5). To facilitate our control purposes (in order to exclude nonlinearities), we shall consider the damper forces as given by (4.6), where u_{ij} is an incremental force (used as control input) and $c_{nom_{ij}} = \frac{(c_{max_{ij}} + c_{min_{ij}})}{2}$ is the nominal damping coefficient. Then, the suspension force given in equation (4.3) can be finally re-written as (4.7).

$$F_{d_{ij}} = c_{ij}(\cdot).(\dot{z}_{s_{ij}} - \dot{z}_{us_{ij}}) \tag{4.4}$$

$$0 \leq c_{min_{ij}} \leq c_{ij}(\cdot) \leq c_{max_{ij}} \tag{4.5}$$

$$F_{d_{ij}} = c_{nom_{ij}}.(\dot{z}_{s_{ij}} - \dot{z}_{us_{ij}}) + u_{ij} \tag{4.6}$$

$$F_{s_{ij}} = k_{ij}.(z_{s_{ij}} - z_{us_{ij}}) + c_{nom_{ij}}.(\dot{z}_{s_{ij}} - \dot{z}_{us_{ij}}) + u_{ij} \tag{4.7}$$

The position (and, thus velocities) of each sprung mass at each corner of the vehicle ($z_{s_{ij}}$) is derived from the vehicle equations of motion, and considering the roll and pitch angles as small enough, they become linearized as in:

$$\begin{aligned} z_{s_{fl}} &= z_s - l_f.(\phi) + t_f.(\theta) \\ z_{s_{fr}} &= z_s - l_f.(\phi) - t_f.(\theta) \\ z_{s_{rl}} &= z_s + l_r.(\phi) + t_r.(\theta) \\ z_{s_{rr}} &= z_s + l_r.(\phi) - t_r.(\theta) \end{aligned} \tag{4.8}$$

4.3.1 State-Space Representation

One obtains the following state-space representation of this Full Car model, when injecting (4.2) and (4.7) into (4.1), this is:

$$\sum_{FullVeh.} := \left\{ \begin{array}{rcccccc} \dot{x}(t) & = & A.x(t) & + & B_1.w(t) & + & B_2.u(t) \\ y(t) & = & C.x(t) & + & D_1.w(t) & + & D_2.u(t) \end{array} \right\} \tag{4.9}$$

where the system states are given by (4.10), the control inputs are given by (4.11), the unmeasured (disturbances) are given by (4.12) and, finally, the measured outputs are given

in equation (4.13). Remark: A, B_1, B_2, C, D_1 and D_2 are constant matrices

$$x = \begin{bmatrix} z_s & \theta & \phi & z_{us_{fl}} & z_{us_{fr}} & z_{us_{rl}} & z_{us_{rr}} & \dot{z}_s & \dot{\theta} & \dot{\phi} & \dot{z}_{us_{fl}} & \dot{z}_{us_{fr}} & \dot{z}_{us_{rl}} & \dot{z}_{us_{rr}} \end{bmatrix}^T \tag{4.10}$$

$$u = \begin{bmatrix} u_{fl} & u_{fr} & u_{rl} & u_{rr} \end{bmatrix}^T \tag{4.11}$$

$$w = \begin{bmatrix} z_{r_{fl}} & z_{r_{fr}} & z_{r_{rl}} & z_{r_{rr}} \end{bmatrix}^T \tag{4.12}$$

$$y = \begin{bmatrix} \ddot{z}_{s_{fl}} & \ddot{z}_{s_{fr}} & \ddot{z}_{s_{rl}} & \ddot{z}_{s_{rr}} & z_{us_{fl}} & z_{us_{fr}} & z_{us_{rl}} & z_{us_{rr}} \end{bmatrix}^T \tag{4.13}$$

As this work considers a model predictive control approach, an optimization problem must be solved at each sampling period (T_s). For this, the continuous-time model (4.9) will be treated as discrete-time, as in (4.14), considering a discretization at the sampling frequency of $f_s = 200\,\text{Hz}$ (which is the testbed's fixed rate, further explained in section 4.6 of this chapter). Note that the matrices A_d, ..., D_{2d} are constant.

$$\sum_{Full\,Veh.}^{T_s} := \left\{ \begin{array}{rcl} x[k+1] & = & A_d.x[k] + B_{1d}.w[k] + B_{2d}.u[k] \\ y[k] & = & C_d.x[k] + D_{1d}.w[k] + D_{2d}.u[k] \end{array} \right\} \tag{4.14}$$

4.3.2 Input Constraints

Let us, now, depict with more details the dissipativity conditions of the semi-active suspension systems, as given in equation (4.5) - the damper force constraints. As we shall consider an *MPC* approach, these conditions have to be put as state, input or output constraints (upon x, u or y). From (4.5-4.6), considering $z_{def_{ij}} = z_{s_{ij}} - z_{us_{ij}}$ and multiplying each (4.5) by $z_{def_{ij}}$, we have that:

$$\begin{array}{lll} c_{min_{ij}}.\dot{z}_{def_{ij}} \le c_{nom_{ij}}\dot{z}_{def_{ij}} + u_{ij} \le c_{max_{ij}}\dot{z}_{def_{ij}} & \text{if} & \dot{z}_{def_{ij}} \ge 0 \\ c_{max_{ij}}.\dot{z}_{def_{ij}} \le c_{nom_{ij}}\dot{z}_{def_{ij}} + u_{ij} \le c_{min_{ij}}\dot{z}_{def_{ij}} & \text{if} & \dot{z}_{def_{ij}} < 0 \end{array} \tag{4.15}$$

From this, since $c_{nom_{ij}} = \frac{(c_{max_{ij}} + c_{min_{ij}})}{2}$, we must guarantee that: $|u_{ij}| \le \frac{(c_{max_{ij}} - c_{min_{ij}})}{2}.|\dot{z}_{def_{ij}}|$. Equivalently, we can express the dissipativity constraints as linear inequalities between the control inputs u_{ij} and the state variables x, this is:

$$\begin{array}{lll} \text{if} \quad C_{in}.x[k] \ge 0\,, & \text{then} & \left\{ \begin{array}{rcl} u_{ij}[k] & \ge & \frac{(c_{min_{ij}} - c_{max_{ij}})}{2}.C_{in}.x[k] \\ u_{ij}[k] & < & \frac{(c_{max_{ij}} - c_{min_{ij}})}{2}.C_{in}.x[k] \end{array} \right\} \\ \text{if} \quad C_{in}.x[k] < 0\,, & \text{then} & \left\{ \begin{array}{rcl} u_{ij}[k] & \ge & \frac{(c_{max_{ij}} - c_{min_{ij}})}{2}.C_{in}.x[k] \\ u_{ij}[k] & < & \frac{(c_{min_{ij}} - c_{max_{ij}})}{2}.C_{in}.x[k] \end{array} \right\} \end{array} \tag{4.16}$$

where $\dot{z}_{def_{ij}} = \dot{z}_{s_{ij}} - \dot{z}_{us_{ij}} = C_{in}.x$, taking C_{in} as the appropriate matrix for this linear combination of states. This representation of the damper force constraints is given in [71], where a Mixed Integer approach is taken.

4.4 Extended H_2 State Observer

To ensure the feasibility and accuracy of the control objectives, it is of great importance to present the used observer design methodology. The observer design has to take two goals into account: estimate the system's states $x[k]$ and disturbances $w[k]$ and predict the future disturbances $w[k+n]$ and states $x[k+n]$. Future disturbance estimation is well known to improve *MPC* performances.

In order to satisfy these design goals, we must firstly consider a disturbance model. As exploited and discussed thoroughly in [86] and [87], and as the system model (4.14) has no integrating modes (considering input/output dynamics), we can improve the control perfomances by taking a simple constant model. This is, we consider:

$$w[k+n] \;=\; w[k] \quad \text{for} \quad n = 1 \ldots N_p \tag{4.17}$$

where N_p stands for the prediction horizon.

Remark: Differently from [82], this method does not add any complexity in terms of sensors (no need for cameras or added structures to our plant).If some prior knowledge of the road profile is available, a more accurate model can be computed, as seen in [75], but, for this study, it will be considered that there is no information on the type of road profile.

So, we can consider an augmented state-space representation of the system, as follows:

$$\sum_{Aug.Sys.}^{T_s} := \left\{ \begin{array}{rcl} \begin{bmatrix} x[k+1] \\ w[k+1] \end{bmatrix} & = & \overbrace{\begin{bmatrix} A_d & B_{1d} \\ 0 & \mathbb{I} \end{bmatrix}}^{A_{obs}} . \begin{bmatrix} x[k] \\ w[k] \end{bmatrix} + \overbrace{\begin{bmatrix} B_{2d} \\ 0 \end{bmatrix}}^{B_{obs}} . u[k] \\ y[k] & = & \underbrace{\begin{bmatrix} C_d & D_{1d} \end{bmatrix}}_{C_{obs}} . \begin{bmatrix} x[k] \\ w[k] \end{bmatrix} + D_{2d} . u[k] \end{array} \right\} \tag{4.18}$$

Let us also consider the presence of a measurement noise (ν) upon the measured outputs y. This is:

$$y[k] \;=\; \begin{bmatrix} C_d & D_{1d} \end{bmatrix} . \begin{bmatrix} x[k] \\ w[k] \end{bmatrix} + D_{2d} . u[k] + F_u \nu[k] \tag{4.19}$$

This being defined, we can, then, design an observer to estimate the extended states with the following structure:

$$\left\{ \begin{array}{rcl} \begin{bmatrix} \hat{x}[k+1] \\ \hat{w}[k+1] \end{bmatrix} & = & A_{obs} . \begin{bmatrix} \hat{x}[k] \\ \hat{w}[k] \end{bmatrix} + B_{obs} . u[k] + L(y[k] - \hat{y}[k]) \\ \hat{y}[k] & = & C_{obs} . \begin{bmatrix} \hat{x}[k] \\ \hat{w}[k] \end{bmatrix} + D_{2d} . u[k] \end{array} \right\} \tag{4.20}$$

where $L \in \mathbb{R}^{18\times 8}$ is the observer matrix gain to be defined.

To compute this gain, we will consider an H_2 observer with pole placement definition, as seen in [23]. This is an appropriate method to design the observer, for the H_2 norm of a system, from a stochastic point-of-view, is equal to the square root of the asymptotic variance of the output when the input is a white noise, see proof in [22].

4.4.1 Problem Definition:

The (discrete-time) H_2 observer problem (detailed in [23]), is, then, to minimize γ in (4.21), taking into account that (4.22) and (4.23) are true, where $T_{e\nu}(z)$ being the transfer function that represents the effects of $\nu(z)$ upon $e(z) = \begin{bmatrix} x(z) \\ w(z) \end{bmatrix} - \begin{bmatrix} \hat{z}(s) \\ \hat{w}(z) \end{bmatrix}$. Therefore, the observer design consists in computing the gain L so that the transfer function (z-domain) from the measurement noise $\nu[k]$ to the estimation error $e[k]$ meets the H_2-norm upper bond constraints.

In order to improve the convergence performances of the observer, we shall consider that the poles of the computed observer are placed inside a parameterized region $\mathcal{C}(\mu, \varrho)$ (circle centered at μ with radius ϱ), smaller than the unit circle (being fast enough for the problem).

$$\|T_{e\nu}(z)\|_2 \leq \gamma \quad \text{under} \quad e[k=0] = 0 \tag{4.21}$$

$$\lim_{k\to\infty} e[k] \to 0 \quad \text{for} \quad \nu[k] \equiv 0 \tag{4.22}$$

$$e[k+1] = (A_{obs} - L.C_{obs}).e[k] - L.F_u\nu[k] \tag{4.23}$$

4.4.2 Problem Solution

Following [23], the problem is rewritten in terms of Linear Matrix Inequalities. Considering that there is one measurement noise for every measured output ($F_u = \mathbb{I}_8$ and $\nu \in \mathbb{R}^8$), the solution to this problem consists in **minimizing** γ, if and only if there exists two positive definite symmetric matrices P and R and a matrix Y so that the following inequalities hold:

$$\begin{bmatrix} P & P(\frac{A_{obs}-\mu.\mathbb{I}}{\varrho}) - Y.\frac{C_{obs}}{\varrho} & -Y \\ \star & P & 0 \\ \star & \star & \mathbb{I} \end{bmatrix} > 0,$$
$$\begin{bmatrix} R & \mathbb{I} & 0 \\ \star & P & 0 \\ \star & \star & \mathbb{I} \end{bmatrix} > 0, \tag{4.24}$$
$$\text{Trace}(R) < \gamma$$

From this, L is computed as $L = P^{-1}.Y$.

Numerical application of the H_2 filtering observer design: for the studied control application, the numerical computation of these LMIs yields $\gamma = 0.6602$, which leads to a good observer, considering $\varrho = 0.03$ and $\mu = 0.0067$. This poles are chosen so that the observer's errors converge very fast to zero, there is no fixed relationship between these poles and the system's CL poles. This problem's solution was obtained with the use of *Matlab* [7] and of solver *SeDuMi* [88].

Let us remark that the variance of $e[k]$ due to variations on $\nu[k]$ (white noise) can be given by $||\Delta e||_2 = ||T_{e\nu}(z)||_{H_2}.||\Delta\nu||_2$; as we know that the measurement noise has small norm, the variance caused upon the estimation error $e[k]$ is small enough for the study, as seen in the following simulation results.

Let us also remark that there is a trade-off between the convergence velocity of this H_2 observer (given by the pole placement region $\mathcal{C}(\mu, \varrho)$) and the noise-attenuation goals. To better handle this trade-off, an extra output filter is added to the estimation, in order to guarantee high-frequency noise rejection. The continuous-time transfer function of this filter is given by $W_e(s) = \frac{1}{0.001s+1}.\mathbb{I}_{18}$.

4.4.3 Experimental Validation Results

Firstly, let us present a (continuous-time) frequency analysis of $T_{e\nu}(s)$ and $W_e(s).T_{e\nu}(s)$, so we can analyse the effect of measurement noise ν upon the estimated states. Herein, the transfer function $W_e(s)$ represents the high-frequency noise filter for every state. On figure 29, we see the maximal and minimal singular values (σ decomposition) of $T_{e\nu}(s)$ and $W_e(s).T_{e\nu}(s)$. As we can see, the effect of measurement noise (in higher frequencies, over 10^4 Hz) on the (augmented states) estimation will be throughly attenuated.

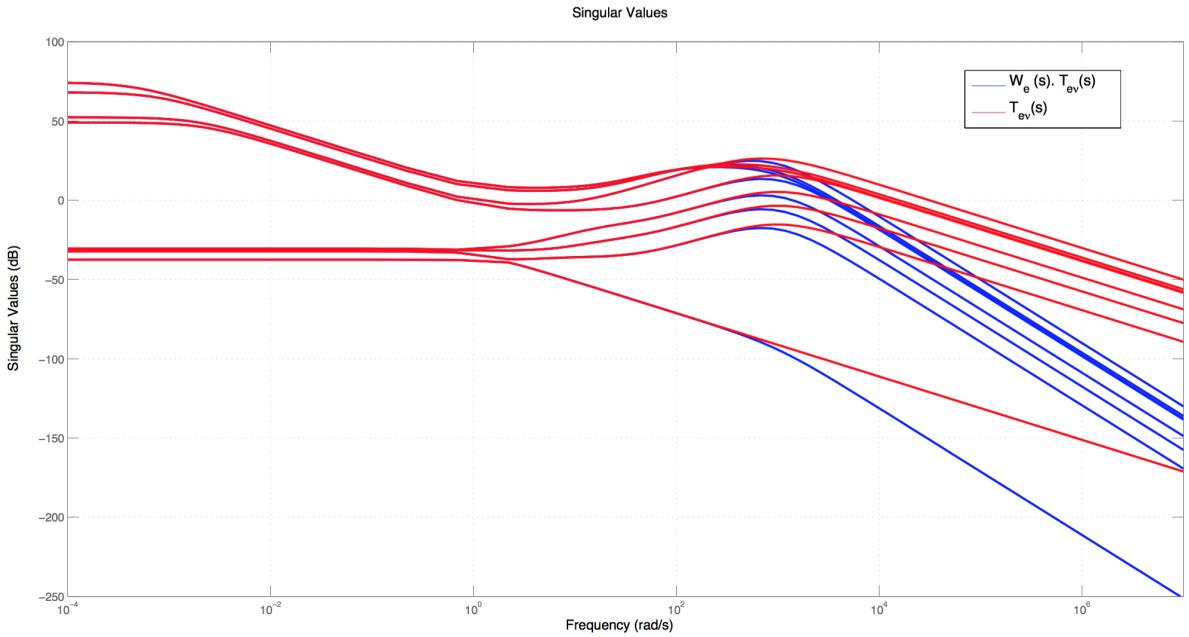

Figure 29 – Frequency σ-Plot: Noise effect on Observer

Let us now present some experimental validation results depicting states (x) and road profile (disturbances, w) estimation by the designed H_2 filtering observer.

These following results herein presented are a validation of the described H_2 observer, for they use real measurement data (y) retrieved from the *INOVE Soben-Car* mechatronic testbed (details on section 4.6), considering a sequence of bumps road profile scenario z_r. The measurement noise, naturally, is present upon each measured output (y).

On figure 30, we also see an accurate estimation of the road profile at each corner of the vehicle. The road profile estimation of the front-left corner is showed in details on figure 31. As it can be seen, the effect of the measurement noise is still present, but the main trend is followed by the estimated augmented states, which is enough from the *MPC* controller's point-of-view.

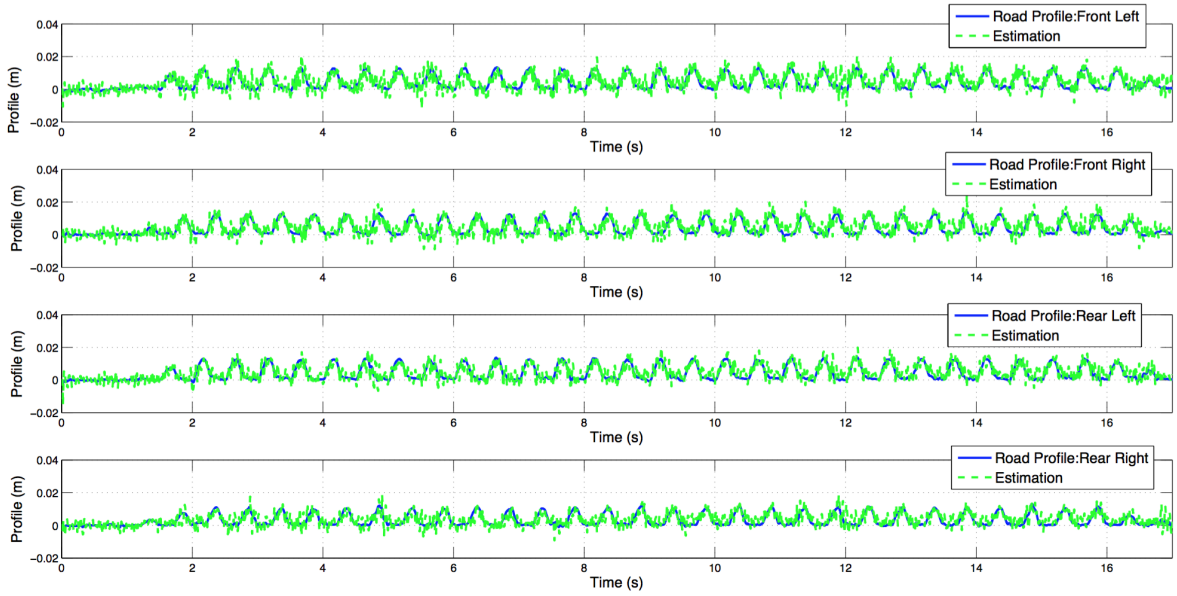

Figure 30 – Road Profile Estimation by H_2 Observer

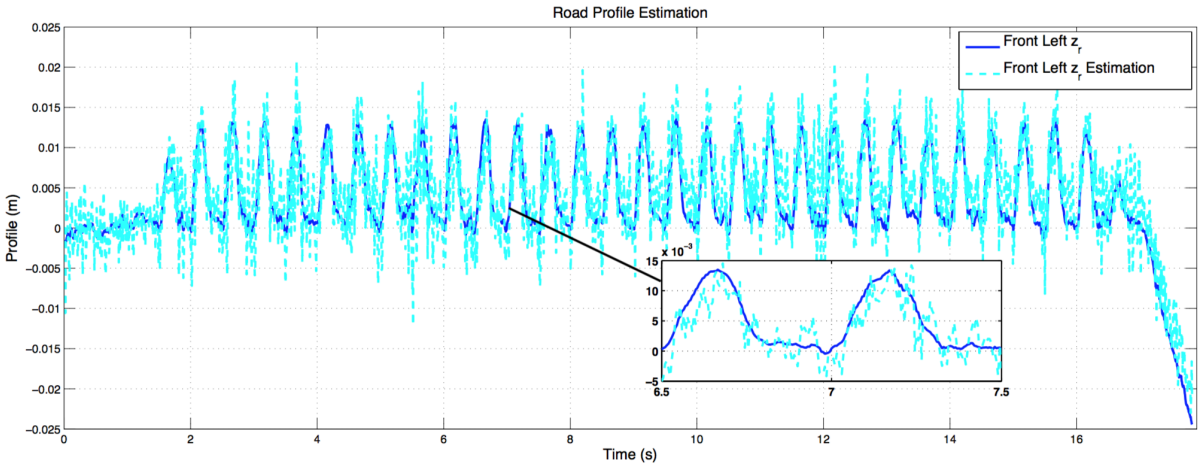

Figure 31 – Front Left Road Profile Estimation by H_2 Observer

On figure 32, we see the (sufficiently) somewhat accurate estimation of the system states (only some important states are shown). Once again, the effect of $\nu(t)$ is still present (but diminished) and the main trend is followed closely by the estimated states.

The proposed H_2 extended observer approach can serve well as to provide an *MPC* controller information on states and disturbances, as it could be seen with the presented results.

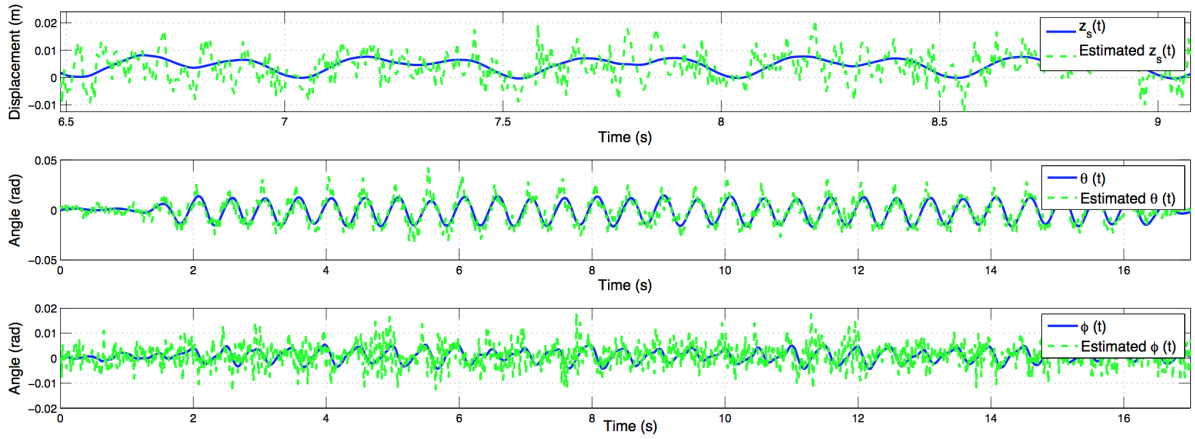

Figure 32 – System States Estimation by H_2 Observer

4.5 A Model Predictive Controller Solution for Semi-Active Suspension Control

The main control objective of this work on semi-active automotive suspensions is to isolate the body from the road disturbances, without deteriorating road handling. These two objectives can be referred to as *comfort performance* and *handling performance*, respectively, and can be described through the vehicle's *COG* acceleration (given by $\ddot{z}_s$) and roll angle (given by θ), as seen in [89].

For control design purposes, let us consider two perfomance indexes, with respect to each control objective: $J_{comfort} = \int_0^\tau \ddot{z}_s^2(t)dt$ and $J_{handling} = \int_0^\tau \theta^2(t)dt$, where τ represents a given time interval. Let us remark that it is well-known that (physically) these two objectives are conflicting. For this reason, the control method must take into account a suitable trade-off between these performance indexes, coupled with the input constraints, given by equation (4.16). We may, also, consider a possible minimization of the displacement of chassis ($z_s(t)$), for other control purposes (can help on comfort perfomance for given road profiles).

Thus, the control problem can be solved by a well-posed constrained optimization problem, formulated in a Model Predictive Control framework. The *MPC* control approach to the semi-active suspension problem consists in solving the minimization of the following cost function at every discrete-time step k in a computational time smaller than the sampling period T_s:

$$J(U, x[k], w, N_p, N_c) = \sum_{j=1}^{N_p}[\xi_1(\frac{\ddot{z}_s[k+j|k]}{\ddot{z}_s^{\max}})^2 + \xi_2(\frac{\theta[k+j|k]}{\theta^{\max}})^2] \tag{4.25}$$
$$+ \sum_{j=1}^{N_p}[\xi_3.(\frac{z_s[k+j|k]}{z_s^{\max}})^2] + \sum_{j=0}^{N_c-1} u^T[k+j|k].Q_u.u[k+j|k]$$

where N_p is the given prediction horizon, N_c is the control horizon, $u[k+j|k]$, $\ddot{z}_s[k+j|k]$, $z_s[k+j|k]$ and $\theta[k+j|k]$ denote, respectively, the control efforts, the chassis displacement, the chassis acceleration and roll angle predicted for instant $k+j$ at instant k, using the prediction model (4.14) and considering the initial states $x[k]$ and disturbance information w, and $U = \begin{bmatrix} u[k|k] & u[k+1|k] & \dots & u[k+N_p-1|k] \end{bmatrix}^T$ represents the vector of control efforts inside the prediction horizon (to be optimized). Q_u is a weighting matrix, ξ_3 is a weighting scalar and ξ_1 and ξ_2 are adequately tuned weighting coefficients that influence the trade-off between handling and comfort performances.

Remarks: for this application to be scale-wise correct, the control inputs u, z_s, $\ddot{z}_s$ and θ are normalized with the use of $z_s^{\max}$, $\ddot{z}_s^{\max}$ and $\theta^{\max}$ - this values were retrieved from experimentation on a real vehicle test-bench. For this study, we shall take $N_c = N_p$.

In regard to what is presented on section 4.4, let us remark that the information about system states used for the solution of the *MPC* problem (4.26) relies on the states estimated by the designed H_2 extended observer ($\hat{x}[k]$) and the information of future road profile disturbances ($\hat{w}$) that is considered constant throughout the prediction horizon. The computation of the estimated states and disturbances by the H_2 extended observer has to be done *before* the *MPC* computation in a fast-enough response time.

Finally, the *MPC* design can be defined as:

$$\begin{array}{ll} \min_U & J(U, \hat{x}[k], \hat{w}, N_p, N_c) \\ \text{s.t.} & \left\{ \begin{array}{c} \hat{x}[k+1] = A_d.\hat{x}[k] + B_{1d}.w + B_{2d}.u[k] \\ \text{dissipativity constraints on (4.16)} \end{array} \right\} \end{array} \tag{4.26}$$

As the usual *MPC* control approach, the problem (4.26) is solved at every iteration k and the control effort to be applied to the real system corresponds to the first entry of the minimized control effort vector U (solution to (4.26)).

In figure 33, the proposed control approach is summarized, considering the *MPC* and the H_2 observer blocs. Remark: $\nu(t)$ is the unknown measurement noise and the plant is subject to an external $w(t)$ road profile.

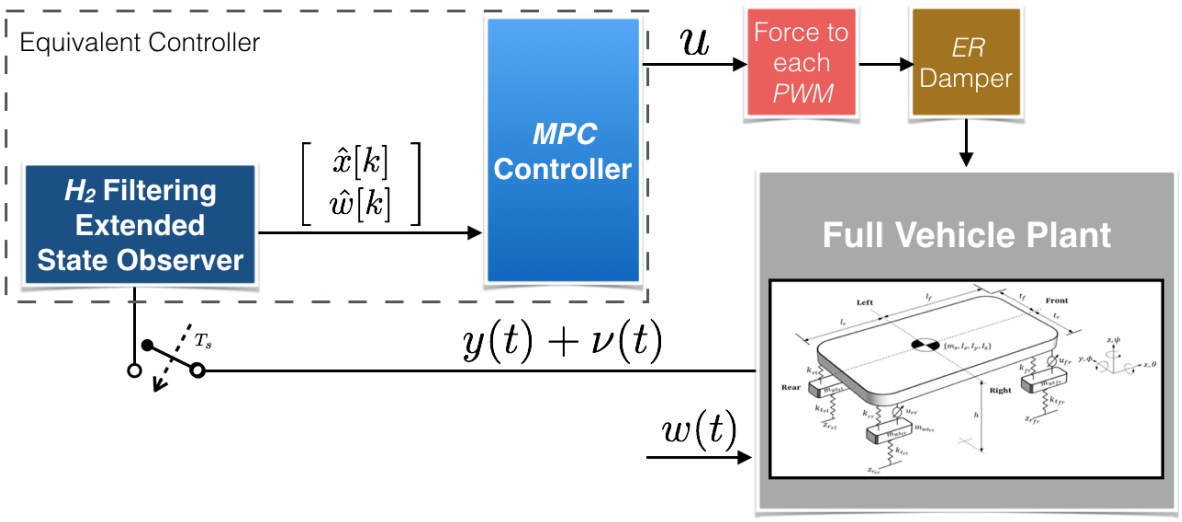

Figure 33 – Proposed Predictive Control Scheme

4.5.1 On Constraints

The computation of the *MPC* optimization problem depends heavily on the constraints. The solution to this problem as put in (4.26) must be $U \in \mathcal{U}$, where $\mathcal{U}$ is the set that represents the constrained region within which the control law is applicable to the real plant.

For the present problem, the set $\mathcal{U}$ is given by every $u[k]$ so that the dissipativity constraints on (4.16) are respected. These constraints **switch** according to the sign of $C_{in}.x[k]$. To solve this issue, the optimization problem can be formulated as a quadratic problem with logical constraints - *Mixed Integer Quadratic Programming problem*, for details see [71], [5]. A practical application is given in [90] and in others throughout literature.

4.6 Practical Implementation

The main goal of this chapter's work is the *Real-Time* implementation of a model-based predictive controller for semi-active suspension systems, as described in the previous sections.

For this, a real testbed is considered for the application of the control scheme proposed in figure 33. This testbed is the *INOVE Soben-Car* experimental platform that allows dealing with several configurations and use-cases (see full details on [6]). Figure 34 shows a picture of this testbed.

Figure 34 – *INOVE Soben-Car* Test-Bench

In table 3, we see the numerical values for each of this vehicles' parameters, considering the full vertical vehicle model presented on section 4.3.

Table 3 – Vehicle Model Parameters: *INOVE Soben-car*

Parameter	Value	Unit
m_s	9.08	kg
$m_{us_{fl}}$	0.32	kg
$m_{us_{fr}}$	0.32	kg
$m_{us_{rl}}$	0.485	kg
$m_{us_{rr}}$	0.485	kg
I_x	5	kg.m^2
I_y	2.5	kg.m^2
t_f	0.23	m
t_r	0.23	m
l_f	0.2	m
l_r	0.37	m
$k_{t_{fl}}$	12270	N/m
$k_{t_{fr}}$	12270	N/m
$k_{t_{rl}}$	12270	N/m
$k_{t_{rr}}$	12270	N/m
k_{fl}	1396	N/m
k_{fr}	1396	N/m
k_{rl}	1396	N/m
k_{rr}	1396	N/m
$c_{max_{fl}}$	111.729	N.s/m
$c_{min_{fl}}$	31	N.s/m
$c_{max_{fr}}$	111.729	N.s/m
$c_{min_{fr}}$	31	N.s/m
$c_{max_{rl}}$	111.729	N.s/m
$c_{min_{rl}}$	31	N.s/m
$c_{max_{rr}}$	111.729	N.s/m
$c_{min_{rr}}$	31	N.s/m

On this plant, the semi-active suspension system involves four Electro-Rheological (ER) dampers which have a force range of $\pm 50\,\text{N}$. These dampers are adjusted using a controlled voltage inside the range of $[0\,,\,5]\,\text{kV}$, generated by amplifier modules. The control input for these modules are PWM signals at 25 kHz. The characteristic set that represents the real nonlinear behaviour of the used semi-active dampers are seen on figure 35, where a force $vs.$ deflection speed graph is seen, for different PWM signals, as presented on [5]. These characteristics imply on the input constraints presented on equation (4.16).

In terms of capturing the vehicle's behaviour, this test-bench is equipped with a wide variety of sensors. For our study, these sensors correspond to the available measured outputs (y) as seen on equation (4.13).

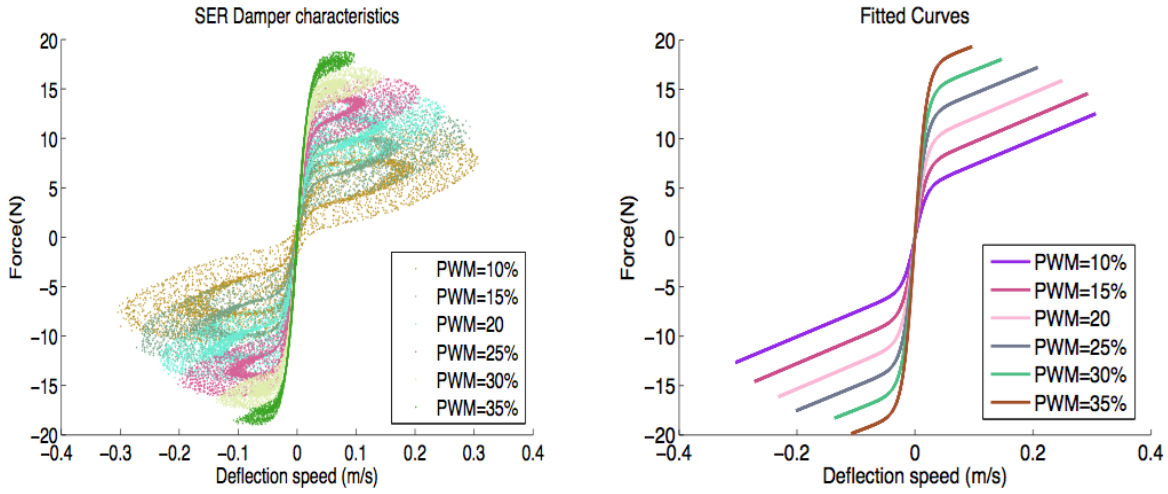

Figure 35 – Force over Speed deflection characteristics of used *ER* Semi-Active Dampers

4.6.1 Computational Time Constraints

On figure 36, we can see a representation of the closed-loop system of this testbed, that is able to interpret *Matlab* and *SimuLink* control laws, operating with a **fixed** sampling frequency of $f_s = 200\,\text{Hz}$. This condition implies that the available working time within which the proposed control scheme (*MPC* and H_2 observer) has to compute the control law is fixed (has to be **smaller** than $0.005\,\text{s}$).

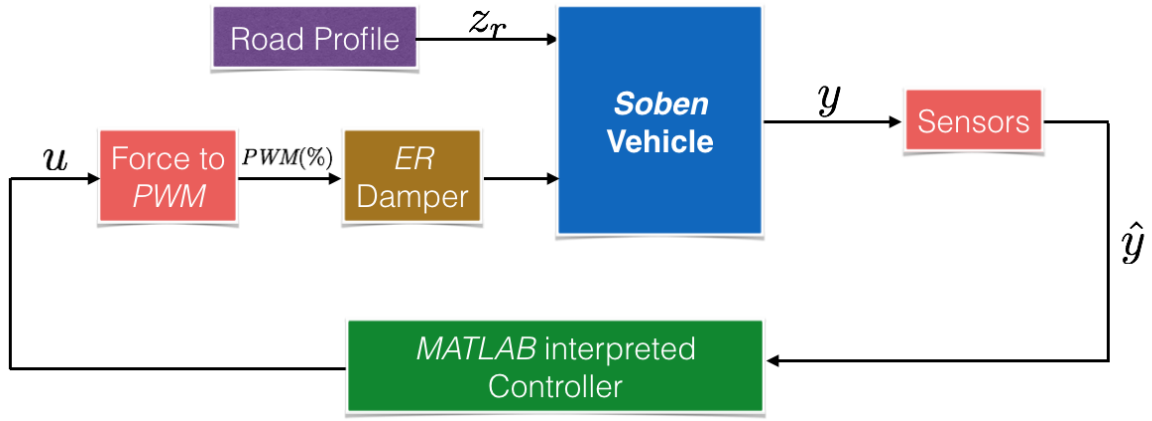

Figure 36 – Closed-Loop of *INOVE Soben-Car* Test-Bench

Through simulation, the online computation of the proposed constrained *MPC* problem was tested, with the use of *Matlab* [7] with *Yalmip* toolbox tools [91] and *Gurobi* solver [92]. The computational time, considering these softwares, is seen compared to the maximal sampling period T_s of the testbed in figure 37 and to the computational time of only the H_2 observer. An efficient discrete controller has to be able to compute the control law in

a period always smaller than the sampling time T_s. The mean computational time is around 0.0295 s and the maximal computational time is around 10 times bigger than T_s. These results come from simulation on a 2.4 GHz, 8 GB *RAM Macintosh* computer. Obviously, **faster approaches have to be considered** for this *real-time MPC* application.

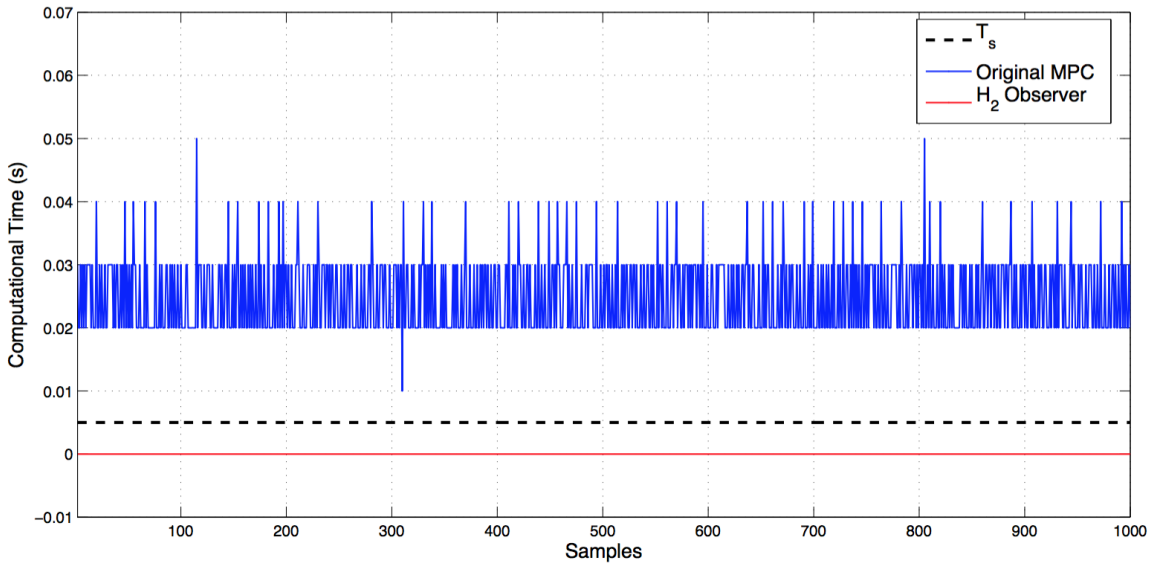

Figure 37 – Computational Time of Constrained *MPC vs* T_s

4.6.2 Faster *MPC* Approaches

4.6.2.1 Analytical Unconstrained *MPC* Approach

The first faster *MPC* approach to be tested is to consider the problem's input constraints only *after* the computation of the control law and *clip* each computed control (compare and saturate in respect to figure 35) before applying to the plant. This is an unconstrained *MPC* approach, as seen in [79], and the minimization of $J(U, x[k], w, N_p, N_c)$ can be computed analytically.

Considering an auxiliary output vector $z[k]$ as in equation (4.27), we can write:

$$z[k] = \begin{bmatrix} \ddot{z}_s[k] & z_s[k] & \theta[k] \end{bmatrix}^T \tag{4.27}$$

$$z[k] = C_z.x[k] + D_{zu}.u[k] + D_{zw}.w[k] \tag{4.28}$$

where C_z and D_z are constant matrices. From this, our cost function to be minimized (4.25) can be re-stated as:

$$J(U, x[k], w, N_p, N_c) = \sum_{j=1}^{N_p} \|z[k+j|k]\|^2_{Q_z} + \sum_{j=0}^{N_c-1} \|u[k+j|k]\|^2_{Q_u} \tag{4.29}$$

where $\|\cdot\|_M$ represents the M-weighted 2-Norm and $Q_z = \text{diag}\{\xi_1, \xi_2, \xi_3\}$.

From equation (4.28), we can evolve onto the future behaviour, considering the disturbances to remain constant during the prediction horizon:

$$Z(k|k) = \begin{bmatrix} z[k|k] & z[k+1|k] & \dots & z[k+N_p-1|k] \end{bmatrix}^T \tag{4.30}$$

$$Z(k|k) = \overbrace{\begin{bmatrix} C_z \\ C_z.A_d \\ \vdots \\ C_z.A_d^{(N_p-1)} \end{bmatrix}}^{\mathcal{A}}.x_0 + \overbrace{\begin{bmatrix} D_{zw} \\ (C_z.B_{1d} + D_{zw}) \\ \vdots \\ (C_z.(A_d^{(N_p-2)}).B_{1d} + \dots + C_z.B_{1d} + D_{zw}) \end{bmatrix}}^{\mathcal{B}_w}.w_0 + \underbrace{\begin{bmatrix} D_{zu} & 0 & \dots & \dots & 0 \\ C_z.B_{2d} & D_{zu} & 0 & \dots & 0 \\ \vdots & \vdots & \vdots & \vdots & \vdots \\ C_z.(A_d^{(N_p-2)}).B_{2d} & C_z.(A_d^{(N_p-3)}).B_{2d} & \dots & C_z.B_{2d} & D_{zu} \end{bmatrix}}_{\mathcal{B}_u}.U \tag{4.31}$$

where x_0 represents the states at given instant k, w_0 the disturbance vector at given instant k (assumed to remain constant) and U represents the future control inputs vector, as previously stated.

This formulation leads us to re-write our cost function (4.29) as quadratic in U as:

$$J(U, x_0, w_0, N_p, N_c) = \frac{1}{2}U^T.\mathcal{H}.U + x_0^T.\mathcal{F}_x.U + w_0^T.\mathcal{F}_w.U + \hat{J}_{ct} \tag{4.32}$$

where $\hat{J}_{ct}$ is a constant matrix and $\mathcal{H}$ is defined positive, posing $\mathcal{H} = 2.(\mathcal{B}_u^T Q_z \mathcal{B}_u + Q_u)$, $\mathcal{F}_x = 2.\mathcal{A}.Q_z.\mathcal{B}_u$ and $\mathcal{F}_w = 2.\mathcal{B}_w.Q_z.\mathcal{B}_u$.

In the absence of constraints, as we shall consider for the moment, the minimal value of $J(U, x_0, w_0, N_p, N_c)$ is given by $U_{min} = -\mathcal{H}^{-1}.[\mathcal{F}_x^T.x_0 + \mathcal{F}_w^T.w_0]$, which corresponds to a static *LTI* feedback control law. Given a suitable choice of Q_z and Q_u, there are guarantees of asymptotic stability of the closed-loop system.

This simplified faster *MPC* approach consists, then, on computing the feedback control at every instant k, given $\hat{x_0}$ and $\hat{w_0}$ as **estimated** by the H_2 observer, saturating (clipping) the control law inside the feasible region (as in figure 35) and applying to the plant. This is clear on the equivalent controller scheme put on figure 38.

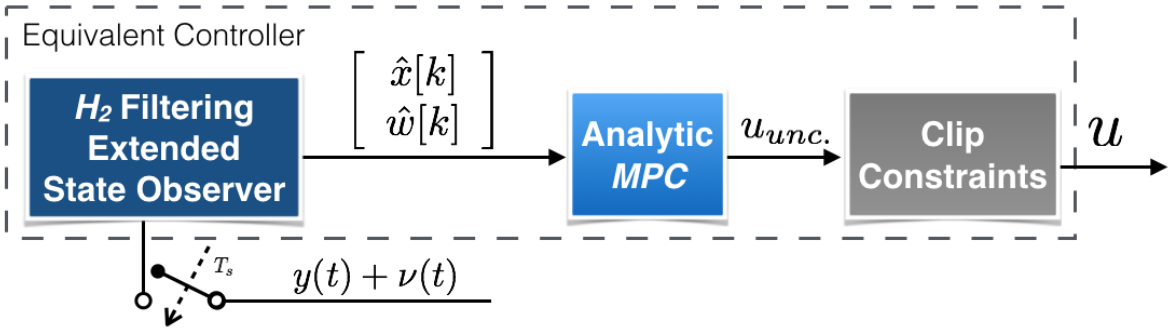

Figure 38 – Simplified Unconstrained Analytical *MPC*

A small remark has to be done: in most pratical applications, an *Anti-Windup* structure is coupled to saturation (clipping) blocks, in order to unload excessive integral action. This means that the computed unconstrained law is summed to an *anti-windup* term u_{AW} so that the control law *"gets out"* of the saturated mode. The *Anti-Windup* structure commonly considers the use of a matrix gain multiplied by the difference between the clipped law (u) and the unclipped law (u_{unc}); this is, if there was clipping action:

$$u_{AW} = K_{AW}.(u - u_{unc}) \tag{4.33}$$

4.6.2.2 Fast *MPC* Approach

Now, let us consider a **stronger** fast control approach to be implemented in *real-time* to the full vehicle testbed. This method has been introduced in [93].

Firstly, let us use the original *non linear* damper force formulation, as given in equation (4.4), instead of using the approximated linear version (4.6). This will imply that the dissipativity constraints of the semi-active suspension system will be linear inequalities on u, as in (4.5), and the use of Mixed Integer Quadratic Programming will not be needed.

The goal here in to use an *LPV* model of the system to handle the nonlinearities of the damper force (4.4). Doing so, the use of Mixed Integer Quadratic Programming is no longer needed.

Then, let us assume that u is no longer what is given in (4.11), but the actual *incremental* damping coefficients $\Delta c_{ij}[k]$, over the nominal values, as given by equation (4.34). The actual damping coefficients will be regulated by the *PWM* signal, given that

$c_{ij}[k] = c_{nom_{ij}}[k] + \Delta c_{ij}[k]$.

$$u = \begin{bmatrix} \Delta c_{fl} & \Delta c_{fr} & \Delta c_{rl} & \Delta c_{rr} \end{bmatrix}^T \tag{4.34}$$

$$\rho = \begin{bmatrix} (\dot{z_{s_{fl}}} - \dot{z}_{us_{fl}}) & (\dot{z_{s_{fr}}} - \dot{z}_{us_{fr}}) & (\dot{z_{s_{rl}}} - \dot{z}_{us_{rl}}) & (\dot{z_{s_{rr}}} - \dot{z}_{us_{rr}}) \end{bmatrix}^T \tag{4.35}$$

Then, the (discrete-time) system representation will change from what was presented in equation (4.14) to

$$\sum_{LPV\,Full\,Veh.}^{T_s} := \left\{ \begin{array}{rcl} x[k+1] & = & A_d.x[k] + B_{1d}.w[k] + B_{2d}(\rho).u[k] \\ y[k] & = & C_d.x[k] + D_{1d}.w[k] + D_{2d}(\rho).u[k] \end{array} \right\} \tag{4.36}$$

The matrices of (4.36) are not equivalent to those of (4.14), since the matrices $B_{2d}(\rho)$ and $D_{2d}(\rho)$ are, now, *LPV*. Let us remark that the difference between these two system representation models are those explained through equations (4.37)-(4.39).

$$B_{2d}^{\text{LPV}} = B_{2d}.\text{diag}\{\dot{z}_{def_{ij}}[k]\} \tag{4.37}$$

$$D_{2d}^{\text{LPV}} = D_{2d}.\text{diag}\{\dot{z}_{def_{ij}}[k]\} \tag{4.38}$$

$$\rho_{ij}[k] = \dot{z}_{def_{ij}}[k] \tag{4.39}$$

LPV systems can be understood as a range of systems well suited for the control of dynamical systems with parameter variations. These systems can be represented as an extension of *LTI* systems, assuming that the classical state-space representation matrix are dependent on **bounded** scheduling parameters ρ.

For this representation, the scheduling parameters taken are those presented on (4.35). Remark: this implicitly assumed that $(\dot{z}_{s_{ij}} - \dot{z}_{us_{ij}})$ is bounded.

Given this representation, the dissipativity constraints, combined with the *LPV* parameter assumption, imply the following (linear) problem constraints:

$$\begin{aligned} u_{min} \leq u[k] \leq u_{max} \\ x_{min} \leq x[k] \leq x_{max} \end{aligned} \tag{4.40}$$

Then, the *MPC* problem consists on minimizing (4.25), subject to (4.40) in avid time. For this, the **Fast Model Predictive Control** approach, using online optimization, first proposed in [93], can be considered. This method can evaluate a *MPC* control rule, at every sampling instant k, even for time-varying input disturbances and space-state representation matrices, which is our case (for $B_{2d}(\rho)$ and $D_{2d}(\rho)$ are time-varying, as well as $w(t)$). This method is also interesting since it has been proved to work with a system with 12 states, 3 control inputs and a horizon of 30 samples, computing the control actions in around 5 ms - the problem herein studied is of similar size.

This method (*FMPC*) greatly speeds up the computational time of the control action. It consists on exploiting the special structure of the *MPC* quadratic problem and solving the problem approximately with the use of an early terminated *primal barrier interior-point* method combined with warm-start techniques. The quality of the achieved control is very high, as demonstrated in [93]. Notice that this method only considers linear inequality constraints on control inputs and states, which, for the present control problem (using the *LPV* formulation) is sufficient.

Note also that the *FMPC* control law that will be obtained at each sampled instant k depends on the matrices $B_{2d}(\rho)$ and $D_{2d}(\rho)$ **fixed** at instant k for $\rho[k]$ (considered constant throughout the prediction horizon N_p). This is, after all, a *gain-scheduling* approach. See [94] for further reading on the stability and optimality issues of this kind of approach, and in particular on the procedure to determine bounds on the suboptimality of this *FMPC* solution.

Let us, now, detail the *FMPC* method applied to the *LPV* system (4.36); this follows [93]: in section 4.6.2.2.1, the primal barrier interior-point method is presented and its application to the quadratic problem is shown; in section 4.6.2.2.2, the infeasible start Newton method is shown, in order to deal with the quadratic problem's constraints; in section 4.6.2.2.3, the used warm start techniques are presented and, finally, in section 4.6.2.2.4, some other possible adjustments are briefly described.

4.6.2.2.1 Primal Barrier Interior-Point Method

From here on, let us consider the quadratic program as expressed in equation (4.41), where z represents an overall optimization variable given by (4.42). It is important to depict that the matrices H, P, ..., b have a special considerable structure, as exposed in [93]. Herein, N_p stands for the prediction horizon, n represents the number of states, whereas m depicts the number of control inputs.

$$\begin{aligned} &\text{minimize} && z^T H z + g^T z \\ &\text{subject to} && Pz \leq h,\ Cz = b \end{aligned} \tag{4.41}$$

$$z = (u[k], x[k+1], \ldots, u[k+N_p-1], x[k+N_p]) \in \mathbb{R}^{N_p(m+n)} \tag{4.42}$$

The primal barrier method resides, roughly speaking, on replacing the inequality constraints of (4.41) by a **barrier term**, finding, then, an approximate problem. This is put on equations (4.43)-(4.44), considering p_i^T as the rows of P. This problem is, after all, a convex optimization problem with linear equality constraints.

$$\begin{aligned} \text{minimize} \quad & z^T H z + g^T z + \kappa.\phi(z) \\ \text{subject to} \quad & Cz = b \end{aligned} \tag{4.43}$$

$$\phi(z) = \sum_{i=1}^{l.N_p+\kappa} -log(h_i - p_i^T.z) \tag{4.44}$$

A complete discussion of this approximate optimization method is discussed on [95].

4.6.2.2.2 Infeasible Start Newton Method and Fast Computation of the Newton Step

The presented *FMPC* approach resides on the primal barrier method, but as well on the infeasible start Newton method (see the book [96], Sect. 11.2.2 for a complete discussion) and fast computations of the Newton step.

Let us associate the equality constraints on z with a dual variable $\mu \in \mathbb{R}^{N_p.n}$. The conditions of optimality for our modified problem (4.43) become those seen on equation (4.45), where $\kappa P^T d$ is the gradient of $\kappa\phi(z)$ and $d_i = \frac{1}{h_i - p_i^T z}$. The residual vector r, composed by the primal residual r_p and the dual residual r_d, is to be stacked by the solver.

$$\begin{aligned} r_d = 2Hz + g + \kappa P^T d + C^T \mu = 0 \\ r_p = Cz - b = 0 \end{aligned} \tag{4.45}$$

The infeasible start Newton method consists, then, on initializing the optimization algorithm at point z_0 (given by any μ_0 such that the inequality constraints are strictly satisfied). From this point, the solution (z_{sol}, μ_{sol}) is maintained if the residuals (r) are small enough; else, the estimative solution is refined by linearizing the optimality conditions (4.45) and computing the dual and primal increments Δz and $\Delta\mu$, to be summed upon z and μ. The search for these increments is done by solving the following linear equations:

$$\begin{bmatrix} 2H + \kappa P^T \text{diag}(d)^2 P & C^T \\ C & 0 \end{bmatrix} . \begin{bmatrix} \Delta z \\ \Delta\mu \end{bmatrix} = - \begin{bmatrix} r_d \\ r_p \end{bmatrix} \tag{4.46}$$

The fast computation of the Newton step, then, resides on the following steps, considering $\Sigma = 2H + \kappa P^T \text{diag}(d)^2 P$:

- Computing the *Schur complement* (see [97]), $Y = C\Sigma^{-1}C^T$ and $\beta = -r_p + C\Sigma^{-1}r_d$ - this is done using the *Cholesky* factorization of each sub-block of Σ and forming Y by backward and forward substitution ;

- Determining $\Delta\mu$ by solving $Y\Delta\mu = -\beta$ - using, once again, the *Cholesky* factorization of Y and backward and forward substitution ;
- Finally, computing Δz by solving $\Sigma\Delta z = -r_d - C^T.\mu$ - this requires only matrices already computed in previous steps.

4.6.2.2.3 Warm Start Techniques

Let us remark that the studied *FMPC* method also uses some warm start techniques for the described approximate optimization method. The used warm start method is, simply, to use the previously computed z as the initial z_0 for the next optimization (Newton) step. Using this technique, it can be proved with self-concordance, that the total number of steps will be bounded by a polynomial function of (4.43)'s dimension.

The application of the warm start to the *MPC* algorithm is, basically, using the previous plan of control actions ($u[k]$ to $u[k+N_p-1]$), shifted in time (z^{+1}) as the starting point for the next Newton loop.

4.6.2.2.4 Other Adjustments and Comments

Some other adjustments can be used upon the Infeasible Start Newton Method coupled with Warm Start techniques and the Approximate Primal Barrier Method applied to *MPC*. These are discussed on [93] and, herein, shall be only enumerated:

- Use of a fixed parameter κ in (4.46);
- Use of a maximal iteration limit, for the Newton algorithm.

Also on [93], we can see a number of problems tested using the *FMPC* method and a *SDPT3*-based (see [98]) *MPC* solution. The *FMPC* method far outperforms the *SDPT3* solver, in terms of computational time.

4.7 Results and Analysis

Given the presented problem and the respective control approaches, in this section we shall analyze the effectiveness of these controllers with respect to the control goals, in simulation, considering the fixed sampling period of 5 ms. The used prediction horizon for all the controllers is fixed at $N_p = N_c = 10$ samples. The tuning parameters of the *fast MPC* method are given in table 5. The use of different prediction horizons was tested, whereas these values were found to be a sufficiently good trade-off between computational time and accuracy of computed control law.

On the following results, *AMPC* represents the analytical unconstrained clipped predictive controller as seen in section 4.6.2.1, whereas *FMPC* represents the stronger fast *LPV MPC* approach presented in section 4.6.2.2.

Let us, before presenting practical results, show that the computational time constraints of the problem (as exposed in section 4.6.1) are **strictly** satisfied with both analytical and fast *MPC* approaches. Through simulation, the online computation of the two proposed *MPC* approaches were tested, with the aid of software tools *Matlab* [7] and *Yalmip* toolbox [91]. Both mean computational times are seen compared to the maximal sampling period T_s of the testbed on figure 39, considering that the computational time of the H_2 observer is embedded into the controller's computational time. As it can be seen, the computational time for the control law with the analytical *MPC* and with the *fast MPC* approach are smaller than 5 ms (testbed's sampling period).

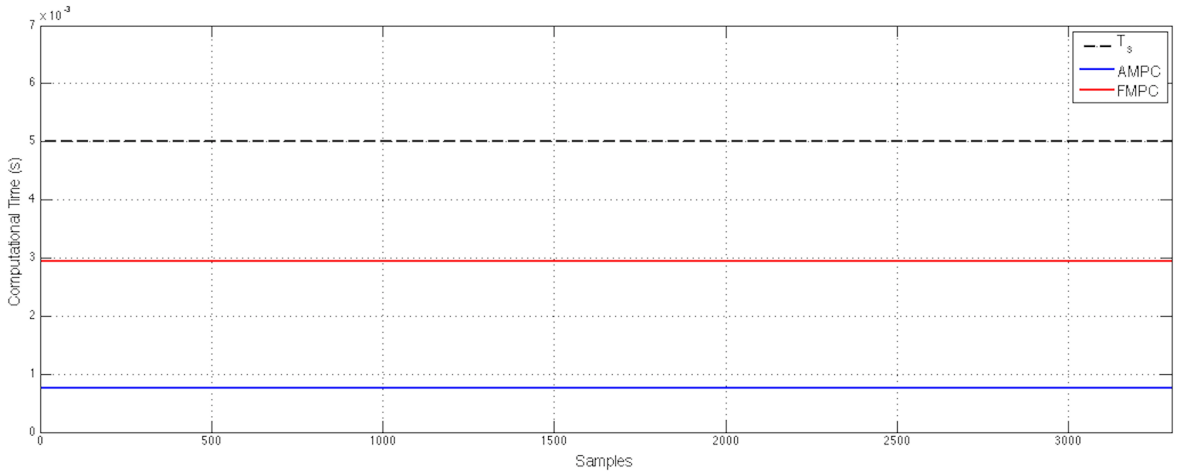

Figure 39 – Sampling Time *vs.* Computational Time: *AMPC* and *FMPC*

Let us consider, now, the scenario of a vehicle running at 120 km/h in a straight line on a dry road, when a first 5 cm bump occurs simultaneously on all wheels, to excite the bounce motion and chassis vibration, a second 5 cm bump occurs afterwards, but only on the left wheels, to cause a roll motion and, finally, a third bump occurs at both front wheels, causing a pitch motion. This road profile and its estimation by the H_2 observer is shown in figure 40; a white measurement noise was added to each measured output (y), in order to mimic real conditions, as shows figure 41.

The used weighting coefficients for the predictive controller are given in table 4. These are settled so that the minimization of the chassis' acceleration is prioritized, while the minimization of the roll angle is not neglected - a suitable trade-off, leading mainly to comfort performances of the vehicle.

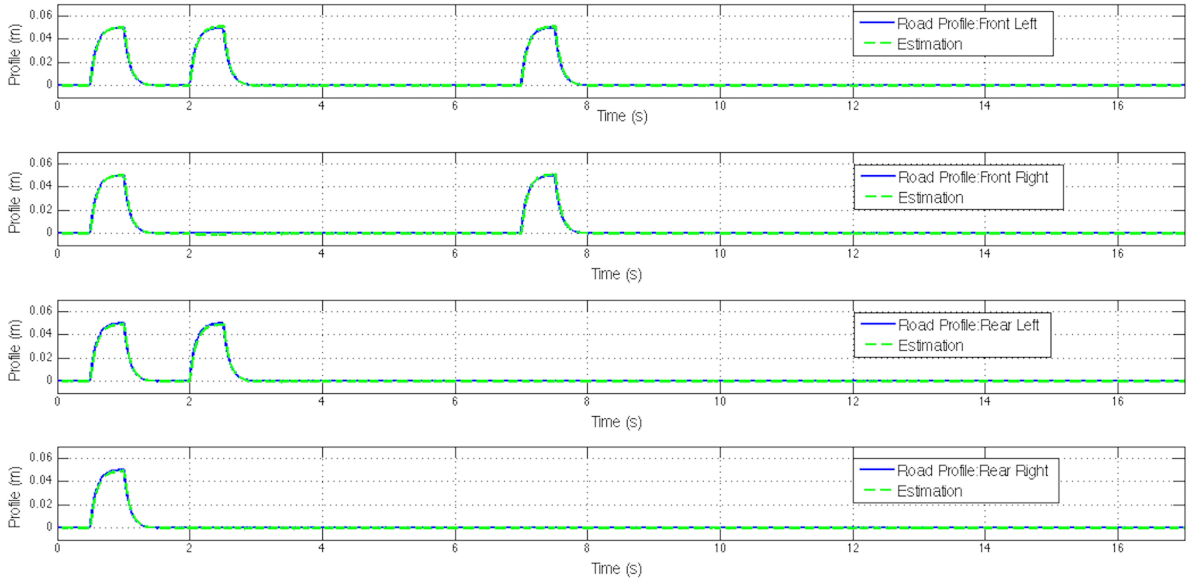

Figure 40 – Road Profile and its Estimation

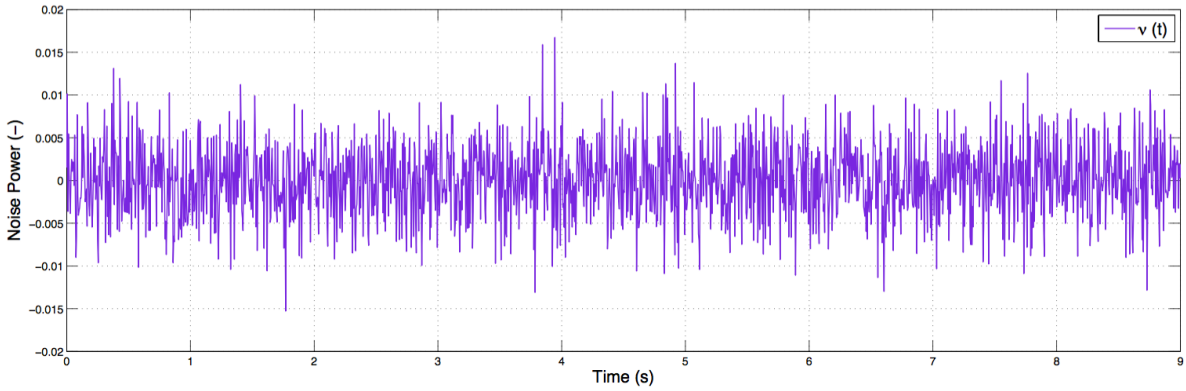

Figure 41 – Measurement Noise

Table 4 – *MPC* Synthesis Parameters

Parameter	Value
ξ_1	0.975
ξ_2	0.025
ξ_3	0.00001
Q_u	$\begin{bmatrix} 0.975 & 0 & 0 & 0 \\ 0 & 0.975 & 0 & 0 \\ 0 & 0 & 0.975 & 0 \\ 0 & 0 & 0 & 0.975 \end{bmatrix}$

Table 5 – *FMPC* Synthesis Parameters

Parameter	Value
κ	0.01
Maximal number of Newton iteration steps	17

4.7.1 Simulation Results

Let us, firstly, analyse the efficiency and the performance of the two proposed *Real-Time MPC* controllers, applied to the semi-active suspension control of a full vehicle.

The chassis' displacement due to the road profile is seen in figure 42, for both proposed control approaches and the nominal damper case. The minimization of $z_s(t)$ is not of great importance for this study, as explained beforehand.

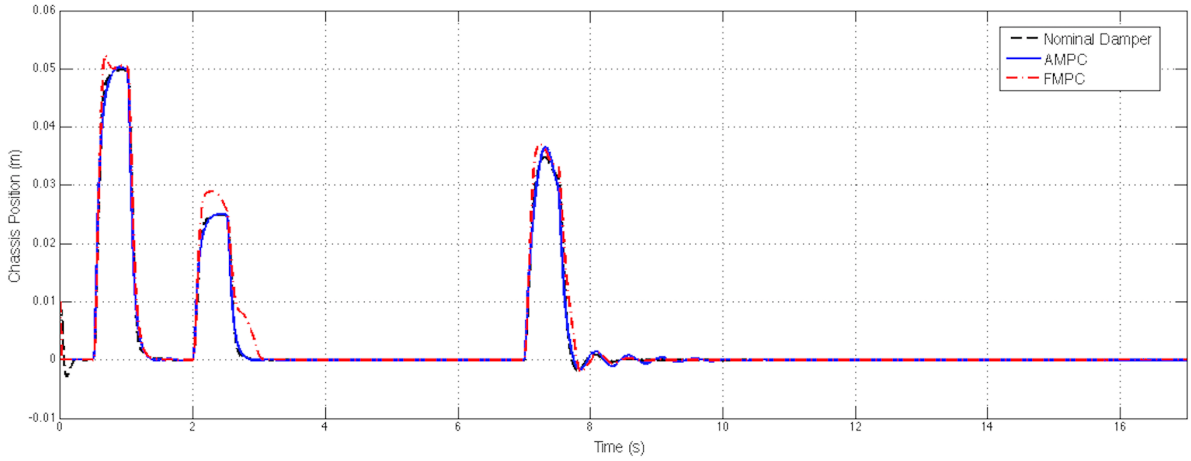

Figure 42 – Chassis' Displacement

Of uttermost importance, in figure 43, we can see the behaviour of the chassis' acceleration ($\ddot{z}_s(t)$, key for comfort performances of a vehicle) due to the road profile, with a comparison between the *AMPC*, *FMPC* and nominal case. As expected, in most situations the response with a controlled damper is more efficient than with a passive nominal suspension system. In table 6, we see the *RMS* values (root mean square over simulation time) for these three cases. It is, thus, clear that the *FMPC* method is the most efficient (specially considering what happens to roll angle behaviour with the *AMPC* approach).

Table 6 – *RMS* Values: Chassis' Acceleration

Control Approach	Value	Unit
Uncontrolled Damper	2.22066	m/s^2_{RMS}
AMPC	2.11640	m/s^2_{RMS}
FMPC	2.10061	m/s^2_{RMS}

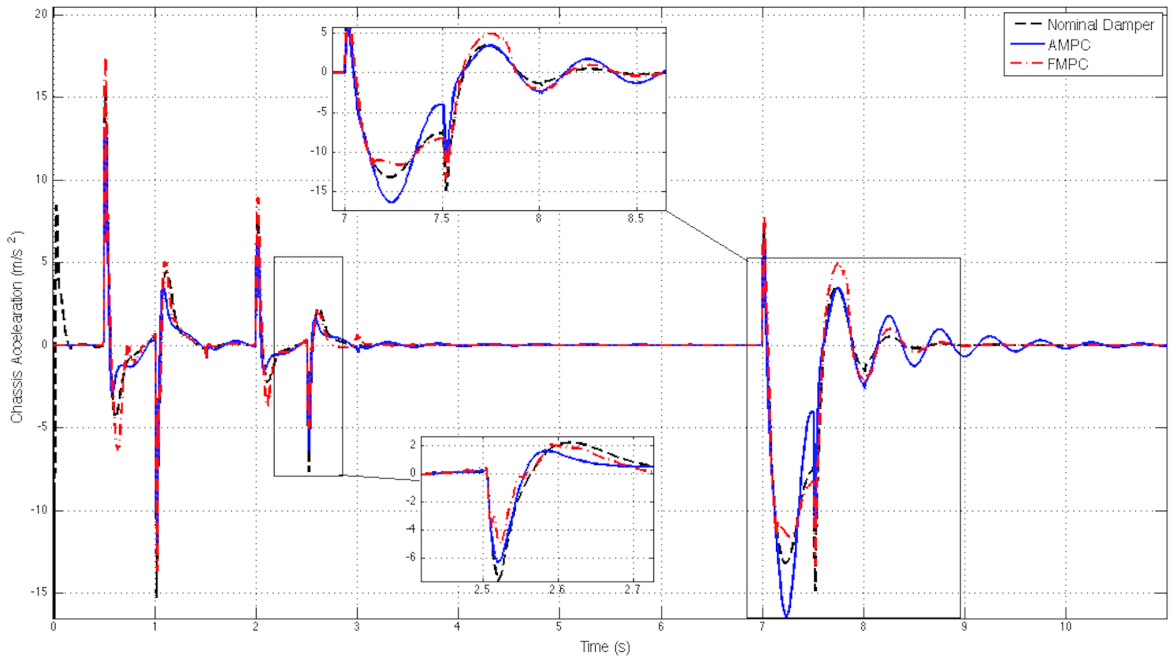

Figure 43 – Chassis' Acceleration

The behaviour of the vehicle's roll angle is, as expected, enhanced due to the sideways bump from the road profile around $t = 2\,\text{s}$. Figure 44 shows the behaviour of the roll angle ($\theta(t)$) considering the nominal passive damper (uncontrolled, taking $\Delta c_{ij} = 0$), and a controlled semi-active damper with the *AMPC* and *LPV FMPC* approaches. In terms of handling performances, the *LPV FMPC* controlled response is, at least, equal to the nominal damper, whereas the *AMPC* controlled response is much worse, because closed-loop system might present internal instabilities (marginal stability) due to the saturation effects (clipping constraints) not taken into account during the design step.

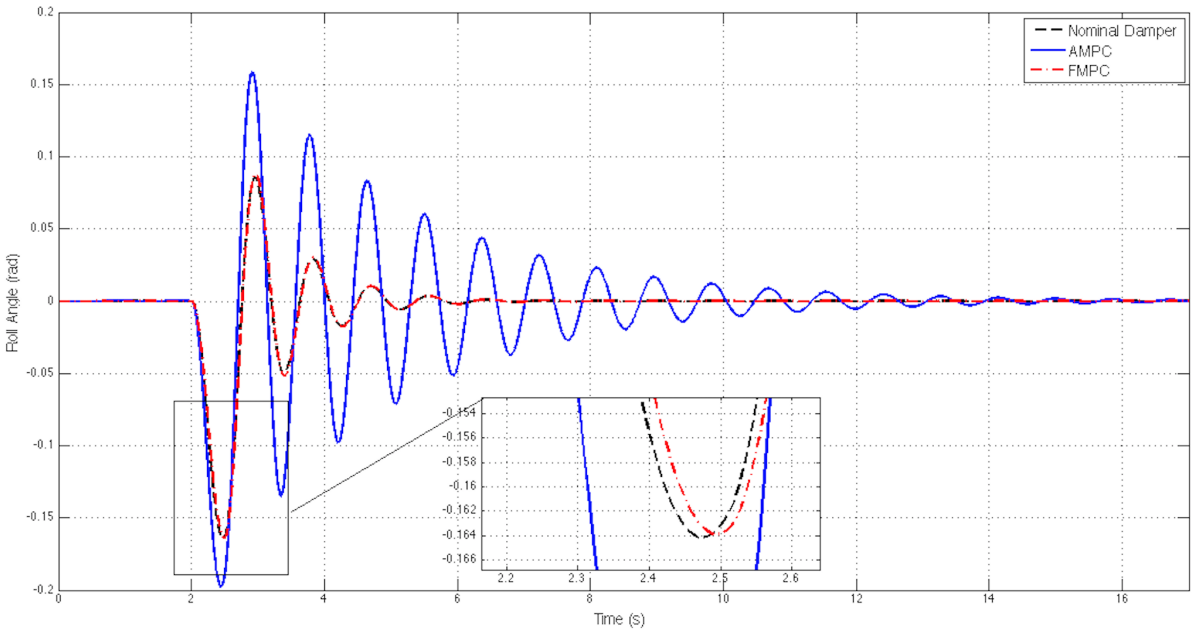

Figure 44 – Roll Angle θ

Finally, on figure 45 we see that the dissipativity constraints of all the four dampers are respected by both *Real-Time MPC* approaches, although, for the *AMPC* method, the controlled damping coefficient stays most of the time forced at $c_{max_{ij}}$. For the *FMPC* method, a wider gamma of values of $c_{ij}(\cdot)$ is used. On figure 46, we see the respective *PWM* signals to be applied to plant, for both control approaches.

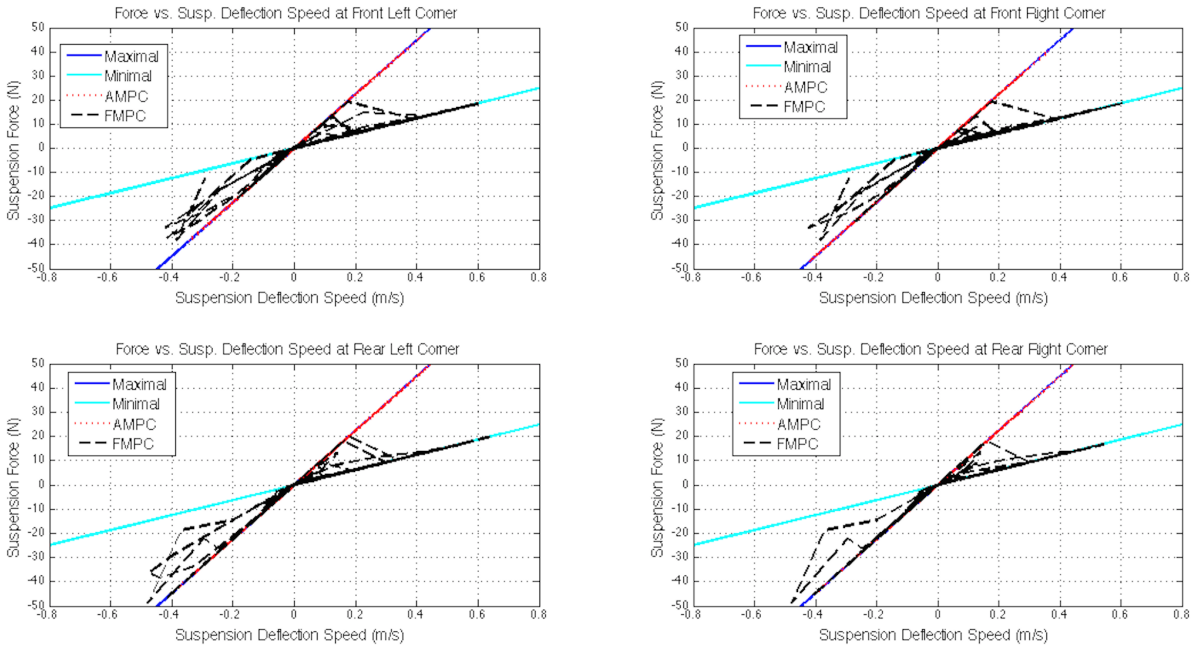

Figure 45 – Suspension Force at Each Corner

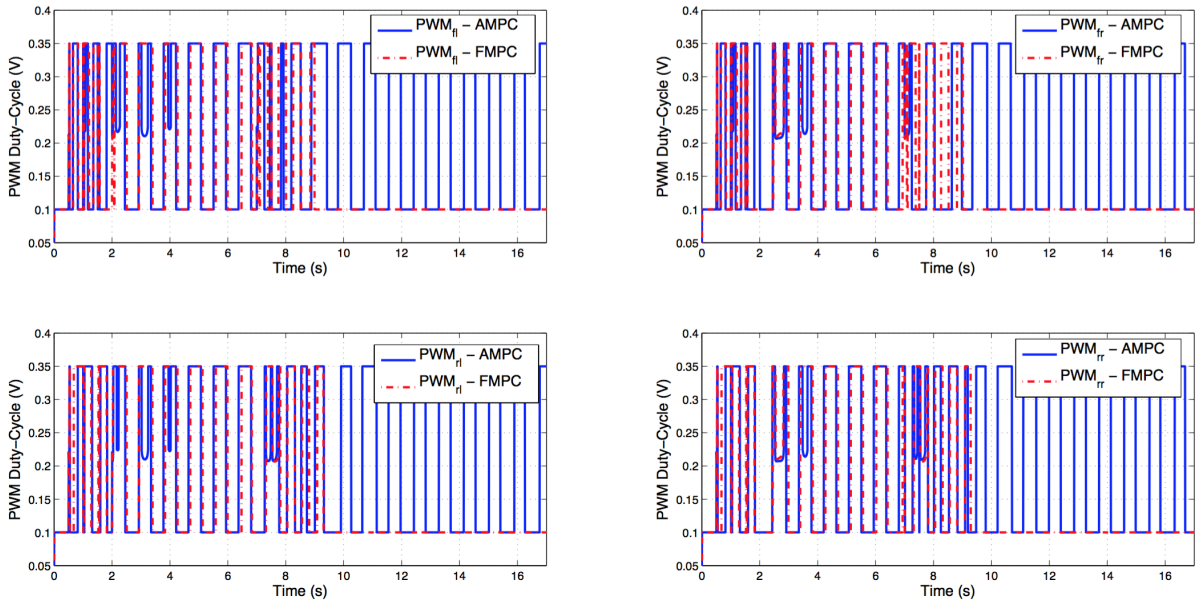

Figure 46 – *PWM* Signal for Each Damper

4.7.2 Second Scenario

Let us also show the results of the proposed control scheme to a different simulation scenario, aiming handling performance (prioritize minimization of $\theta^2(t)$). The same road profile (see figure 40) and measurement noise are considered.

On table 7, we see the chosen tuning parameters for the *MPC* scheme.

Table 7 – *MPC* Synthesis Parameters: Second Scenario

Parameter	Value
ξ_1	0.1
ξ_2	0.9
ξ_3	0
Q_u	$\begin{bmatrix} 0.9 & 0 & 0 & 0 \\ 0 & 0.9 & 0 & 0 \\ 0 & 0 & 0.9 & 0 \\ 0 & 0 & 0 & 0.9 \end{bmatrix}$

The chassis' displacement behaviour is seen on figure 47 and its acceleration is seen on figure 48. As it can be seen, once again, the *FMPC* still outperforms the uncontrolled damper and the *AMPC* method in terms of comfort performances, given the *RMS* values for this simulation, as put on table 8.

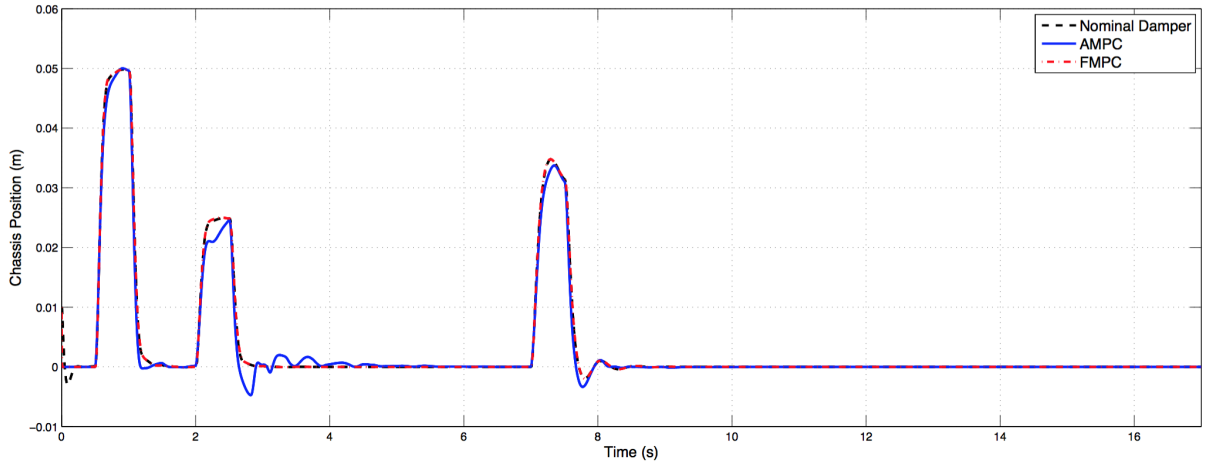

Figure 47 – Chassis' Displacement - Scenario 2

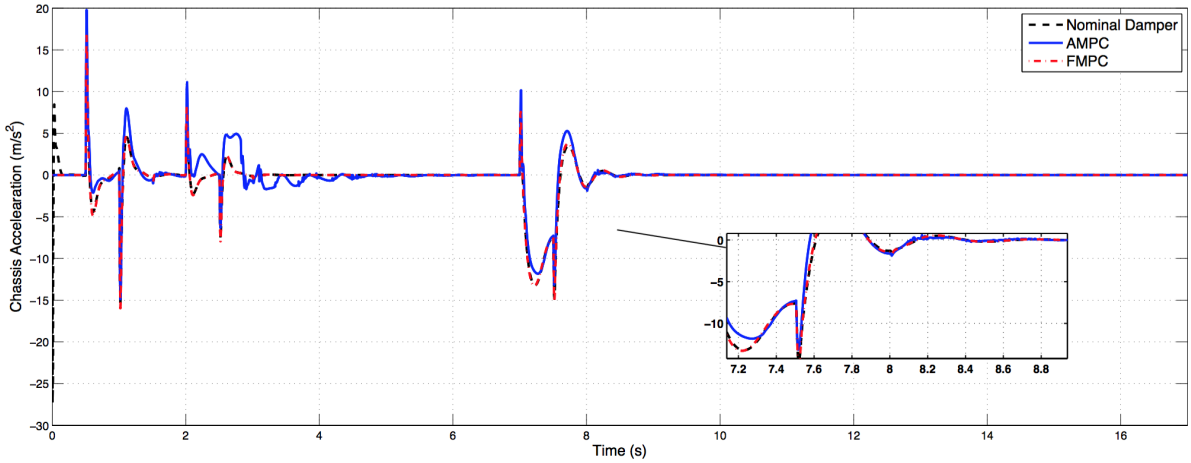

Figure 48 – Chassis' Acceleration - Scenario 2

Table 8 – *RMS* Values: Chassis' Acceleration - Scenario 2

Control Approach	Value	Unit
Uncontrolled Damper	2.2206	m/s^2_{RMS}
AMPC	2.1842	m/s^2_{RMS}
FMPC	2.1412	m/s^2_{RMS}

Finally, as this scenario considers mostly handling performances, we can analyse the roll angle behaviour, with each approach and with the uncontrolled damper, on figure 49. Once again, analyzing the *RMS* values for $\theta(t)$, on table 9, we can see the efficiency of the *FMPC* method, compared to the uncontrolled damper situation.

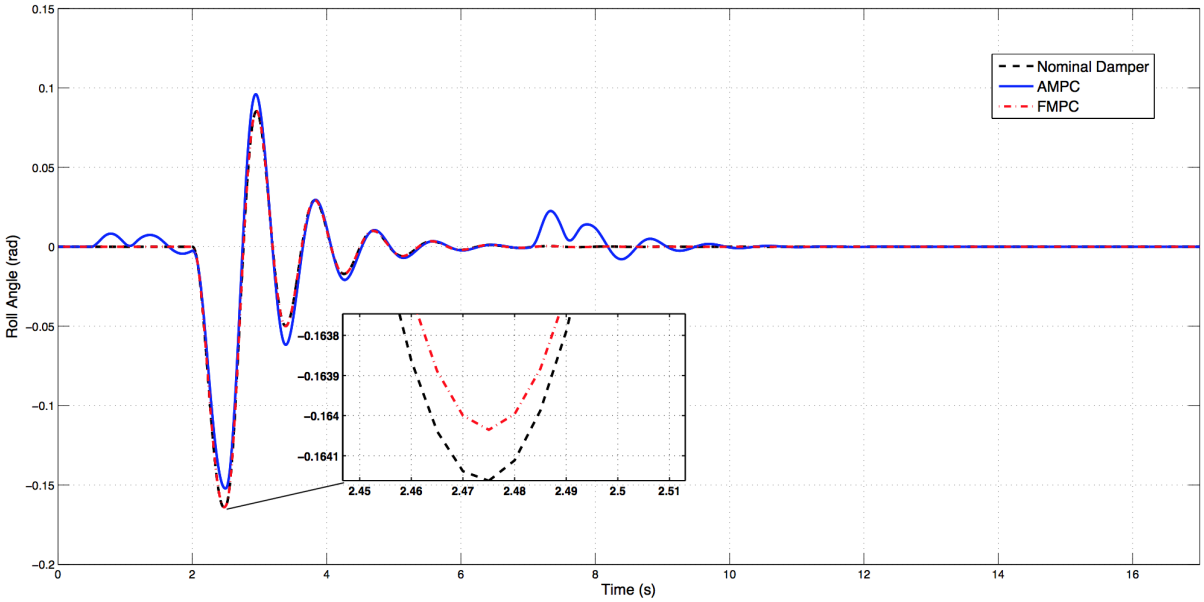

Figure 49 – Roll Angle θ - Scenario 2

Table 9 – *RMS* Values: Roll Angle - Scenario 2

Control Approach	Value	Unit
Uncontrolled Damper	$25.7122.10^{-3}$	rad_{RMS}
FMPC	$25.7044.10^{-3}$	rad_{RMS}

4.7.3 Discussion

After detailing the behaviour of the closed-loop system (presented in figure 33), we can deepen a discussion on the efficiency of the proposed control approaches, given that they aim to be implemented on a real vehicle system.

The trade-off between handling and comfort performances is the main goal of this work. For the first simulation scenario, the tuning parameters ξ have been set so that the comfort performance is better than with an uncontrolled damper and so that the handling performance is, at least, equal. For the second simulation scenario, the tuning parameters were set so that handling performance is prioritized.

Firstly, let us say that there is no guarantee that the closed-loop system would remain stable with the *AMPC* approach, since the saturation (clipping) blocks, see figure 38, might affect the internal stability. This is seen on the handling performances sense, as the *AMPC* presents a much worse behaviour than that of the uncontrolled damper. In figure 46, we can also see that the *PWM* signal, with this approach continues to vary after the road profile stabilizes, trying to stabilize internal modes.

On the other hand, the proposed *FMPC* control approach presents extremely efficient results, abiding to constraints, guaranteeing internal stability (as expected) and being able to enhance comfort performances ($\ddot{z}_s$ is well minimized, compared to the uncontrolled damper behaviour) and to maintain good handling performances ($\ddot{\theta}$ is, at least, as small as when the damper is uncontrolled). The tuning parameters can be adjusted so that an adequate trade-off is achieved, as it was shown through the two different simulation scenarios.

4.8 Conclusions

This chapter presented the issue of controlling a *semi-active* suspension system, considering a full vertical vehicle model and using a fast model-based predictive control framework. A H_2 observer is designed to estimate the system states and future road disturbances, considering the attenuation of measurement noise. A *fast* Linear Parameter Varying *MPC* control scheme is designed for a *real-time* application with a sampling frequency of 200 Hz and tested through realistic simulation scenarios, considering nonlinearities and measurement noise. Thanks to the *MPC*-based strategy, a multi-objective problem is considered, implementing a trade-off between road handling and passenger comfort, while ensuring dissipativity constraints, with the adequate choice of tuning parameters. As showed by the simulation results, the proposed control structure behaves very well. A comparison is done to a simplified analytical unconstrained *MPC*.

The proposed control scheme has not yet been implemented on a full vehicle system due to practical instrumentation issues, but this shall be done in the near future. On the other hand, some validation was already done using the experimental platform *INOVE Soben-Car*, as presented herein. The fixed sampling time constraints of 5 ms are set in order to respect a plausible implementation on a real vehicle, with the use of a fast microcontroller.

For further works, an interesting theme is to study different kinds of implementations of this *MPC* proposition, considering the use of Mixed Integer Quadratic Programming in *Real-Time MPC* controllers.

5 A Robust LPV-H_∞ Approach as a Fault-Tolerant Control Framework: Application to Full Vehicle Semi-Active Suspension Systems

5.1 About Chapter

The previous two chapters presented background results that shall be used herein. This chapter presents a Robust LPV-H_∞ approach for the goal of Fault-Tolerant Reconfiguration Technique. Previous work on FT reconfiguration techniques, by the author, is seen in [3].

This chapter considers a full vehicle model, as presented on the previous chapter and **loss of effectiveness** faults on each actuator.

The main problem herein exposed is how to maintain system performance whenever there is a faulty situation.

Remark 3. Not all the development proposed herein was finished until the end of the internship period by the author at *gipsa-lab*. Anyhow, this chapter represents a sketch for future works in terms of FTC applied to vehicle systems. All the theoretical background, contextualization, motivations and justification have already been developed. The last part focused on controller synthesis, result analysis and robustness analysis has been sketched but shall be finished post-$July$ 2017 (end of internship).

5.1.1 Abstract

In this chapter, the problem of designing a Robust Fault Tolerant dynamic output-feedback controller for Semi-Active Suspension Systems is considered. The suspension system is considered as subject to Loss of Effectiveness (time-varying) faults on each of the four actuators (suspension's dampers). An active reconfiguration fault tolerant scheme is proposed, considering a *Polytopic* LPV-H_∞ approach. The proposed solution aims to maintain the plant's driving performances (considering handling and comfort indexes) whenever there are sudden actuator faults. These faults are identified through a parallel LPV-based FDI scheme, which is also thoroughly detailed. A robustness analysis is presented for the case sensor faults and of different estimation errors on actuator faults. The validity and performance of the proposed control structure are demonstrated through

simulation. Results show the overall good operation of this control scheme, which is compared to other standart control approaches.

Keywords: Fault Tolerant Control; *LPV* Control; H_∞ Control; Robustness; Vehicle System; Semi-Active Suspensions.

5.2 Contextualization

For several years, the automotive engineering sector rapidly has come to know the use of passive safety features, such as modern seat belts and *state-of-the-art* airbags, evermore present on vehicles. On the other hand, active safety and comfort features are still arising. There is an incipient trade-off when dealing with comfort and road handling performances, for these characteristics are naturally conflicting [55]. In order to enhance a vehicle's driving performance aiming road handling **and** ride comfort, a trade-off can be achieved if the vehicle's suspension system is carefully controlled.

Evermore present in the automotive industry, *Semi-Active* suspension systems have to be given attention: these systems are efficient and altogether less expensive and energy-consuming than purely active suspensions. This type of suspension is present on new *state-of-the-art top*-cars and a good deal of academic and industrial research is focused on this topic, as seen on [56], [12] and others. Further details on semi-active suspension systems are throughly discussed on [14], and [13].

This study shall consider, thus, this type of suspension system, where the controlled input is the suspension's damper's damping coefficient $c(\cdot)$. Numerous approaches have been studied for semi-active suspension control, on [72], and more recently on [73] and [74], we can find an extensive review of semi-active suspension control. Some of the most recent and modern control techniques have been applied for this kind of problem, as presented by the author on [99], where a fast model-based predictive controller is designed.

5.2.1 Why Fault Tolerant Control?

Most of the practical control systems are subject to possible faults, failures, component malfunctions and others. These might imply on significant performance degradation or even loss of control and instability.

Accordingly, in recent years attention has been considerably been given to fault tolerant control (FTC) schemes. A FTC system has the goal to allow a system to recover performances when faults occur (or, at least, guarantee continuous stability). FTC systems are categorized into two types: passive and active approaches, as seen in [38] and (firstly) [37]. Passive approaches usually reside on more conservative control schemes, as details [1], whereas active approaches reside on continuous reconfiguration of the controller,

due to identified faults.

The accurate behaviour of active *FTC* schemes, then, dependes on a solid Fault Detection and Isolation (*FDI*) system. Adaptive control techniques have been designed to integrate *FDI* and *FTC*, as seen in [100] and [101]. It is recognised that the combined *FDI*/*FTC* design could be profitable, but, yet, very challenging, [102].

On the other hand, the modulated design (*FDI* and *FTC* designed separately) also presents its benefits, being more flexible for practical applications and easier to test and implement. This is the approach used herein.

It is important to remark that, for this modulated design approach, scientific breakthrough has been achieved with gain-scheduling and *LPV* approaches for active *FTC*, as seen in [103] and [104]. Notice that, therein, the *FTC* framework considers the imperfect estimation of fault effect by the *FDI* structure, aiming robustness.

5.2.2 Linear Parameter Varying Systems

Synthesis and investigation techniques for Linear Parameter Varying (*LPV*) Systems have gathered evermore attention from the Control Systems community, see [30] and [32].

Firstly introduced in [105], the *LPV* system paradigm has become an established formalism in systems and control, in terms of analysis, controller synthesis and system identification. This kind of system can be understood as a representation methodology to be well suited for the control of dynamical systems with parameter variations, as it is exploited in [47], [48], [49] and [50]. These (*LPV*) structures can be represented as an extension of *LTI* systems, assuming the classical state-space representation matrices are dependent on known **bounded** scheduling parameter ρ. Briefly, these scheduling parameters must abide to:

$$\{\rho \in \Omega \,|\, \rho_{\min} \leq \rho \leq \rho_{\max}\} \tag{5.1}$$

Sometimes, bounds are also needed on the scheduling parameters' variations, $\dot{\rho}$.

Within the *LPV* framework, developments regarding the architecture of observers [106], [59], state-feedback controllers [78], H_∞ controllers [107], [108] and model reference controllers [109] have been obtained. This work shall be preoccupied with the use of the *LPV* methodology on extended-state observers for the case of fault estimation and dynamic output-feedback controllers for the case of Fault Tolerant reconfiguration (explained further on).

An *LPV*-based fault estimation is able to autonomously adjust and schedule observer or detection filter gains. This is suitable trade-off between full scaled nonlinear designs and *LTI* methods based on a fixed operating condition, for *LPV*-based *FDI*

methods provides most of the conveniencies of *LTI* design and still guarantees good performance and stability conditions over a wider operating set.

5.2.3 H_∞ Control

H_∞ Control Theory has been used for suspension control in some works throughout literature, as in [110] and [107]. This technique shall be used herein for it presents some efficient tools for our performance control goal: provide a trade-off between handling and comfort performances, which shall be done with the use of adequate weighting functions. *LPV* control design for suspension control, on the other hand, is evermore present in literature, as seen in [51], [52] and [53].

5.2.4 Problem Statement

Considering the given contextualization, the problem dealt within this chapter is the following: how to design an efficient (and robust) Fault Tolerant Control scheme, considering actuator faults, for the control of a full vehicle model with four semi-active suspension systems, maintaining (sufficient) comfort and handling performances whenever occurs a faulty scenario ?

This shall be treated by a threefold:

- Firstly, a *LPV*-based Fault Detection and Isolation structure shall be presented, in order to detect *Loss of Effectiveness* faults on each of the suspensions' dampers (actuation);
- Secondly, an internal Force Control System scheme is designed to deal with reference tracking and disturbance rejection for each damper;
- Lastly, a *LPV*-H_∞ *FTC* scheme shall be detail, in order to guarantee closed-loop stability and performances, based on controller reconfiguration in the case of faulty scenarios.

It is also important to state that very few works have dealt with robustness analysis (performance and stability) due to parameter uncertainties, in the automotive industry and research. This issue is essentially due to the mass production and nonlinearities of vehicle components, that become more and more susceptible to faults. As of this, this work shall also present a robustness analysis for the case sensor faults and estimation errors (from the *FDI* scheme) on actuator faults.

5.2.5 About Chapter

This chapter is outlined as follows:

- The considered full vehicle model with 4 semi-active suspension systems is presented in section 5.3, as well as a reduced quarter-of-vehicle model, used for fault identification goals;
- In section 5.4, the proposed LPV Fault Diagnosis and Isolation structure is described and some validation results are already presented;
- In section 5.5, an internal control scheme is designed to rapidly track force references to each of the semi-active dampers;
- In section 5.6, performance and robustness specifications for our control goals are presented and the proposed Robust LPV-H_∞ Fault Tolerant controller is designed;
- A complete robustness analysis is done in section 5.7;
- Simulation results and a thorough discussion are seen in 5.8 and, finally, conclusions are drawn in section 5.9.

5.3 Vehicle Modelling

An automative suspension system comprises, basically, two components: a spring and a damping (shock absorbing) structure, as it can be seen on figure 50. These components have to work together to maintain the tire's contact with the ground. The goal of the damping structure is to reduce the effect of travelling upon a rough road by absorbing shock and helping with driving performance, ensuring a smoother and safer drive. An automative suspension without an efficient damping system might be able to absorb damps, but continues to bounce, and this might lead the tires to leave the road.

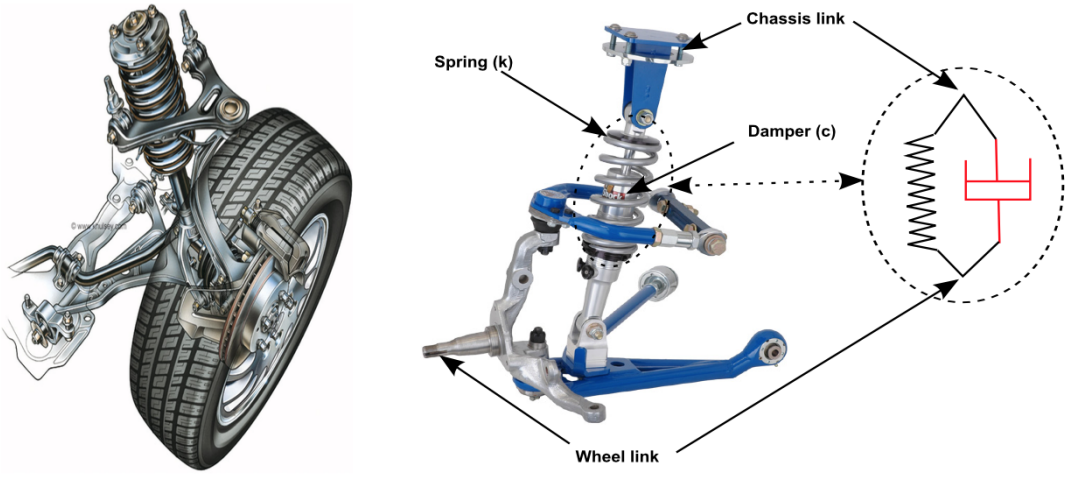

Figure 50 – Outline of Studied Suspension System

Throughout literature there are some established dynamical models of vehicles and automotive suspension systems. Herein, two models shall be considered: a full vertical vehicle model (FVV) for the vehicle's suspension control and a reduced quarter-of-vehicle model (QoV), used for fault detection and identification goals. Further details on each of this models are seen on [5].

5.3.1 Full Vertical Vehicle Model

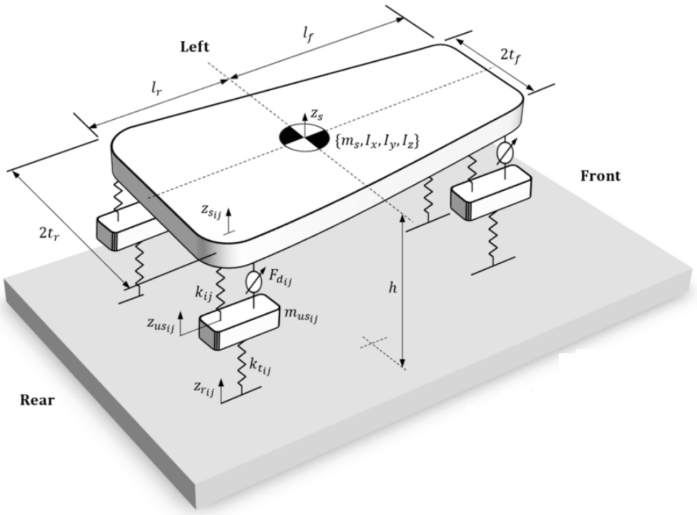

Figure 51 – Full Vehicle Model with 4 *ER* Semi-Active Suspensions

Let us first present the dynamical model that represents a vehicle's vertical dynamical behaviour, considering the suspension system comprised by four Electro-Rheological (ER) dampers (which have a force range of $\pm 50\,\mathrm{N}$). This is a classic 7 degrees of freedom suspension model, as seen in figure 51 and referred to in [85], and shall be used for analysis and control purposes. This model comprises the chassis dynamics (vertical displacement (z_s), roll angle (θ) and pitch angle (ϕ)) and the vertical displacements of the wheels ($z_{us_{ij}}$) at the front/rear - left/right corners ($i = (f, r)$ and $j = (l, r)$). This described $7 - DOF$ model is governed by the following equations:

$$\begin{aligned} m_s.\ddot{z}_s &= -F_{sfl} - F_{sfr} - F_{srl} - F_{srr} \\ I_x.\ddot{\theta} &= (-F_{sfr} + F_{sfl}).t_f + (F_{srl} - F_{srr}).t_r \\ I_y.\ddot{\phi} &= (F_{srr} + F_{srl}).l_r - (F_{sfr} + F_{sfl}).l_f \\ m_{us_{ij}}.\ddot{z}_{us_{ij}} &= F_{s_{ij}} - F_{tz_{ij}} \end{aligned} \tag{5.2}$$

where I_x and I_y represent the moments of inertia of the sprung mass around the longitudinal and lateral axis, respectively, h represents the height of the center of gravity (COG). l_f,l_r,t_f and t_r are the COG-front, rear, left and right distances, respectively.

The position (and, thus velocities) of each sprung mass at each corner of the vehicle ($z_{s_{ij}}$) is derived from the vehicle equations of motion, and considering the roll and pitch angles as small enough, they become linearized as in:

$$\begin{aligned} z_{s_{fl}} &= z_s - l_f.(\phi) + t_f.(\theta) \\ z_{s_{fr}} &= z_s - l_f.(\phi) - t_f.(\theta) \\ z_{s_{rl}} &= z_s + l_r.(\phi) + t_r.(\theta) \\ z_{s_{rr}} &= z_s + l_r.(\phi) - t_r.(\theta) \end{aligned} \tag{5.3}$$

In terms of the forces, $F_{tz_{ij}}$ depicts the vertical tire forces, given by:

$$F_{tz_{ij}} = k_{t_{ij}}.(z_{us_{ij}} - z_{r_{ij}}) \tag{5.4}$$

where $k_{t_{ij}}$ represent the stiffness coefficients of the tires and $z_{r_{ij}}$ are the road profile disturbances that the vehicle is subject to.

Each vertical suspension forces (for each of the 4 corners of the vehicle) is represented by $F_{s_{ij}}$ and, in this study, will be modeled by a spring and a damper with linear and nonlinear characteristics, respectively. This is:

$$F_{s_{ij}} = k_{ij}.(z_{s_{ij}} - z_{us_{ij}}) + F_{d_{ij}} \tag{5.5}$$

where k_{ij} representes the nominal spring stiffness coefficient and $F_{d_{ij}}$ the semi-active damper force. Herein, we shall consider a two-level control scheme, where the damper force is treated by an internal lever control structure.

Anyhow, the damper force is given by equation (5.6), divided into passive and controlled parts, where $d_{c_{ij}}(t)$ represents a controlled PWM signal inside $[0\,,\,100]\,\%$. The dissipativity constraints of each of these semi-active dampers will be treated by the lower level controllers; this will be dealt with in later sections.

$$F_{d_{ij}}(t) = \overbrace{c_{0_{ij}}.(\dot{z}_{s_{ij}} - \dot{z}_{us_{ij}})}^{\text{passive}} + \overbrace{f_{c_{ij}}.d_{c_{ij}}(t).\tanh(a_{1_{ij}}.\dot{z}_{def_{ij}}(t) + a_{2_{ij}}.z_{def_{ij}}(t))}^{\text{controlled}} \tag{5.6}$$

Remark: herein we shall use the notation $z_{def_{ij}} = z_{s_{ij}} - z_{us_{ij}}$ as the suspension deflection.

To facilitate our control purposes, the full vehicle's control inputs are, thus, given by:

$$u = \begin{bmatrix} F_{d_{fl}} & F_{d_{fr}} & F_{d_{rl}} & F_{d_{rr}} \end{bmatrix}^T \tag{5.7}$$

5.3.1.1 *FVV* State-Space Representation

This studied (FVV) system model can be represented, thus, by a *state-space* representation, when injecting (5.4) and (5.7) into (5.2). This is:

$$\sum_{FVV} := \left\{ \begin{array}{rcl} \dot{x}(t) & = & A.x(t) + B_1.w(t) + B_2.u(t) \\ y(t) & = & C.x(t) + D_1.w(t) + D_2.u(t) \end{array} \right\} \tag{5.8}$$

where the system states are given by (5.9), the controlled inputs are given by (5.7), the disturbances (unmeasured) are given by (5.10) and, finally, the measured outputs are seen on equation (5.11). Remark: A, B_1, B_2, C, D_1 and D_2 are constant matrices. This model is continuous-time, obviously.

$$\begin{aligned} x &= \left[\begin{array}{cccccccc} z_s & \theta & \phi & z_{us_{fl}} & z_{us_{fr}} & z_{us_{rl}} & z_{us_{rr}} & \dot{z}_s \quad \dots \\ \dot{\theta} & \dot{\phi} & \dot{z}_{us_{fl}} & \dot{z}_{us_{fr}} & \dot{z}_{us_{rl}} & \dot{z}_{us_{rr}} & & \end{array} \right]^T \qquad (5.9) \\ w &= \left[\begin{array}{cccc} z_{r_{fl}} & z_{r_{fr}} & z_{r_{rl}} & z_{r_{rr}} \end{array} \right]^T \qquad (5.10) \\ y &= \left[\begin{array}{cccccccc} z_{def_{fl}} & z_{def_{fr}} & z_{def_{rl}} & z_{def_{rr}} & \dot{z}_{def_{fl}} & \dot{z}_{def_{fr}} & \dot{z}_{def_{rl}} & \dot{z}_{def_{rr}} \quad \dots \\ z_{us_{fl}} & z_{us_{fr}} & z_{us_{rl}} & z_{us_{rr}} & & & & \end{array} \right]^T \qquad (5.11) \end{aligned}$$

5.3.2 Quarter-of-Vehicle Model

Let us, also, present a reduced-order model that can be used to analyse the behaviour of an automotive system on a single of its corner. Considering the same type of ER damper, a representation of a Quarter-of-Vehicle model (QoV) is seen in figure 52.

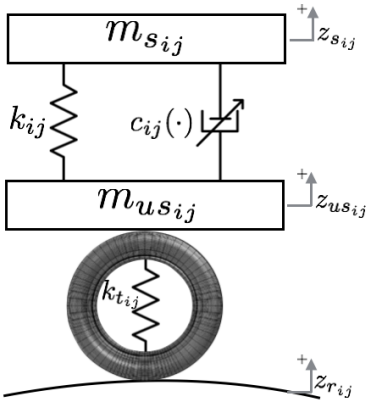

Figure 52 – Semi-Active Suspension of Quarter-Vehicle with ER Damper

The dynamical equations that rule this model are similar to those for the FVV model. These are, for each corner $(i-j)$ of the vehicle:

$$\begin{aligned} m_{s_{ij}}.\ddot{z}_{s_{ij}}(t) &= -k_{ij}.z_{def_{ij}} + F_{d_{ij}}(t) \\ m_{us_{ij}}.\ddot{z}_{us_{ij}}(t) &= k_{ij}.z_{def_{ij}} - F_{d_{ij}}(t) - k_{t_{ij}}.(z_{us_{ij}}(t) - z_{r_{ij}}(t)) \end{aligned} \tag{5.12}$$

where $F_{d_{ij}}$ represents the semi-active *ER* damper's force (controlled and passive) at the given corner. As of the proposed *FVV* model, herein $F_{d_{ij}}(t)$ is also the controlled damper force.

5.3.2.1 *QoV* State-Space Representation

A *state-space* representation can be found if considering system states as of equation (5.13), a disturbance input as of equation (5.14) and finally, the measured outputs as of equation (5.15).

$$x^{ij}_{qov}(t) = \left[\begin{array}{cccc} z_{s_{ij}}(t) & \dot{z}_{s_{ij}}(t) & z_{us_{ij}}(t) & \dot{z}_{us_{ij}}(t) \end{array} \right]^T \tag{5.13}$$

$$w^{ij}_{qov}(t) = z_{r_{ij}}(t) \tag{5.14}$$

$$y^{ij}_{qov}(t) = \left[\begin{array}{ccc} z_{def_{ij}}(t) & \dot{z}_{def_{ij}}(t) & z_{us_{ij}}(t) \end{array} \right]^T \tag{5.15}$$

This measurements are, in a certain way, common on vehicular suspension systems. They can be acquired using relative displacement sensors. The deflection velocity ($\dot{z}_{def_{ij}}(t)$) can be used with certain carefullness, as they arise from derivative filters. Finally, this leads us to the following *LTI* model:

$$\sum_{QoV}^{ij} := \left\{ \begin{array}{rcl} \dot{x}^{ij}_{qov}(t) &=& A^{ij}_{qov}.x^{ij}_{qov}(t) + B^{ij}_{1_{qov}}.w^{ij}_{qov}(t) + B^{ij}_{2_{ij}}.F_{d_{ij}}(t) \\ y^{ij}_{qov}(t) &=& C^{ij}_{qov}.x^{ij}_{qov}(t) + D^{ij}_{1_{qov}}.w^{ij}_{qov}(t) + D^{ij}_{2_{qov}}.F_{d_{ij}}(t) \end{array} \right\} \tag{5.16}$$

where the matrices A^{ij}_{qov} to $D^{ij}_{2_{qov}}$ are all constant. Notice that this representation repeats itself for every corner of the full vehicle.

5.4 Fault Detection and Isolation Scheme

Now that the used vehicle models have been detailed, let us introduce the proposed Fault Detection and Isolation (*FDI*) scheme.

As explained beforehand, this work shall consider **actuator faults** on each of the *ER* dampers of the full vehicular suspension system. Considering the studied suspension system, a fault can occur due to oil leakage, physical deformation or even the presence of air on the *ER* fluid. The study of faults on Electro-Rheological Dampers is thoroughly discussed in [111].

5.4.1 Loss of Effectiveness Faults

Faults on each of the actuators, in a practical sense, result on a **loss of effectiveness** of these components. For this, in this study, the actuator faults shall be represented by a multiplicative factor α_{ij} upon each damper force $F_{d_{ij}}$.

Remark 4. In a faultless situation, we shall have $\alpha_{ij} = 1$ and, in the worst of scenarios (where the damper is completely *broken*), we shall have $\alpha_{ij} = 0$. For this, $\alpha_{ij} \in [0\,,\,1]$. In figure 53, we see a representation of the studied loss of effectiveness fault scenario.

It is also worth noting that even if α is assumed to be constant, the corresponding additive fault magnitude on nth semi-active damper is given by $f(t) = (1-\alpha)u(t)$ is a time varying signal and depends on the value of the control input $u(t)$. Thanks to the multiplicative representation, the information about the actuator fault α is considered as constant or slow-varying and $\dot{\alpha} = 0$.

This multiplicative fault representation has been firstly presented in [112], and introduces a solid framework for the identification of damper faults.

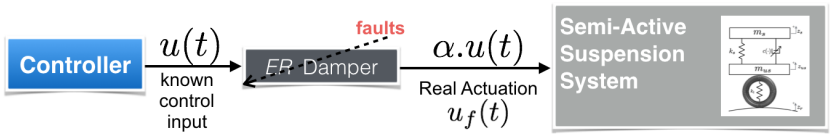

Figure 53 – Damper Loss of Effectiveness Fault Problem

Synthetically: The problem herein is, thus, to identify this loss of effectiveness fault factor α only through the available measurements $y(t)$, see equation (5.11).

Then, these loss of effectiveness faults on the dampers on each corner of a full vehicle results on nonlinear system model representation. By using the QoV model, we are cast into the following representation of each corner of the studied suspension system:

$$\sum_{QoV}^{ij} := \left\{ \begin{array}{rcl} \dot{x}^{ij}_{qov}(t) & = & A^{ij}_{qov}.x^{ij}_{qov}(t) + B^{ij}_{1_{qov}}.w^{ij}_{qov}(t) + B^{ij}_{2_{ij}}.\mathrm{diag}\{\alpha_{ij}\}.F_{d_{ij}}(t) \\ y^{ij}_{qov}(t) & = & C^{ij}_{qov}.x^{ij}_{qov}(t) + D^{ij}_{1_{qov}}.w^{ij}_{qov}(t) + D^{ij}_{2_{qov}}.\mathrm{diag}\{\alpha_{ij}\}.F_{d_{ij}}(t) \end{array} \right\} \quad (5.17)$$

In terms of the FVV model, we arrive at:

$$\sum_{Full\,Veh.} := \left\{ \begin{array}{rcl} \dot{x}(t) & = & A.x(t) + B_1.w(t) + B_2(\mathrm{diag}\{\alpha_{ij}\}).u(t) \\ y(t) & = & C.x(t) + D_1.w(t) + D_2(\mathrm{diag}\{\alpha_{ij}\}).u(t) \end{array} \right\} \quad (5.18)$$

5.4.2 *LPV*-based *FDI* Design

Considering an automotive suspension system subject to actuator *loss of effectiveness* faults, we can design a reduced-order *FDI* structure for each of the full vehicle's suspensions systems, considering the use of the *QoV* model.

For this goal, we can re-write our faulty damper *QoV* system with an augmented *space-state* representation considering $x_a^{ij}(t) = \left[\begin{array}{ccc} (x_{qov}^{ij})^T(t) & \alpha_{ij} & w_{qov}^{ij}(t) \end{array} \right]^T$. We also assume that each fault factor α_{ij} is statical, so $\dot{\alpha_{ij}} = 0$. As of this, we have:

$$\overbrace{\left[\begin{array}{c} \dot{x}_{qov}^{ij}(t) \\ \dot{\alpha}_{ij} \\ \dot{w}_{qov}^{ij}(t) \end{array} \right]}^{\dot{x_a^{ij}}(t)} = \overbrace{\left[\begin{array}{ccc} A_{qov}^{ij} & \underbrace{B_{2_{qov}}^{ij}.F_{d_{ij}}(t)}_{B_\alpha^{ij}} & B_{1_{qov}}^{ij} \\ 0 & 0 & 0 \\ 0 & 0 & A_{mw}^{ij} \end{array} \right]}^{A_a^{ij}} .x_a(t)$$

$$y_{qov}^{ij}(t) = \underbrace{\left[\begin{array}{ccc} C_{qov}^{ij} & \overbrace{D_{2_{ij}}^{ij}.F_{d_{ij}}(t)}^{D_\alpha^{ij}} & D_{1_{qov}}^{ij} \end{array} \right]}_{C_a^{ij}} .x_a^{ij}(t)$$

where we assume to have information on the type of road profile disturbance. This is, we have a model of the disturbance: $\dot{w}_{qov}^{ij}(t) = A_{mw}.w(t)$. This information may come from an external adaptive road profile estimator, as proposed on [57]. Remark that different road profiles may have greater *state-space* models with more than one state (say n_w states), which leads to the augmentation of matrices $B_{1_{qov}}^{ij}$ and $D_{1_{qov}}^{ij}$ with $(n_w - 1)$ *null* columns - for example, a sinusoidal road profile has, at least, $n_w = 2$ states.

It is important to notice that the matrices A_a^{ij} and C_a^{ij} are affine on $F_{d_{ij}}(t)$, due to the terms (respectively) B_α^{ij} and D_α^{ij}. Let us remark, then, that damper force signal $F_{d_{ij}}(t)$ is *perfectly know* (use of compression force sensors), and **bounded** (due to saturation constraints of each semi-active damper) inside the convex set $\mathcal{U}_{\text{sat}}$, delimited by the minimal and maximal values of $F_{d_{ij}}$, $\underline{F_{d_{ij}}}$ and $\overline{F_{d_{ij}}}$, respectively.

Thus, we can assume $F_{d_{ij}}(t)$ as a scheduling parameter $\rho^{ij}(t)$, as it satisfies $0 < \rho_{min}^{ij} \leq \rho^{ij} \leq \rho_{max}^{ij}$. From this, we arrive at $B_\alpha^{ij} = B_{2_{qov}}^{ij}.\rho^{ij}$ and $A_a^{ij} = A_a^{ij}(\rho^{ij})$ and, similarly, $D_\alpha^{ij} = D_{2_{qov}}^{ij}.\rho^{ij}$ and $C_a^{ij} = C_a^{ij}(\rho)$. Thus, the augmented system (5.19) becomes *LPV*.

Finally, we can design an asymptotical state observer to estimate the value of each fault factor α^{ij}. This is:

$$\sum_{\text{FDI}} := \left\{ \begin{array}{rcl} \dot{\hat{x}}_a^{ij}(t) & = & A_a^{ij}.\hat{x_a^{ij}}(t) + L^{ij}(\cdot).[y_{qov}^{ij}(t) - C_a^{ij}.x_a^{ij}(t)] \\ \hat{\alpha}_{ij} & = & \underbrace{\left[\begin{array}{ccc} 0_{\text{size}(x_{qov}^{ij})} & \mathbb{I}_{\text{size}(\alpha_{ij})} & 0_{\text{size}(w_{qov}^{ij})} \end{array} \right]}_{C_\alpha} .\hat{x_a^{ij}}(t) \end{array} \right\} \quad (5.19)$$

Finally, let us consider the dynamics of the estimation error. These dynamics are presented in equation (3.7). Then, the *LPV FDI* design resided on computing the gain matrix $L(\cdot)$ as dependent of the scheduling parameter ρ^{ij} so that $(A_a^{ij} - L^{ij}(\rho^{ij}).C_a^{ij})$ is Lyapunov-sense stable.

$$\dot{e}^{ij}(t) = \dot{x_a}^{ij}(t) - \dot{\hat{x}}_a^{ij}(t) = [A_a^{ij} - L^{ij}(\rho^{ij}).C_a^{ij}].e^{ij}(t) \tag{5.20}$$

From here, we shall consider a *Polytopic LPV*-based solution. Notice, once again, that what is subsequently presented has to be solved for each of the four $(i-j)$ corners of the automotive suspension system.

To compute the matrix gain $L^{ij}(\cdot)$ of the proposed extended observer and guarantee the stability of each (5.20), we shall follow a H_2 (noise filtering) criterion, as seen in [23]. The H_2 norm of a system, through a stochastic point-of-view, is equal to the square root of the asymptotic variance of the output when the input is a white noise (proof is seen on [22]), which means that the measurement noise effect will be diminished when estimating the loss of effectiveness fault factor α (impulse to energy gain minimization), taking the measurement noise as the input to the estimation error system (5.20);

Definition 5.1. The H_2 observer problem definition resides, then, on minimizing the following objective function:

$$J = ||T_{e\nu}^{ij}(s)||_2^2 \quad \text{under} \quad e^{ij}(t)|_{t=0} = 0 \tag{5.21}$$

under the two following conditions (exponential stability of $T_{e\nu}^{ij}(s)$ and *closed-loop* observation error dynamics):

$$\lim_{t\to\infty} e^{ij}(t) \to 0 \quad \text{for} \quad \nu^{ij} \equiv \overrightarrow{0} \tag{5.22}$$

$$\dot{e}^{ij}(t) = (A_a^{ij}(\cdot) - L^{ij}(\cdot).C_a^{ij}(\cdot)).e(t) + B_\nu^{ij}\nu^{ij}(t) \tag{5.23}$$

where $T_{e\nu}^{ij}(s)$ represents the *Laplace*-domain transfer function between the estimation error $e^{ij}(t)$ and an additive measurement noise $\nu^{ij}(t)$ on each component of $x^{ij}(t)$. Notice, also, that the matrix B_ν^{ij} represents the influence of the measurement noise on the system states.

Lemma 5.2. This problem's solution, then, is obtained by minimizing the scalar γ^{ij} on:

$$\text{Trace}(N) \leq \gamma^{ij} \tag{5.24}$$

and solving the following *LMI*s, exposed in equations (5.25)-(5.27), taking $Q^{ij} = P^{ij}.L^{ij}(\cdot)$, with P and N being two positive define matrices.

$$\begin{bmatrix} (A_a^{ij})^T(\rho^{ij}).P^{ij} + P^{ij}.A_a^{ij}(\rho^{ij}) - (C_a^{ij})^T(\rho^{ij}).(Q^{ij})^T - Q^{ij}.C_a^{ij}(\rho^{ij}) & -Q^{ij} \\ \star & -\mathbb{I} \end{bmatrix} < \quad (5.25)$$

$$\left[2\beta^{ij}.P^{ij} + (A_a^{ij})^T(\rho^{ij}).P^{ij} + P^{ij}.A_a^{ij}(\rho^{ij}) - (C_a^{ij})^T(\rho).(Q^{ij})^T - Q^{ij}.C_a^{ij}(\rho)\right] < \quad (5.26)$$

$$\begin{bmatrix} N^{ij} & (B_\nu^{ij})^T.P^{ij} \\ \star & P^{ij} \end{bmatrix} > \quad (5.27)$$

Proof of Lemma 5.2 1. Is immediate from what is seen in [23].

Remark 5. The gain matrix $L^{ij}(\cdot)$ is taken, thus, as $L^{ij} = (P^{ij})^{-1}.Q^{ij}$.

Remark 6. The maximal variance of the estimation error, with this solution, is given by $\text{Trace}(N^{ij}) = \gamma_{H_2}^{ij}$.

Remark 7. The maximal amplification of the estimation error, with this solution, due to the presence of the uncertain disturbance $\delta w(t)$ is given by $\gamma_{H_\infty}^{ij}$.

Remark 8. The scalar β^{ij} in the *LMI* (5.26) is a *root-locus* condition imposed on the eigenvalues of $(A_a^{ij}(\rho^{ij}) - L^{ij}(\rho^{ij}).C_a^{ij}(\rho^{ij}))$: these must be greater, in module, than β^{ij}.

Remark 9. A weighting function can be appropriately introduced to specify the frequency range on which sensor noises should be attenuated. Besides, (obviously) sensor noise is considered as a high frequency signal.

As, to our problem, we have only one scheduling parameter ρ^{ij} for each corner of the vehicle, we shall solve the observer synthesis problem (5.24) at $\rho^{ij} = \underline{F_{d_{ij}}}$, finding $\underline{L^{ij}}$, and at $\rho^{ij} = \overline{F_{d_{ij}}}$, finding $\overline{L^{ij}}$. Finally, our gain matrix $L^{ij}(\cdot)$ is given by:

$$L^{ij}(\rho^{ij}) = \left(\frac{\rho_{max}^{ij} - \rho^{ij}}{\rho_{max}^{ij} - \rho_{min}^{ij}}\right).\underline{L^{ij}} + \left(\frac{\rho^{ij} - \rho_{min}^{ij}}{\rho_{max}^{ij} - \rho_{min}^{ij}}\right).\overline{L^{ij}} \quad (5.28)$$

5.4.3 Validation of Proposed *FDI* Scheme

To finalize this section of this work, we shall present some simulation results to prove the proposed fault identification and diagnosis scheme is accurate. The validation simulation is detailed from here on, considering a single corner of a vehicle (front-right). The indexes $i - j$ are omitted for simpler notation purposes.

For goals of simulation, we shall use small sinusoidal road profile $w(t)$, that could represent a series of bumps for a vehicle running on a dry road at constant speed. In terms of the expected damper force, which is computed with the use of equation (5.6), the manipulated *PWM* signal $d_c(t)$ is taken as a series of steps, to simulate changes upon the damping coefficient $c(\cdot)$. This is shown in figure 54.

The simulated vehicular suspension system is initially considered close to its origin (this is, $x(0) \neq 0$), and the initial conditions on $w(t)$ are also non-null. The suspension damper is initially fault-less ($\alpha = 1$). An additive (high-frequency) measurement noise is added on each measured output $y(t)$, in order to better represent a real situation.

As explained, the information used on the dynamics of each road profile disturbance $w(t)$ is considered to be provided by a road identification scheme, prior to the proposed Fault Detection and Identification structure. For the following simulation results, the disturbance model A_{mw} is different than the disturbance's dynamic behaviour, to induce a modelling error and to check if this error is overlapped by the robustness of the H_2 extended observer approach. This modelling error is detailed on equation (5.29).

$$A_{mw}^{\text{real}} = \begin{bmatrix} 0 & -2.4674 \\ 4 & 0 \end{bmatrix} \qquad (5.29)$$

$$A_{mw}^{\text{used}} = \begin{bmatrix} 0 & -2.5 \\ 3 & 0 \end{bmatrix}$$

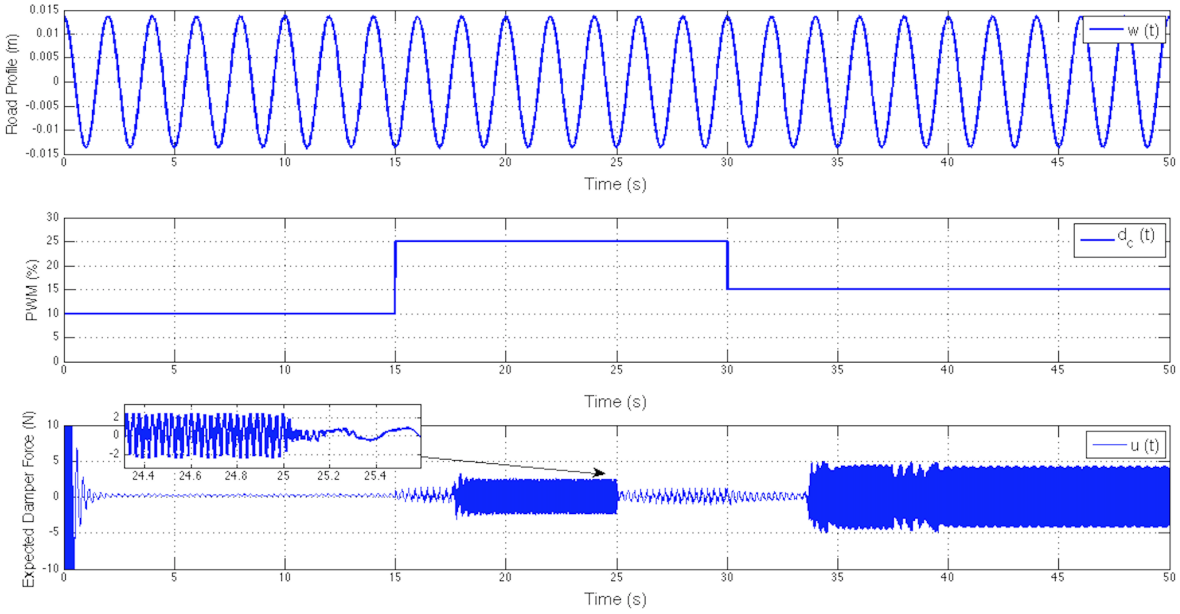

Figure 54 – Simulation Scenario

For these simulation results, we consider a sequence of steps as the loss of effectiveness fault. This can represent, for instance, a successive oil leakage scenario. At $t = 13\,\text{s}$, α decreases to 0.735. This is done once again at $t = 25\,\text{s}$, when the loss of effectiveness fault α decreases to 0.375. Finally, at $t = 37\,\text{s}$, α decreases to 0.275. The estimation $\hat{\alpha}$ is seen in figure 55, in comparison with the actual value of α. This is a satisfactory simulation

result, for the accurateness of the approach proposed herein is very strong. In table 10, we see the used parameters for the computation of the damper force F_d.

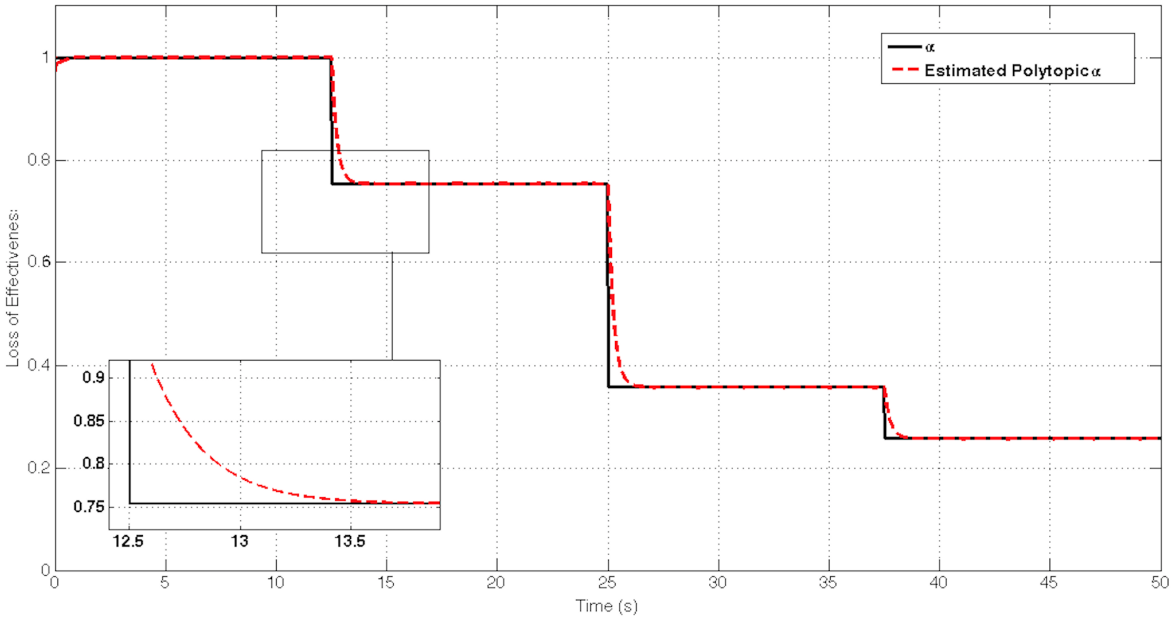

Figure 55 – Simulation of Fault Estimation: *Polytopic LPV* Observer Approach

Table 10 – Semi-Active *ER* Damper Parameters

Parameter	Value	Unit
f_c	6.5137	N
a_1	27.7154	s/m^2
a_2	1.3297	1/m
c_0	37.2670	N/m

As it can be seen, the fault factor α^{ij} is well detected and, thus, the proposed polytopic *LPV FDI* scheme can be used to gather information on actuator faults for a posterior Fault Tolerant Control scheme. This kind of *FDI* scheme has already been discussed and validated in a real test-bench, as details chapter 3.

5.5 Internal Controller: Damper Control

Let us, now, present a proposition for a internal level controller, to track references of desired damper forces. Herein, we shall consider that there is an availability of the following measurements: suspension deflections (z_{def}), suspension deflection velocities ($\dot{z}_{def}$) and damper forces (F_d). Once again, we shall suppress the $i-j$ notation for simplicity, but the following proposition is repeated for each corner of the vehicle.

The use of force control system to handle fast force reference tracking for semi-active dampers is discussed on [2] and other previous works. This is not the main goal of this chapter, but a necessary paradigm.

As we know, the damper force is given by the nonlinear characteristic presented on equation (5.6), considering the controlled portion of the damper force (passive part is already included in the dynamical equation (5.5) given the nominal damping coefficient $c_{0_{ij}}$). Because of this nonlinear condition, it is possible to attain same force levels at different conditions. This is seen in figure 56, where points (i), (ii) and (iii) indicate the same controlled damper force value $F_d(t) = 10\,\text{N}$ (the passive part is set to 0), with different PWM duty-cycles ($d_c(t)$) and average deflection velocity ($\dot{z}_{def}(t)$).

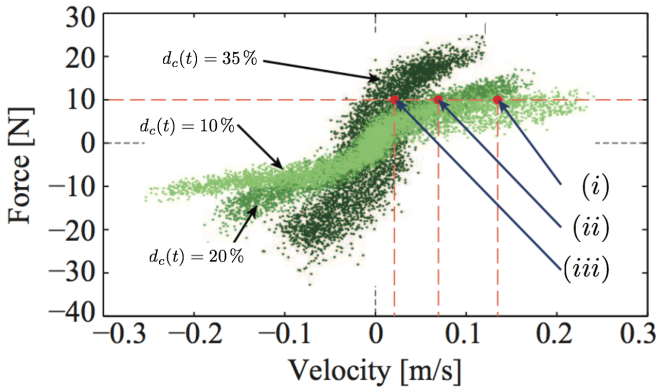

Figure 56 – Force *vs.* Deflection Velocity - Different PWM signals, adapted from [2]

We shall also consider that the controlled and passive parts of the damper force are given, respectively, by:

$$F_{SA}(t) = \mathcal{F}(d_c(t), z_{def}(t), \dot{z}_{def}(t)) \tag{5.30}$$

$$F_{Pass}(t) = \mathcal{H}(\dot{z}_{def}(t)) \tag{5.31}$$

Then, let us consider the compensation nonlinear function $\mathcal{G}$, used to compute a PWM signal $d_c(t)$ so that F_{SA} tracks a desired reference $u^g(t)$. For simplicity, up to now, no saturation constraints or disturbances are considered. Thus, we can take:

$$\mathcal{G}(u^g(t), z_{def}(t), \dot{z}_{def}(t)) = \frac{u^g(t) - F_{Pass}(t)}{f_c.\tanh(a_1.\dot{z}_{def}(t) + a_2.z_{def}(t))} \tag{5.32}$$

Then, let us take the function $\text{sat}(u^\star(t))$ as the saturation of $u^\star(t)$ inside the bounded PWM percentage region $[0\,,\,100]\,\%$.

Let us remark that a dynamical behaviour shall be considered upon the damper's actuation. This means the damper force is not purely statical as described by equation (5.6), but also depends on a second-order (*Laplace*) transfer function, as proposes [113]. This transfer function shall be given by:

$$D(s) = \frac{1}{(\frac{1}{w_d^2}).s^2 + (\frac{2.m_d}{w_d}).s + 1} \tag{5.33}$$

Table 11 details the values used for this transfer function's parameters.

Table 11 – Damper Dynamical Parameters

Parameter	Value
w_d	$20\ \frac{\text{rad}}{\text{s}}$
m_d	1

From this, our proposed internal damper force control scheme is detailed on figure 57. Therein, $\nu(t)$ represents an additive measurement noise, $q(t)$ represents an output (unknown) disturbance, $\text{FF}(t)$ represents the actual full (dynamical) damper force that should track a reference signal $\text{Ref}_{F_d}(t)$. Notice that the transfer function from $u^g(s)$ to $\text{FF}(s)$ is, ideally, equal to $D(s)$.

As of this, a double *PID* controller is added considering the tracking error $e_{F_d}(t)$ and its output $u^g(t)$. This *PID* is used to ensure the rejection of $q(t)$ and high-frequency $\nu(t)$, tuned with classical control techniques, guaranteeing some robustness in terms of phase and gain margins. This *PID*'s transfer-function shall be considered as:

$$\begin{aligned} \frac{u^g(s)}{e_{F_d}(s)} &\equiv \text{PID}(s) \\ \text{PID}(s) &= \left(k_{c_1}.\frac{(\tau_{z_1}s+1)}{s.(\tau_{p_1}.s+1)}\right).\left(k_{c_2}.\frac{(\tau_{z_2}s+1)}{(\tau_{p_2}.s+1)}\right) \end{aligned} \tag{5.34}$$

The parameters k_{c_1}, k_{c_2}, τ_{z_1}, τ_{z_2}, τ_{p_1} and τ_{p_2} are set in order to determine the closed-loop response of this scheme. From the point-of-view of the outer loop, ideally, the closed-loop force control system can be approximated by:

$$\frac{\text{FF}(s)}{\text{Ref}_{F_d}(s)} \approx \frac{1}{(\tau s+1)} \tag{5.35}$$

Remark 10. The gain K_{AW} represents an anti-windup action in order to discharge the integral action whenever there is a saturation of $u^\star(t)$.

This proposed internal control framework is simple enough to be implemented quickly, so that, from the point-of-view of an exterior-layer controller, the response to a damper force references $u_{ij}(t)$ is immediate (considering τ is relatively small enough). In figure 58, we see the outline of the force control system, from the point-of-view of the outer loop.

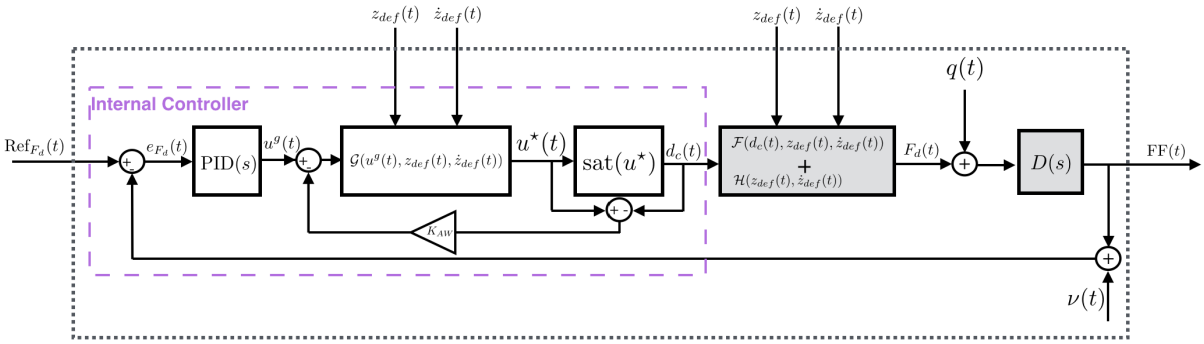

Figure 57 – Proposed Internal Damper Force Controller

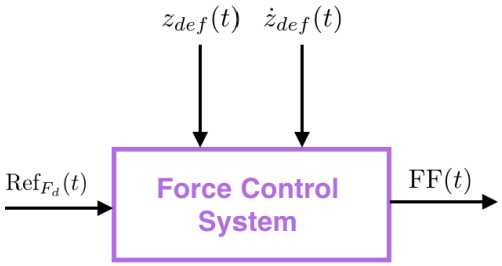

Figure 58 – Outline of Force Control System

5.5.1 Semi-Active Dissipativity Constraints

It is very important to state that some adaptations on the presented Force Control System have to be done in order to strictly guarantee the dissipativity constraints of the semi-active dampers.

A Semi-Active damper must always dissipate energy, which implies that the direction and sense of the force must be the same as the connected mass's velocity. As of this, in a Force *vs.* Velocity graph, only the second and fourth quadrants can be used as of desired forces. This is clearer to be understood as of figure 59.

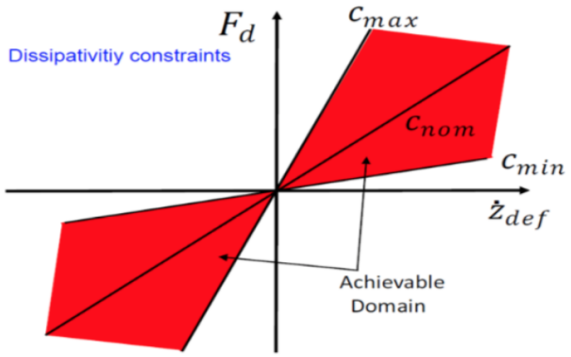

Figure 59 – Achievable Domain of Damper Forces

Let us also state that each semi-active damper has its maximal and minimal damping constraints. If the damper force equation (5.6) is approximated by the following equation

$$F_{d_{ij}}(t) \quad = \quad c_{ij}(\cdot).\dot{z}_{def_{ij}} \tag{5.36}$$

these constraints are converted to:

$$c_{min_{ij}} \quad \leq \quad c_{ij}(\cdot) \leq c_{max_{ij}} \tag{5.37}$$

Then, the force references $\text{Ref}_{F_d}(t)$ that are actually passed onto the Force Control System have to be previously treated in order to abide to the dissipativity contraints. This is done by the use of a Force Clipping block, as presents [2].

If the desired damper force (chosen by the controller, given by $F_{\text{des}}(t)$) is inside the admissible force region $\mathcal{R}_F$ (so to abide to the constraints), this is the reference to be tracked by the Force Control System. Else, the reference is taken as the orthogonal projection of the desired force over the region $\mathcal{R}_F$, given by $F^{\perp}$. Synthetically, this means that the damper force reference is given by:

$$\begin{aligned} \text{Ref}_{F_d} \quad &= \quad \text{Clip}(F_{\text{des}}(t), \dot{z}_{def}) \\ \text{Clip}(F_{\text{des}}(t), \dot{z}_{def}) \quad &:= \quad \begin{cases} F_{\text{des}}(t) & \text{if} \quad F_{\text{des}}(t) \in \mathcal{R}_F \\ F^{\perp}_{\text{des}}(t) & \text{if} \quad F_{\text{des}}(t) \notin \mathcal{R}_F \end{cases} \end{aligned} \tag{5.38}$$

Before showing some simulation results, let us depict the chosen values for the double *PID*'s parameters and the closed-loop gain and phase margins. These values and margins are seen in tables 12 and 13, respectively.

Table 12 – Double *PID*: Parameters

Parameter	Value
k_{c_1}	3.1058167
τ_{z_1}	0.0107 s
τ_{p_1}	$0.33\,10^{-3}$ s
k_{c_2}	1000
τ_{z_2}	0.0118 s
τ_{p_2}	$0.33\,10^{-3}$ s

Table 13 – Closed-Loop Margins

Margin	Value
Gain Margin M_K	34.78
Phase Margin M_ϕ	44.3568 ^{o}

5.5.2 Simulation Results

In order to asses the effectiveness of the proposed control approach, let us present some simple simulation results of this scheme. A simulation scenario using data $(z_{def}(t), \dot{z}_{def}(t))$ from a real mechatronic testbed (see [6]) is presented below, in figure 60.

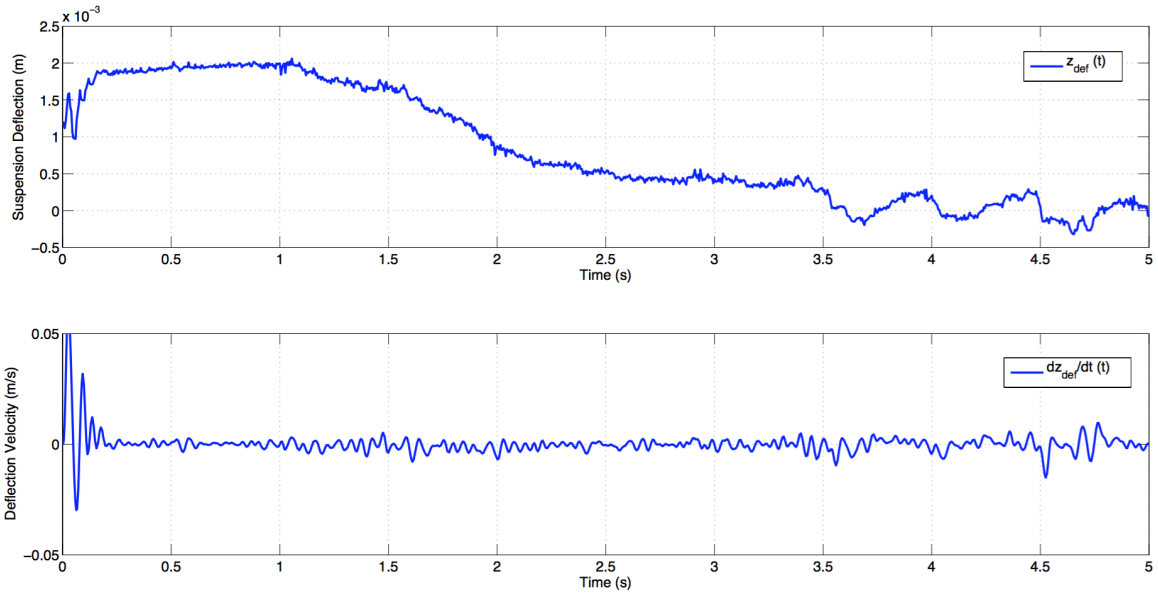

Figure 60 – Internal Damper Force Control System: Simulation Scenario

In figure 61, we can see this proposed internal Force Control System (*FCS*) tracking a reference of 20 N of force and the rejection of an additive output load disturbance of −3 N, at $t = 2.5$ s. Notice that $q(t)$ is a step signal and a high-frequency noise $\nu(t)$ was added to the loop (and is well rejected). The response time of this internal loop, as it can be seen, is approximately 0.05 s, which means this *FCS* can be approximate by the transfer function in equation (5.35), with $\tau = 0.015$ s.

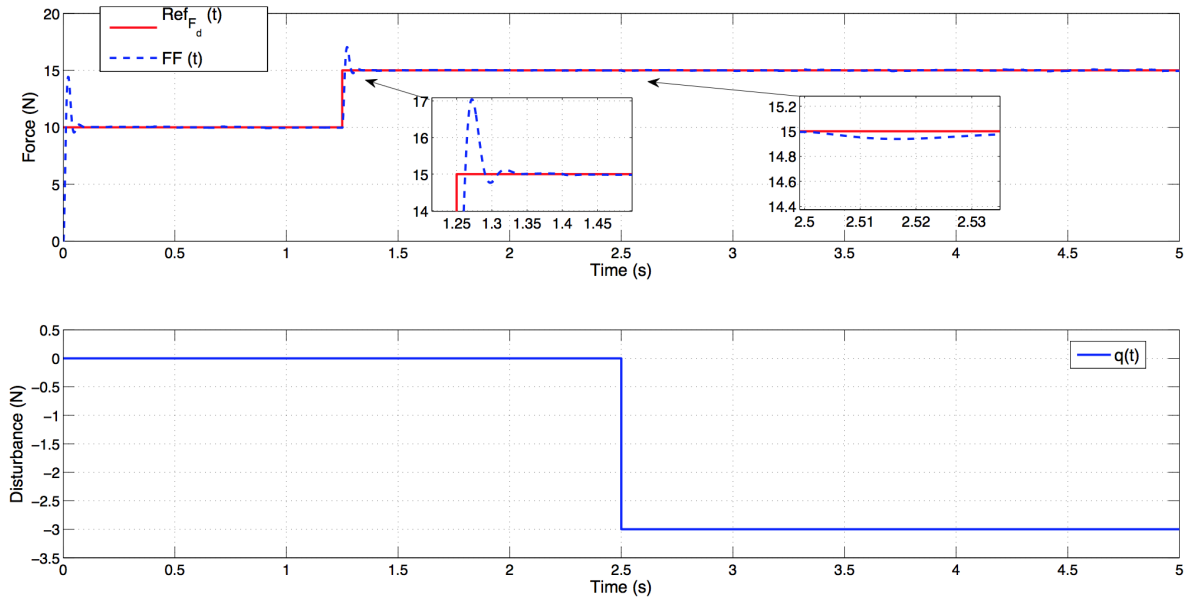

Figure 61 – Internal Damper Force Control System: Reference Tracking and Disturbance Rejection

Remark 11. Notice that, as the system's response shall be approximate by a first order dynamic, a filter can be added in order to reduze the overshoot due to reference changes.

Finally, the respective control signals $u^g(t)$ (LTI control signal), $u^\star(t)$ (nonlinear compensation signal) and $d_c(t)$ (final control law) are seen on figure 62, compared with the tracking error $e_{F_d}(t)$. Remark that $u^g(t)$ stabilizes as the tracking error $e_{F_d}(t)$ converges to zero. The saturation law implied on $u^\star(t)$ is sometimes attained and the anti-windup gain K_{AW} unloads the integral action so that $u^\star(t)$ leaves the saturated mode.

5.6 Proposed Robust *LPV-*H_∞ Fault Tolerant Controller

This section presents the main interest of this chapter's study: the design of an efficient (and robust) Fault Tolerant Control scheme considering actuator loss of effectiveness fault for the control of a full vehicle suspension system. Herein, for obvious reasons, the considered model is the fault-prone FVV model, presented beforehand on (5.18), considering the depicted states (5.9), measured outputs (5.11), disturbances (5.10) and control inputs (5.7).

Firstly, let us remember that, in order to enhance a vehicle's driving performance aiming road handling and ride comfort, one should take special care with the vehicle's suspension system. The main goal of a vehicle suspension control is to isolate the body from the road disturbances, without deteriorating road handling. These two objectives can be referred to as *comfort performance* and *handling performance*, respectively, and can be

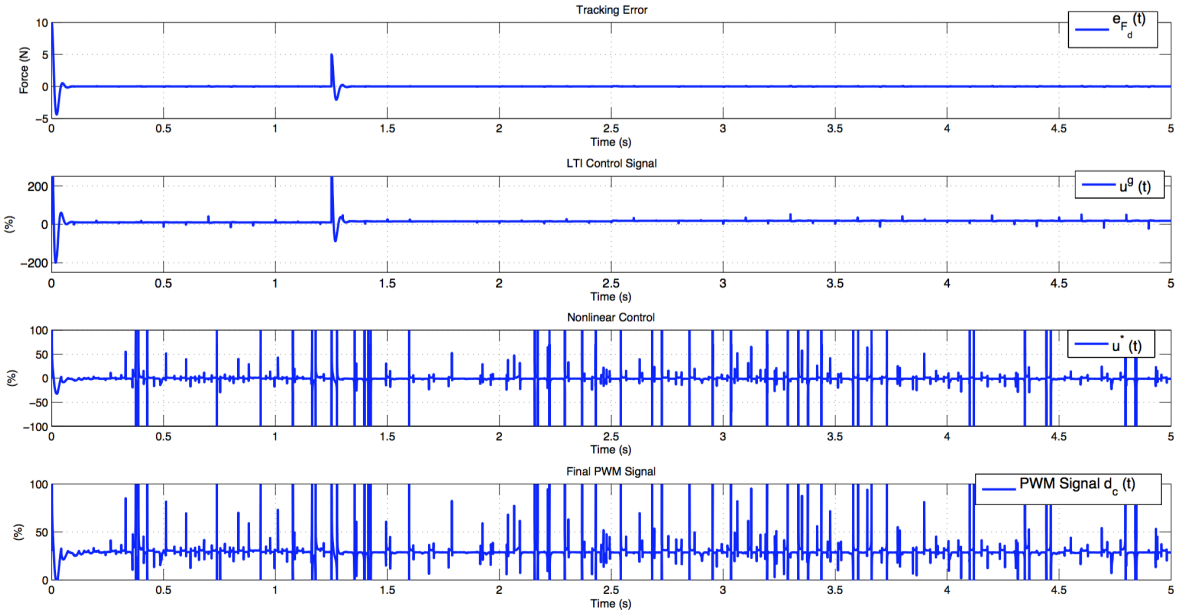

Figure 62 – Simulation of Internal Damper Force Control Loop: Control Signals

described through the vehicle's *COG* acceleration (given by $\ddot{z}_s$) and roll angle (given by θ), as seen on [89].

For control design purposes, let us consider two perfomance indexes, with respect to each control objective: $J_{comfort} = \int_0^\tau \ddot{z}_s^2(t)dt$ and $J_{handling} = \int_0^\tau \theta^2(t)dt$, where τ represents a given time interval. Let us remark that it is well-known that (physically) these two objectives are conflicting. For this reason, our control method must take into account a suitable trade-off between these performance indexes.

As of this, our control approach will be based on the H_∞ control framework. This means this work aims to solve the following problem:

Definition 5.3. Find a controller $C(\cdot)$, which, based on the information of some measured output y (as of equation (5.11)), generates a control signal u (as of equation (5.7)) that counteracts the influence of the disturbances w (as of equation (5.10)) on some controlled outputs z, thereby minimizing the closed-loop H_∞ norm from w to z.

As the control objectives depend on the vehicle's chassis acceleration and roll angle, we shall consider our controlled outputs as:

$$z(t) = \left[\begin{array}{ccc} z_{\ddot{z}_s}(t) & z_\theta(t) & z_u(t) \end{array} \right]^T \tag{5.39}$$

$$z(t) = E.x(t) + F_1.w(t) + F_2(\text{diag}\{\alpha_{ij}\}).u(t) \tag{5.40}$$

$$z_{\ddot{z}_s}(t) = W_{\ddot{z}_s}(s).\ddot{z}_s(s) \tag{5.41}$$

$$z_\theta(t) = W_\theta(s).\theta(s) \tag{5.42}$$

$$z_u(t) = W_u(s).u(s) \tag{5.43}$$

where W_u, $W_{\ddot{z}_s}$ and W_θ are adequate weighting functions, soon to be detailed, the matrices E and F_1 are constant and F_2 is dependent on collection of fault factors α_{ij}, likewise to the matrix B_2 in (5.18). The controlled output $z_u(t)$ is to constrain the controlled damper force by the FTC controller.

From this point forward, let us remark that the control signal u actually determines set-points to the internal force control system, described on the previous section. As the transfer function seen on (5.35) is adequately fast, we shall assume that, at this control level, the reference tracking is perfect and instantaneous (for $\tau << 1\,\mathrm{s}$). The faults occur *a posteriori* to the Force Control System, although the measured force $FF(t)$ is faulty but the reference shall be corrected by the fault tolerant controller scheme.

Considering the paradigm of actuator loss of effectiveness faults, that imply on each α_{ij}, as explained on section 5.4, we need to solve the described H_∞ control problem for fault-less and fault-prone situations (at any value of each α_{ij}, inside their respective bounded sets). As of this, the achieved controller $C(\cdot)$ has to be autonomously reconfigured with the information form the prior FDI scheme.

In figure 63, we see the outline of the studied Fault Tolerant Control problem, where, once again, the notation ν is used to represent measurement noise.

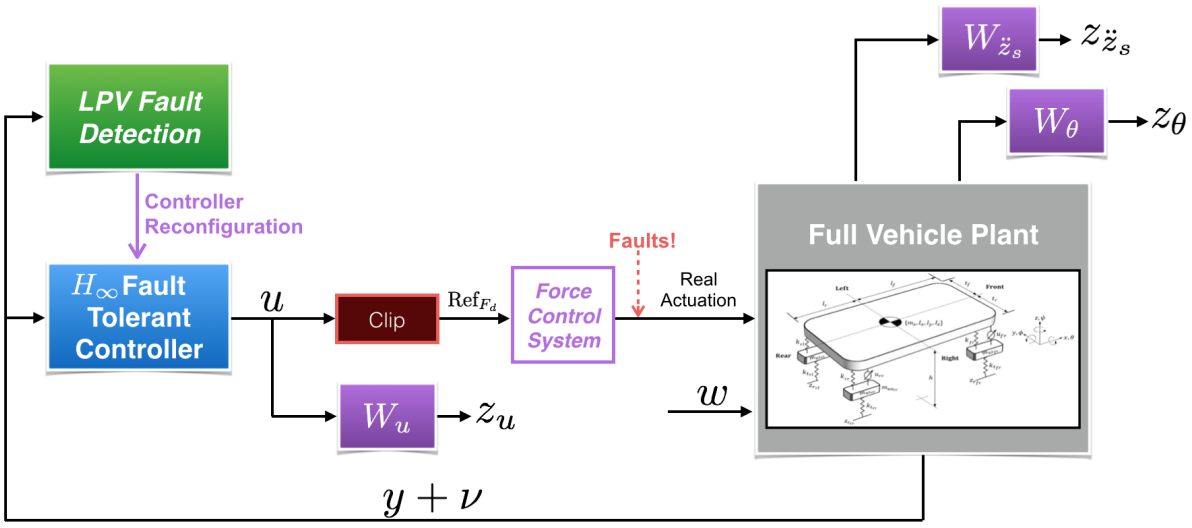

Figure 63 – Outline of Studied Fault Tolerant Control Problem

Remark 12. Notice that the velocity of the FDI scheme might influence the closed-loop dynamics. As of this, for the controller synthesis, this is ignored, supposing that each fault is perfectly detected. Further on, in the results analysis, this is taken into account. Note, nonetheless, that the convergence speed of the proposed FDI scheme, as seen in figure 55, is relatively small (around 1 s).

5.6.1 *LPV* Problem Solution

To treat this H_∞, problem, we should remark that the studied faulty system seen in equation (5.18) can be represented in a polytopic form, as this systems has an affine dependence on the fault factors α_{ij} and these are assumed to be bounded within the following set:

$$\{\mathcal{K}_\alpha \subset \mathbb{R}^4 \,||\, \mathcal{K}_\alpha \;=\; [0\,,\,1]\times[0\,,\,1]\times[0\,,\,1]\times[0\,,\,1]\} \tag{5.44}$$

So, the faulty full vertical vehicle system, augmented with controlled outputs z, can be re-written as:

$$\sum_{\text{Full Veh.}}^{LPV}(\alpha) \;:=\; \sum_{k=1}^{\mathcal{Z}}\beta^k(\alpha).\left[\begin{array}{c|c|c} A & B_1 & B_2^k \\ \hline C & D_1 & D_2^k \\ \hline E & F_1 & F_2^k \end{array}\right] \tag{5.45}$$

with

$$\sum_{k=1}^{\mathcal{Z}}\beta^k(\alpha) \;=\; 1 \tag{5.46}$$

$$\beta^k(\alpha) \;>\; 0 \tag{5.47}$$

where the vector of faults α (as of equation (5.49)) evolves inside a polytope $\mathcal{L}_p$ defined by $\mathcal{Z} = 2^4$ vertices. Notice that the *LTI* system (5.48) corresponds to the *LPV* system frozen at vertex $k \in \mathcal{Z}$.

$$\sum_{\text{Full Veh.}}^{k} \;:=\; \left[\begin{array}{c|c|c} A & B_1 & B_2^k \\ \hline C & D_1 & D_2^k \\ \hline E & F_1 & F_2^k \end{array}\right] \tag{5.48}$$

$$\alpha \;=\; \left[\begin{array}{cccc} \alpha_{fr} & \alpha_{fl} & \alpha_{rl} & \alpha_{rr} \end{array}\right]^T \tag{5.49}$$

Finally, the H_∞ Fault Tolerant controller $C(\cdot)$ can be designed considering a convex sum of $\mathcal{Z}$ controllers, solved at each vertex k of the described polytope $\mathcal{L}_p$. This is:

$$C(\alpha, s) \;=\; \sum_{k=1}^{\mathcal{Z}}\beta^k(\alpha).C^k(s) \tag{5.50}$$

Notice that this controller shall reconfigure itself autonomously, as desired, due to variations on each loss of effectiveness factor α_{ij}.

5.6.2 H_∞ Problem Solution

Then, to finalize the *LPV-FTC* framework design, one has to solve the described H_∞ control problem at each vertex k of the polytope defined by α, finding each $C^k(s)$.

Let us, now, present the Generalized H_∞ Control Problem Formulation, commonly named as the $P-K$ form. This is depicted in figure 64, where P^k is the generalized plant, containing the actual plant and the chosen weights, see equation (5.51). Notice that, therein, $w(t)$ contains the road profile disturbances and, also, the measurement noise $\nu(t)$. Therein, $W_w(s)$ is a weighting function considered upon the road profile disturbances in order to *inform* the controller, at least, the amplitude of this disturbance (normally given in mm).

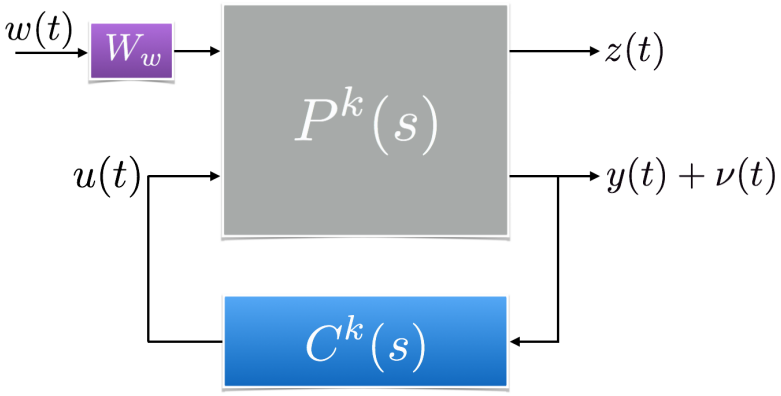

Figure 64 – P-K Generalized Formulation

$$\begin{bmatrix} z(t) \\ y(t)+\nu(t) \end{bmatrix} = P^k . \begin{bmatrix} \text{col}\{z_{r_{ij}}(t)\} \\ \nu(t) \\ u(t) \end{bmatrix} \tag{5.51}$$

Now, the controller $C^k(s)$ is to be found for the system P^k such that, given γ_∞,

$$\|\mathcal{F}_l(P^k, C^k)\|_\infty < \gamma_\infty \tag{5.52}$$

where the operator $\mathcal{F}_l$ represents the lower Linear Fractional Transformation, see [33].

The solution to this problem can be found by the use of Linear Matrix Inequalities, as presents the following lemma.

Lemma 5.4. A dynamical *LPV* output feedback controller of the following form:

$$\begin{bmatrix} \dot{x}_c(t) \\ u(t) \end{bmatrix} = \begin{bmatrix} A_c(\alpha) & B_c(\alpha) \\ C_c(\alpha) & D_c(\alpha) \end{bmatrix} . \begin{bmatrix} x_c(t) \\ y(t)+\nu(t) \end{bmatrix} \tag{5.53}$$

defined inside the polytope $\mathcal{L}_p$, which is LTI when frozen at each of the polytope's vertex k, as of:

$$C^k(s) \;:=\; \left[\begin{array}{c|c} A_c^k & B_c^k \\ \hline C_c^k & D_c^k \end{array}\right] \tag{5.54}$$

has $x_c(t)$ as internal controller states and can solve the LPV/H_∞ control problem defined on 5.3 and given explicitly by equation (5.52). Remark that herein the general case is solved, with linear parameter variations upon all matrices A to F_2.

The resulting closed-loop system, also denoted through the use of the Linear Fractional Transformation (LFT) is given, thus, by:

$$\left[\begin{array}{c} \dot{\xi}(t) \\ z(t) \end{array}\right] \;=\; \left[\begin{array}{cc} \mathcal{A}(\alpha) & \mathcal{B}(\alpha) \\ \mathcal{C}(\alpha) & \mathcal{D}(\alpha) \end{array}\right].\left[\begin{array}{c} \xi(t) \\ w(t) \end{array}\right] \tag{5.55}$$

where these internal LPV matrices are given by:

$$\mathcal{A} \;=\; \left[\begin{array}{cc} A(\alpha) + B_2(\alpha).D_c(\alpha).C(\alpha) & B_2(\alpha).C_c(\alpha) \\ B_c(\alpha).C(\alpha) & A_c(\alpha) \end{array}\right] \tag{5.56}$$

$$\mathcal{B} \;=\; \left[\begin{array}{c} B_1(\alpha) + B_2(\alpha).D_c(\alpha).D_1(\alpha) \\ B_c(\alpha).D_1(\alpha) \end{array}\right] \tag{5.57}$$

$$\mathcal{C} \;=\; \left[\begin{array}{cc} E(\alpha) + F_2(\alpha).D_c(\alpha).C(\alpha) & F_2(\alpha).C_c(\alpha) \end{array}\right] \tag{5.58}$$

$$\mathcal{D} \;=\; F_1(\alpha) + F_2(\alpha).D_c(\alpha).D_1(\alpha) \tag{5.59}$$

Then, the dynamical output feedback controller $C(s,\alpha)$, of the form presented on equation (5.53), that solves the LPV/H_∞ control problem is obtained by solving the following LMIs in $(X(\alpha), Y(\alpha), \breve{A}(\alpha), \breve{B}(\alpha), \breve{C}(\alpha), \breve{D}(\alpha))$, while minimizing γ_∞:

$$\left[\begin{array}{cccc} M_{11} & (\star)^T & (\star)^T & (\star)^T \\ M_{21} & M_{22} & (\star)^T & (\star)^T \\ M_{31} & M_{31} & M_{33} & (\star)^T \\ M_{41} & M_{41} & M_{43} & M_{44} \end{array}\right] \;\prec\; 0 \tag{5.60}$$

$$\left[\begin{array}{cc} X & \mathbb{I} \\ \mathbb{I} & Y \end{array}\right] \;\succ\; 0 \tag{5.61}$$

where,

$$\begin{aligned}
M_{11} &= A(\alpha).X(\alpha) + X(\alpha).A^T(\alpha) + \frac{\partial X(\alpha)}{\partial \alpha}.\dot{\alpha} && (5.62)\\
&+ B_2(\alpha).\breve{C}(\alpha) + \breve{C}^T(\alpha).B_2^T(\alpha)\\
M_{21} &= \breve{A} + A^T(\alpha) + C^T(\alpha).\breve{D}^T(\alpha).B_2^T(\alpha) && (5.63)\\
M_{22} &= Y(\alpha).A(\alpha) + A^T(\alpha).Y(\alpha) + \frac{\partial Y(\alpha)}{\partial \alpha}\dot{\alpha} + \breve{B}(\alpha).C(\alpha) + C^T(\alpha).\breve{B}^T(\alpha) && (5.64)\\
M_{31} &= B_1^T(\alpha) + D_1^T(\alpha).\breve{D}^T(\alpha).B_2^T(\alpha) && (5.65)\\
M_{32} &= B_1^T(\alpha).Y(\alpha) + D_1^T(\alpha).\breve{B}^T(\alpha) && (5.66)\\
M_{33} &= -\gamma_\infty.\mathbb{I} && (5.67)\\
M_{41} &= E(\alpha).X(\alpha) + F_2(\alpha).\breve{C}(\alpha) && (5.68)\\
M_{42} &= E(\alpha) + F_2(\alpha).\breve{D}.C(\alpha) && (5.69)\\
M_{43} &= F_1(\alpha) + F_2(\alpha).\breve{D}.D_1^T(\alpha) && (5.70)\\
M_{44} &= -\gamma_\infty.\mathbb{I} && (5.71)
\end{aligned}$$

Then, the controller reconstruction is obtained by the following equivalent transformation, considering $\frac{\partial X(\alpha)}{\partial \alpha}.\dot{\alpha} = 0$ and $\frac{\partial Y(\alpha)}{\partial \alpha}.\dot{\alpha} = 0$:

$$\left\{\begin{array}{rcl}
D_c(\alpha) &=& \breve{D}(\alpha)\\
C_c(\alpha) &=& (\breve{C}(\alpha) - D_c(\alpha).C(\alpha).X(\alpha)).M^{-T}(\alpha)\\
B_c(\alpha) &=& N^{-1}(\alpha).(\breve{B}(\alpha) - Y(\alpha).B_2(\alpha).D_c(\alpha))\\
A_c(\alpha) &=& N^{-1}(\alpha).(\breve{A} - Y(\alpha).A(\alpha).X(\alpha) - Y(\alpha).B_2(\alpha).D_c(\alpha).C(\alpha).X(\alpha)\\
&-& N(\alpha).B_c(\alpha).C(\alpha).X(\alpha) - Y(\alpha).B_2(\alpha).C_c(\alpha).M^T(\alpha)).M^{-T}(\alpha)
\end{array}\right. \quad (5.72)$$

where $M(\alpha)$ and $N(\alpha)$ are defined so that $M(\alpha).N^T(\alpha) = \mathbb{I} - X(\alpha).Y(\alpha)$. This can be solved through a singular value decomposition and the use of a *Cholesky* factorization.

Proof. This lemma is an adaptation (addition of some relaxations) of the *Bounded Real Lemma* and proof is immediate from what is seen in [114]. □

Remark 13. The first requirement for the application of this lemma is that there exists no direct energy transfer between input and output. This is, that the generalized plant P must be strictly proper and implies that $D_2 = 0$, which is true for our system, given the measured outputs seen on equation (5.11).

Remark 14. The second and final requirement for the application of this lemma is that the input and output matrices ought to be paramater independent. This is: matrices $\begin{bmatrix} B_2(\alpha) & F_2(\alpha) \end{bmatrix}$ and $\begin{bmatrix} C(\alpha) & D_1(\alpha) \end{bmatrix}$ must be constant.

Remark 15. This second requirement is not fulfilled for our studied system. A simple solution to overcome this problem, then, consists in filtering the input and/or output through strictly proper transfer functions. This is exemplified and detailed in [19].

Remark 16. Once again, as the *LPV* problem studied herein is polytopic, defined by the polytope $\mathcal{L}_p$, then the lemma above has to be applied at each of its vertex $\mathcal{Z}$, with the scheduling parameter vector α frozen. Then, the full controller is given as of equation (5.50). In order to ensure the global stability, each of these controllers (at the frozen vertex) must share the same *Lyapunov* function (quadratic stability). This means that the controllers found are stabilizing the entire set formed by the system's polytope $\mathcal{L}_p$.

5.6.2.1 Choice of Weighting Functions

Let us now depict the methodology used to choose appropriate weighting functions $W_{\ddot{z}_s}(s)$, $W_\theta(s)$ and $W_u(s)$.

Firstly, let us present the frequency response plots for $\ddot{z}_s(j.w)$ and $\theta(j.w)$ in the case of purely passive suspension systems - taking the controlled part of the damper force as null and keeping only the nominal passive part (given by $c_{0_{ij}}.\dot{z}_{def_{ij}}$), bare in mind that the suspension force is considered to be given by equation (5.5), neglecting dynamical behaviour described in section 5.5.

The following results consider the use of the *FVV* model, as presented in the first sections of this chapter, considering equation (5.8). These plots consider the maximal values for **singular value decomposition** of $\ddot{z}_s(j.w)$ and $\theta(j.w)$, considering only the effect of the road profile disturbance. Remark that the proposed controller has the goal to minimize the chassis' acceleration ($\ddot{z}_s$) and the vehicle's roll motion (angle, θ) in order to enhance comfort and handling performances, respectively. These performances are affected by the external road profile (disturbance to the system) and, with the use of the proposed controller, should be enhanced.

The parameters used for the computation of the *FVV* model consider those of *INOVE Soben-Car* experimental platform, present in the facilities of *gipsa-lab*, allows the user to deal with several configurations and use cases (see full details on [6]). Figure 65 shows the outline of this test-bench.

Figure 65 – *INOVE Soben-Car* Test-Bench

On this plant, the Semi-Active suspension system involves four Electro-Rheological (ER) dampers which have a force range of $\pm 50\,\mathrm{N}$. These dampers are adjusted using a controlled voltage inside the range of $[0\,,\,5]\,\mathrm{kV}$, generated by amplifier modules. The control input for these modules are PWM signals at $25\,\mathrm{kHz}$. On terms of capturing the vehicle's behaviour, this testbed is equipped with a wide variety of sensors and can accurately measure the chassis' acceleration, given by $\ddot{z}_s(t)$, and the vehicle's roll angle, given by $\theta(t)$.

Finally, in figure 66 we see the singular values decomposition frequency response for the chassis' acceleration, and in figure 67, the *sigma*-plot for the roll angle.

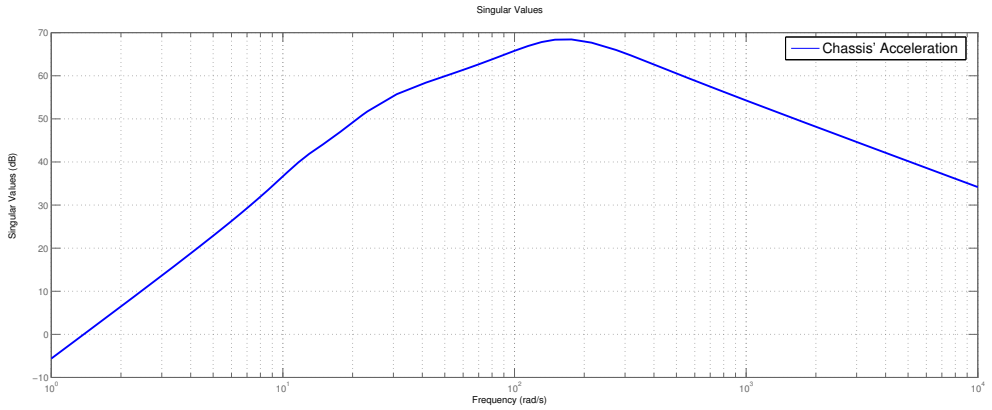

Figure 66 – Frequency Response: Chassis' Acceleration $\ddot{z}_s(j.w)$

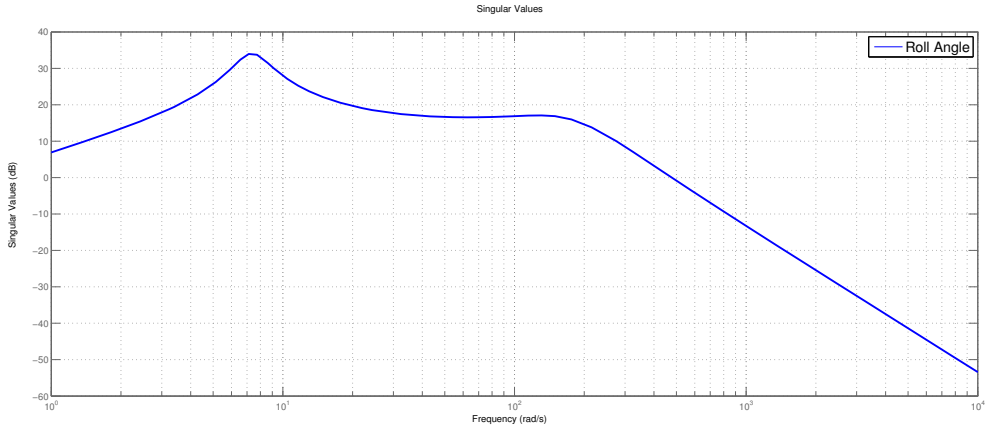

Figure 67 – Frequency Response: Roll Angle $\theta(j.w)$

Now, as we want to choose weighting functions $W_{\ddot{z}_s}(s)$ and $W_\theta(s)$ in order to minimize, respectively, $\ddot{z}_s(s)$ and $\theta(s)$, we shall define them in order to reduce the peaks present on the *open-loop* response (uncontrolled damper), as seen in the figures above.

As of this, we should remind that our H_∞ control problem resides on guaranteeing that:

$$|\ddot{z}_s(jw)| \leq \frac{1}{|W_{\ddot{z}_s}(jw)|} \ \forall w \Leftrightarrow \|W_{\ddot{z}_s}.\ddot{z}_s\|_\infty \leq 1 \tag{5.73}$$

$$|\theta(jw)| \leq \frac{1}{|W_\theta(jw)|} \ \forall w \Leftrightarrow \|W_\theta.\theta\|_\infty \leq 1 \tag{5.74}$$

$$|u(jw)| \leq \frac{1}{|W_u(jw)|} \ \forall w \Leftrightarrow \|W_u.u\|_\infty \leq 1 \tag{5.75}$$

by the minimization of the H_∞ norm from the disturbances $(w(t))$ to the controlled outputs $(z(t))$, as explained beforehand.

5.6.2.1.1 Weighting Function $W_u(s)$

This weighting function shall be used, mainly, to limit the amplitude of the response of $u(t)$, as it shall be treated as a reference to be tracked by an internal Force Control System, as detailed beforehand.

As of this, we shall define $W_u(s)$ as simple first order transfer function in order to guarantee some low-frequency performances, due to the damper actuation constraints and specifications. This is:

$$\frac{1}{W_u}(s) \equiv \frac{\epsilon_u s + w_u}{s + \frac{w_u}{M_u}} \tag{5.76}$$

where the parameters ϵ_u, w_u and M_u are defined so that:

- there is a better limitation of measurement noises and possible high-frequency modelling errors, with the use of ϵ_u;
- and there is an upper bound on the control signal $u(t)$, with the use of M_u.

This template is detailed on figure 68. The used parameters are seen in table 14.

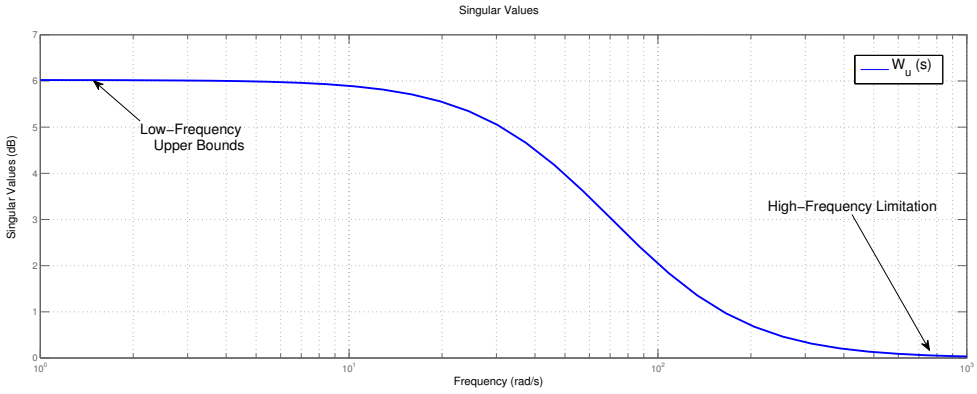

Figure 68 – Template for Control Signal

Table 14 – Weighting Function Parameters: $W_u(s)$

Parameter	Value
ϵ_u	10^{-3}
w_u	$100\ \frac{\text{rad}}{\text{s}}$
M_u	2

5.6.2.1.2 Weighting Function $W_{\ddot{z}_s}(s)$

Firstly lets us remark that the range on frequencies wherein the chassis' acceleration response has the greatest peaks (in terms of the H_∞ norm) is $r_{\ddot{z}_s} = [1\ ,\ 10^4]\ \frac{\text{rad}}{\text{s}}$.

As of this, we shall define $W_{\ddot{z}_s}(s)$ as simple first order transfer function in order to guarantee some robustness and bandwidth specifications. This is:

$$\frac{1}{W_{\ddot{z}_s}}(s) \quad \equiv \quad \frac{\epsilon_{\ddot{z}_s} s + w_{\ddot{z}_s}}{s + \frac{w_{\ddot{z}_s}}{M_{\ddot{z}_s}}} \tag{5.77}$$

where the parameters $\epsilon_{\ddot{z}_s}$, $w_{\ddot{z}_s}$ and $M_{\ddot{z}_s}$ are defined so that:

- there is a rejection of measurement noises and possible high-frequency modelling errors, with the use of $\epsilon_{\ddot{z}_s}$;
- there is a fast enough bandwidth, given by $w_{\ddot{z}_s}$, hence the transient behaviour of the minimization of the effect of the disturbances (road profile);
- and there is a limit on the overshoot of the response, with the use of $M_{\ddot{z}_s}$.

This template is detailed on figure 69. The used parameters are seen in table 15.

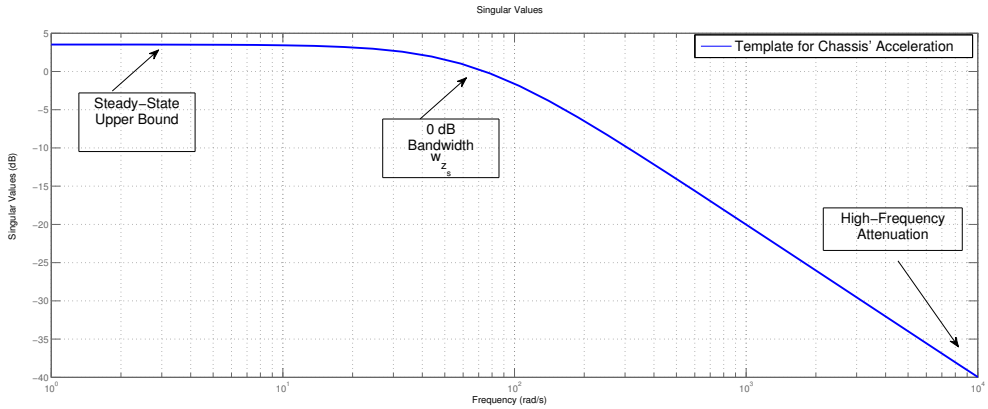

Figure 69 – Template for Chassis' Acceleration

Table 15 – Weighting Function Parameters: $W_{\ddot{z}_s}(s)$

Parameter	Value
$\epsilon_{\ddot{z}_s}$	10^{-3}
$w_{\ddot{z}_s}$	$100\ \frac{\text{rad}}{\text{s}}$
$M_{\ddot{z}_s}$	1.5

5.6.2.1.3 Weighting Function $W_\theta(s)$

Firstly lets us remark that the range on frequencies wherein the roll motion response has the greatest peaks (in terms of the H_∞ norm) is $r_\theta = [1\ ,\ 400]\ \frac{\text{rad}}{\text{s}}$.

As of this, we shall define $W_\theta(s)$ as simple first order transfer function in order to guarantee some robustness and bandwidth specifications. This is:

$$\frac{1}{W_\theta}(s) \quad \equiv \quad \frac{\epsilon_\theta s + w_\theta}{s + \frac{w_\theta}{M_\theta}} \tag{5.78}$$

where the parameters ϵ_θ, w_θ and M_θ are defined so that:

- there is a rejection of measurement noises and possible high-frequency modelling errors, with the use of ϵ_θ;
- there is a fast enough bandwidth, given by w_θ, hence the transient behaviour of the minimization of the effect of the disturbances (road profile);
- and there is a limit on the overshoot of the response, with the use of M_θ.

This template is detailed on figure 70. The used parameters are seen in table 16.

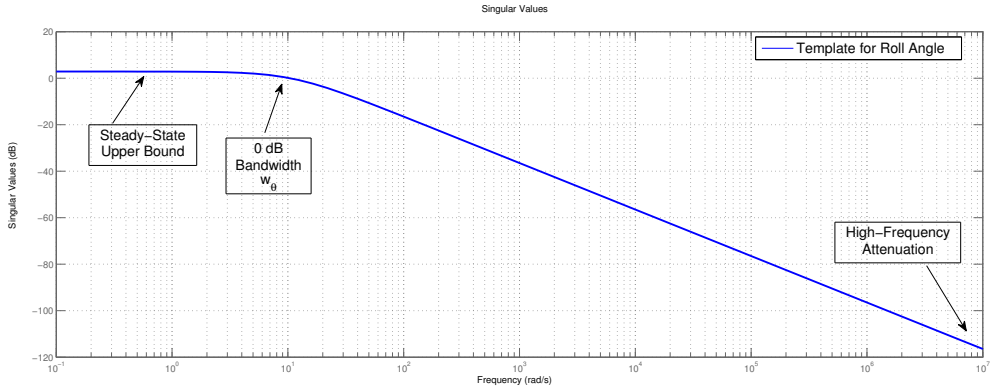

Figure 70 – Template for Roll Motion

Table 16 – Weighting Function Parameters: $W_\theta(s)$

Parameter	Value
ϵ_θ	10^{-7}
w_θ	$15\ \frac{\text{rad}}{\text{s}}$
M_θ	1.39

Finally, in figures 71 and 72 we see, respectively, the comparisons between the real frequency-domain response and the templates.

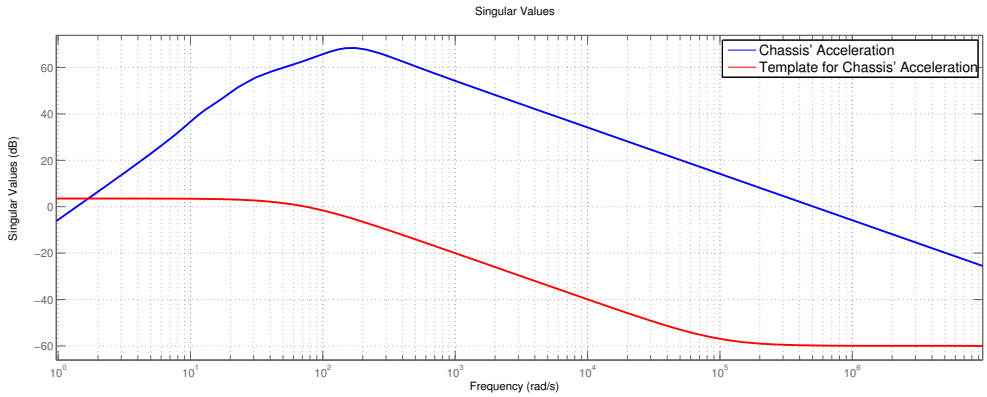

Figure 71 – Chassis' Acceleration: Uncontrolled *vs.* Template

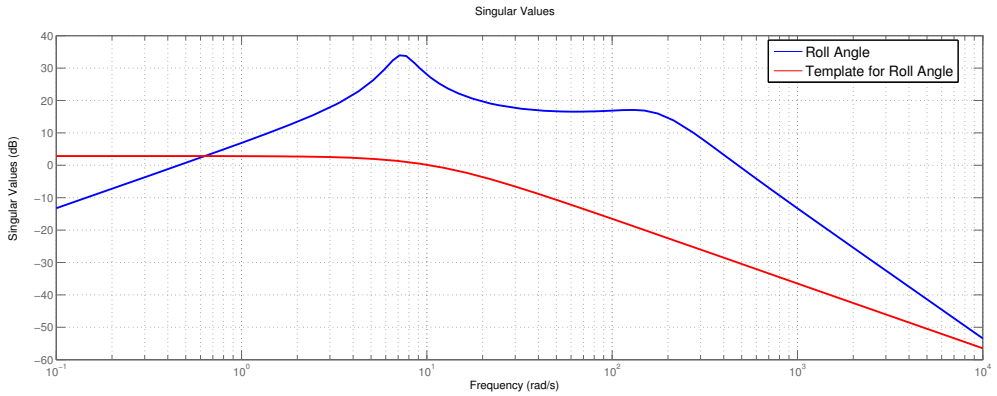

Figure 72 – Roll Angle: Uncontrolled *vs.* Template

5.6.2.2 Controller Synthesis

The proposed H_∞ controller synthesis has to be solved at each vertex of the polytope $\mathcal{L}_p$ using a single Lyapunov matrix function, as seen in lemma 5.4, specifically in the *LMI* (5.60)-(5.61). This can be done with the use of *MATLAB* [7] and *Yalmpi* [91], as proposed by [19].

This synthesis leads us to the solution of the H_∞ Control Problem, as shows equation (5.52), finding a minimal scalar γ_∞ of 0.1.

Let us, then, show the H_∞ frequency plots for the controlled outputs $z(t)$, presented in equation (5.39), compared to their respective Weighting Functions.

Firstly, in figure 73 we see the σ-plot for $u(t)$. As it can be seen, the controller synthesis is able to guarantee that the H_∞ norm of the control signal $u(s)$ is always bounded by the chosen template $W_u(s)$.

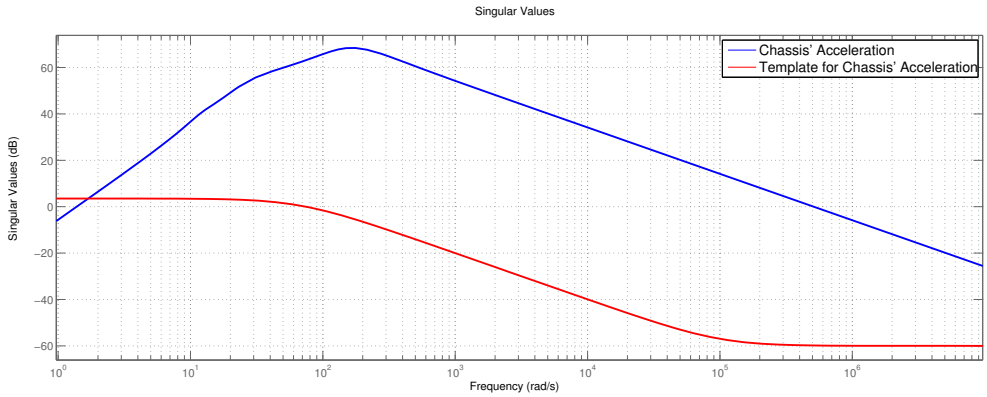

Figure 73 – Final Controller: σ-plot for Control Signal $u(t)$

Then, in figures 74 and 75 we see, respectively, the σ- for $\ddot{z}_s(t)$ (chassis's acceleration) and $\theta(t)$ (roll angle). As it can be seen, the controller synthesis is able to guarantee that the H_∞ norm of these controlled output signals are always bounded by their respectful chosen templates $W_{\ddot{z}_s}(s)$ and $W_\theta(s)$.

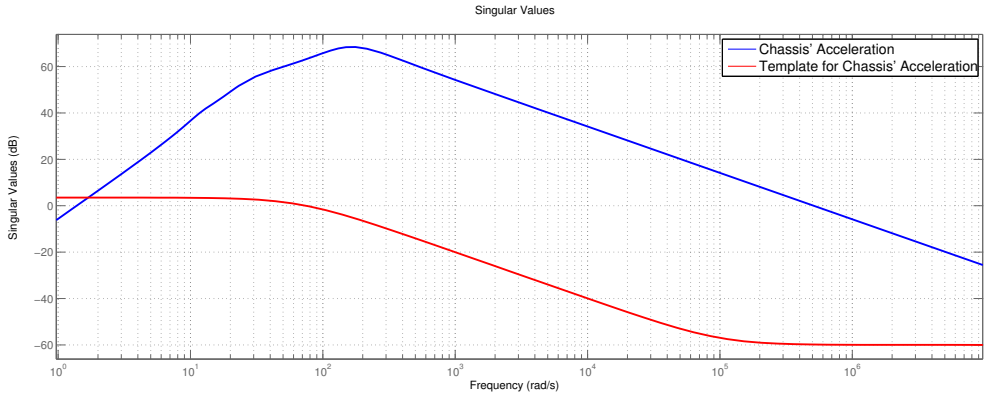

Figure 74 – Final Controller: σ-plot for Chassis' Acceleration $\ddot{z}_s(t)$

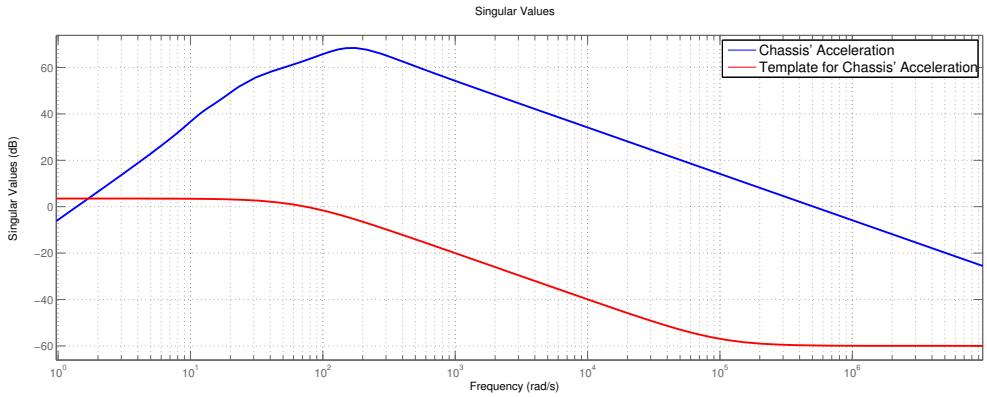

Figure 75 – Final Controller: σ-plot for Roll Angle $\theta(t)$

5.7 Robustness Analysis

The part on robustness analysis has been already partially developed by author. Anyhow, it shall be herein only mentioned as a perspective to be finished in the near future. Nonetheless, avid readers can find theoretical development in Annex A.

5.8 Results and Discussion

Finally, in this section we shall present some simulation results to asses the overall behaviour of the proposed Fault Tolerant Control scheme, as seen in figure 63. Then, we shall discuss these results and conclude on the performance of the proposed control scheme.

On the following results, *LPVFTC* represents the proposed *LPV* H_∞ Fault Tolerant Controller, *HINF* represents a H_∞ Controller solved with the same weighting functions and controlled inputs, but not taking into account the effect of the faults (α_{ij} fixed at 1), and *Unc.* represents the use of purely passive damper, uncontrolled, taking every $d_{c_{ij}}(t)$ as 0. For these results, we should also mention that a high-frequency measurement noise was added to each measured output (y), in order to mimic realistic conditions.

First of all, we have to show the chosen simulation scenario. Let us consider, thus, the scenario of a vehicle running at 120 km/h in a straight line on a dry road, when a first 5 cm bump occurs simultaneously on all wheels, to excite the bounce motion and chassis vibration, a second 5 cm bump occurs afterwards, but only on the left wheels, to cause a roll motion and, finally, a third bump occurs at both front wheels, causing a pitch motion. This road profile is shown in figure 76.

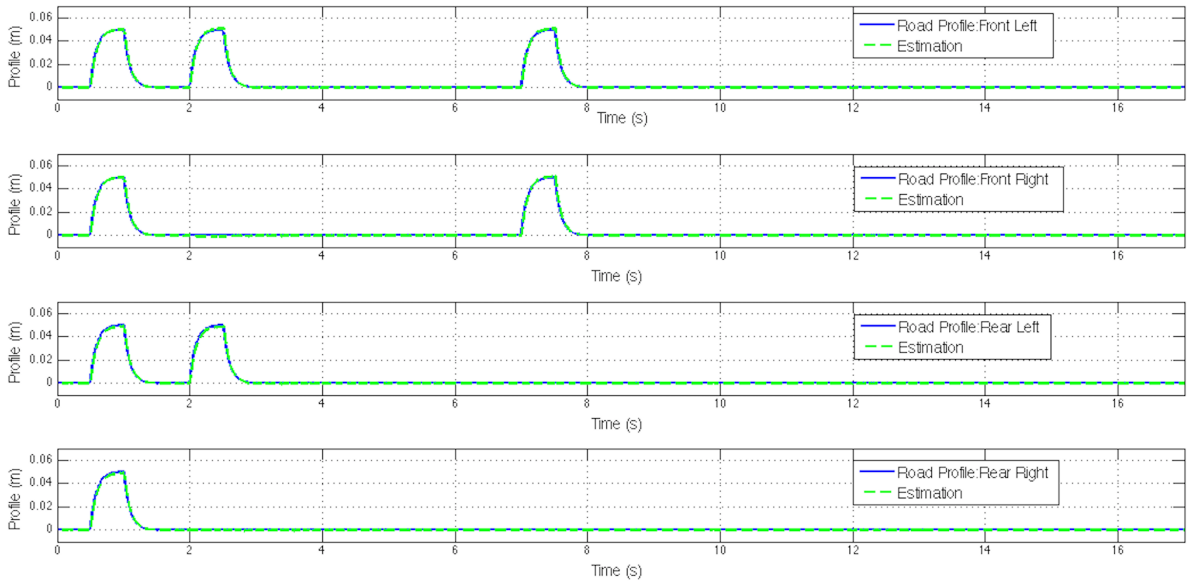

Figure 76 – Simulation Scenario: Road Profile at Every Corner

The final results considering the proposed controller as an *FTC* scheme shall be presented in future works.

5.9 Conclusions

This chapter presented the issue of controlling a full vehicle *semi-active* suspension system, during fault-less and fault-prone situations on the dampers' actuations.

A polytopic *LPV*-based Fault Detection and Diagnosis structure is designed to provide accurate informations on *loss of effectiveness* of each of the vehicle's suspension system's dampers.

An internal controller is designed to track damper force references quickly. Finally, a *LPV*-H_∞ Fault Tolerant Controller is presented, with some performance specifications as to provide a trade-off between the vehicle's comfort and handling performance indexes. An additional robustness analysis was also drawn, considering the structured singular value approach, in order to analyse the proposed controller in the case of parametric uncertainties and, also, sensor faults.

For further works, the author shall finish the simulation results. Also, an interesting theme is to consider the same presented (efficient) control strategies applied to other processes, like the control of energy *Microgrids*.

6 Conclusion

This chapter finally concludes on the work herein presented as an end-of-studies monograph (*Projeto de Final de Curso*, *Projet de Fin d'Études*) supported by the project **PERSYVAL** *LPV4FTC – A Linear Parameter Varying approach for Fault Tolerant Control design*, in collaboration with *CRAN* Nancy and the Academy of sciences of Budapest (*MTA SZTAKI*).

6.1 What Was Done, Effectively

In sum, this work presented:

- As of chapter 2, a thorough literature review was done, providing a full theoretical background for further chapters;
- The issue of Fault Identification of actuator loss of effectiveness faults was considered on chapter 3, wherein three different *LPV* techniques were designed and analysed for *FDI* goals;
- An implementation of a *Real-Time* Model Predictive Control scheme for the Semi-Active suspension control of a Full Vehicle was presented on chapter 4;
- Finally, a full vehicle Fault Tolerant Control was presented and designed on chapter 5, considering an *LPV* approach to deal with actuator faults on each suspension system.

6.2 Comparison to Initial Schedule: *PERSYVAL* Project

Let us, also, compare the results achieved with the initial monograph's objectives, in the context of the *PERSYVAL* Project:

1) As of chapter 3, the author completed the first scheduled goal:

Present and compare Linear Parameter Varying approaches on Fault Estimation for loss of efficiency on **actuators**

2) As of chapter 4, the author completed, then, the second scheduled goal:

Test and develop viable ways for a *real-time* high-complexity Model Predictive Controller for the *Soben-Car* test-bench

It is important to remark that the proposed fast (*Real-Time*) *MPC* was, for now, only tested in simulation. Application to the testbed is soon to be developed.

3) As of chapter 5, the author completed, then, the third scheduled goal:

Present and justify new approaches for Fault Tolerant Control (of Multi-Input Multi-Output systems) in the case of sensor and **actuator** faults

considering the case of several actuator faults, instead of actuator and sensor faults.

4) Finally, the last scheduled task was completed with validation and experimental results presented throughout all chapters:

Present the results of experimental validation of the *Soben-Car* test-bench.

6.3 Scientific Work

Let us point out that the work presented herein enabled the development of some scientific work (in terms of papers and proceedings). These are:

- **Design of a Fast *Real-Time LPV* Model Predictive Control System for Semi-Active Suspension Control of a Full Vehicle**, to be submitted to *International Journal of Control*, First Author;
- **Damper Fault Estimation for Automotive Suspension Systems: An *LPV*-based Extended State Observer Approach**, to be submitted to *Control Engineering Practice*, First Author;
- **Complete Modelling of Electro-Rheological Dampers: A Thorough Analysis for Faultless and Faulty Scenarios**, to be submitted to *Mechanical Systems and Signal Processing*, Co-Author;
- **A Robust *LPV*/H_∞ Approach as Fault Tolerant Control Framework: Application to Full Vehicle Semi-Active Suspension System**, to be submitted to the 9$^{\text{th}}$ *IFAC* Symposion on Robust Control Design, Florianópolis, 2018, First Author.

6.4 Personal Analysis

Writing from the author's point of view: The work developed on *Gipsa-lab* was most pleasurable for me. I was really well received and guided by professors Olivier Sename and Luc Dugard. I hope to have presented some interesting results on *LPV* Control Approaches for further researches. My personal and academic development during this internship was enormous.

6.5 On Future Works

As the author previously worked with renewable energy systems, some topic for further research are:

- LPV (H_∞) Control of the load/charge process of *microgrids* and its connection to the external power grid;
- Detection of faults on renewable *microgrids*;
- Robust Fault Tolerant Control of distributed *microgrids*.

Bibliography

1 JIANG, J.; YU, X. Fault-tolerant control systems: A comparative study between active and passive approaches. *Annual Reviews in control*, Elsevier, v. 36, n. 1, p. 60–72, 2012. Citado 5 vezes nas páginas 9, 41, 42, 44, and 113.

2 VIVAS-LOPEZ, C. A. et al. Force control system for an automotive semi-active suspension. *IFAC-PapersOnLine*, Elsevier, v. 48, n. 26, p. 55–60, 2015. Citado 3 vezes nas páginas 10, 127, and 130.

3 MORATO, M. M. *Study of Different Approaches as Fault Tolerant Control Reconfiguration Techniques*. [S.l.], 2017. Citado 4 vezes nas páginas 23, 42, 43, and 112.

4 FERGANI, S. *Commande Robuste LPV/Hinf Multivariable pour la dynamique véhicule*. Tese (Doutorado) — Université Grenoble Alpes, 2015. Citado na página 24.

5 NGUYEN, M. Q. *LPV approaches for modelling and control of vehicle dynamics: application to a small car pilot plant with ER dampers*. Tese (Doutorado) — Université Grenoble Alpes, 2017. Citado 8 vezes nas páginas 24, 29, 31, 78, 80, 91, 93, and 117.

6 VIVAS-LOPEZ, C. et al. Inove: a testbench for the analysis and control of automotive vertical dynamics. In: *14th International Conference on Vehicle System Dynamics, Identification and Anomalies (VSDIA 2014)*. [S.l.: s.n.], 2014. Citado 5 vezes nas páginas 26, 71, 91, 131, and 139.

7 MATHWORKS. *MATLAB R2017a*. 2017. Citado 5 vezes nas páginas 27, 86, 94, 102, and 145.

8 XPC Target. Citado na página 27.

9 INSTRUMENTS, N. *Data Acquisition Cards*. Citado na página 28.

10 AUBOUET, S.; DUGARD, L.; SENAME, O. Experimental results of an h_∞-observer for an industrial semi-active suspension. *IFAC Proceedings Volumes*, Elsevier, v. 43, n. 7, p. 318–323, 2010. Citado na página 30.

11 ISERMANN, R. *Mechatronic systems: fundamentals*. [S.l.]: Springer Science & Business Media, 2007. Citado 2 vezes nas páginas 30 and 31.

12 SAVARESI, S. M. et al. *Semi-active suspension control design for vehicles*. [S.l.]: Elsevier, 2010. Citado 5 vezes nas páginas 31, 32, 45, 79, and 113.

13 FISCHER, D.; ISERMANN, R. Mechatronic semi-active and active vehicle suspensions. *Control engineering practice*, Elsevier, v. 12, n. 11, p. 1353–1367, 2004. Citado 5 vezes nas páginas 31, 32, 45, 79, and 113.

14 PATTEN, W. et al. Suppression of vehicle induced bridge vibration via hydraulic semi-active vibration dampers. In: *Proceeding of the 1st world conference on structural control*. [S.l.: s.n.], 1994. v. 3, p. 30–38. Citado 4 vezes nas páginas 32, 45, 79, and 113.

15 GILLESPIE, T. D. *Fundamentals of vehicle dynamics*. [S.l.], 1992. Citado na página 33.

16 MILLIKEN, W. F.; MILLIKEN, D. L. *Race car vehicle dynamics*. [S.l.]: Society of Automotive Engineers Warrendale, 1995. Citado na página 33.

17 KIENCKE, U.; NIELSEN, L. *Automotive control systems: for engine, driveline, and vehicle*. [S.l.]: Springer Science & Business Media, 2005. Citado na página 33.

18 ZIN, A. et al. A nonlinear vehicle bicycle model for suspension and handling control studies. In: *Proceedings of the IFAC Conference on Advances in Vehicle Control and Safety AVCS, Genova, Italy*. [S.l.: s.n.], 2004. p. 638–643. Citado na página 34.

19 POUSSOT-VASSAL, C. *Robust multivariable linear parameter varying automotive global chassis control*. Tese (Doutorado), 2008. Citado 3 vezes nas páginas 34, 139, and 145.

20 FERGANI, S. et al. Full vehicle dynamics control based on LPV/h_∞ and flatness approaches. In: IEEE. *Control Conference (ECC), 2014 European*. [S.l.], 2014. p. 2346–2351. Citado na página 34.

21 BOYD, S. P. et al. *Linear matrix inequalities in system and control theory*. [S.l.]: SIAM, 1994. Citado na página 34.

22 DETTORI, M. *LMI techniques for control-with application to a compact disc player mechanism*. Tese (Doutorado) — TU Delft, Delft University of Technology, 2001. Citado 4 vezes nas páginas 34, 49, 85, and 123.

23 TROFINO, A.; COUTINHO, D.; BARBOSA, K. A. *Sistemas Multivariáveis: Uma abordagem via LMIs*. [S.l.]: UFSC, 2003. Citado 5 vezes nas páginas 34, 49, 85, 123, and 124.

24 CHEN, C.-T. *Linear system theory and design*. [S.l.]: Oxford University Press, Inc., 1995. Citado 2 vezes nas páginas 35 and 40.

25 KHALIL, H. K.; GRIZZLE, J. *Nonlinear systems*. [S.l.]: Prentice hall New Jersey, 1996. Citado 2 vezes nas páginas 35 and 40.

26 ISIDORI, A. *Nonlinear control systems*. [S.l.]: Springer Science & Business Media, 2013. Citado na página 35.

27 JR, N. R. S. On newton's method for riccati equation solution. 1974. Citado na página 38.

28 LAVRETSKY, E.; WISE, K. A. Optimal control and the linear quadratic regulator. In: _____. *Robust and Adaptive Control: With Aerospace Applications*. London: Springer London, 2013. p. 27–50. ISBN 978-1-4471-4396-3. Disponível em: <http://dx.doi.org/10.1007/978-1-4471-4396-3_2>. Citado na página 38.

29 BEMPORAD, A. et al. The explicit linear quadratic regulator for constrained systems. *Automatica*, Elsevier, v. 38, n. 1, p. 3–20, 2002. Citado na página 38.

30 MOHAMMADPOUR, J.; SCHERER, C. W. *Control of linear parameter varying systems with applications*. [S.l.]: Springer Science & Business Media, 2012. Citado 2 vezes nas páginas 38 and 114.

31 WU, F. et al. Induced l_2-norm control for LPV systems with bounded parameter variation rates. In: *IEEE conference on Decision and Control*. [S.l.: s.n.], 1997. Citado na página 38.

32 SENAME, O.; GASPAR, P.; BOKOR, J. *Robust control and linear parameter varying approaches: application to vehicle dynamics*. [S.l.]: Springer, 2013. Citado 2 vezes nas páginas 38 and 114.

33 ZHOU, K.; DOYLE, J. C. *Essentials of robust control*. [S.l.]: Prentice hall Upper Saddle River, NJ, 1998. Citado 4 vezes nas páginas 39, 136, 163, and 165.

34 SILVEIRA TITLE = Notas de Aula em Sinais e Sistemas Lineares I, y. . . p. H. B. Citado na página 40.

35 LATHI, B. P. et al. *Linear systems and signals*. [S.l.]: Oxford University Press New York:, 2005. Citado na página 40.

36 WU, F. Control of linear parameter varying systems. 1995. Citado na página 41.

37 BLANKE, M. et al. Fault-tolerant control systems - a holistic view. Elsevier, 1997. Citado 3 vezes nas páginas 41, 43, and 113.

38 LUNZE, J.; RICHTER, J. H. Reconfigurable fault-tolerant control: a tutorial introduction. *European journal of control*, Elsevier, v. 14, n. 5, p. 359–386, 2008. Citado 2 vezes nas páginas 41 and 113.

39 ZHANG, Q.; BASSEVILLE, M.; BENVENISTE, A. *Fault detection and isolation in nonlinear dynamic systems: A combined input-output and local approach*. Tese (Doutorado) — INRIA, 1997. Citado 2 vezes nas páginas 42 and 44.

40 ZHANG, Y.; JIANG, J. Bibliographical review on reconfigurable fault-tolerant control systems. *Annual reviews in control*, Elsevier, v. 32, n. 2, p. 229–252, 2008. Citado na página 43.

41 BLANKE, M.; STAROSWIECKI, M.; WU, N. E. Concepts and methods in fault-tolerant control. In: IEEE. *American Control Conference, 2001. Proceedings of the 2001*. [S.l.], 2001. v. 4, p. 2606–2620. Citado na página 44.

42 PERSIS, C. D.; ISIDORI, A. A geometric approach to nonlinear fault detection and isolation. *IEEE transactions on automatic control*, IEEE, v. 46, n. 6, p. 853–865, 2001. Citado na página 44.

43 HAMMOURI, H.; KINNAERT, M.; YAAGOUBI, E. E. Observer-based approach to fault detection and isolation for nonlinear systems. *IEEE transactions on automatic control*, IEEE, v. 44, n. 10, p. 1879–1884, 1999. Citado na página 44.

44 CHEN, J.; PATTON, R. J. *Robust model-based fault diagnosis for dynamic systems*. [S.l.]: Springer Science & Business Media, 2012. Citado na página 44.

45 GERTLER, J. Fault detection and isolation using parity relations. *Control engineering practice*, Elsevier, v. 5, n. 5, p. 653–661, 1997. Citado na página 44.

46 ISERMANN, R. Supervision, fault-detection and fault-diagnosis methods—an introduction. *Control engineering practice*, Elsevier, v. 5, n. 5, p. 639–652, 1997. Citado na página 44.

47 PATTON, R.; KLINKHIEO, S. LPV fault estimation and FTC of a two-link manipulator. In: *2010 American Control Conference, Baltimore, MD, USA*. [S.l.: s.n.], 2010. p. 4647–4652. Citado 3 vezes nas páginas 44, 76, and 114.

48 OCA, S. de et al. Fault-tolerant control strategy for actuator faults using LPV techniques: Application to a two degree of freedom helicopter. *International Journal of Applied Mathematics and Computer Science*, v. 22, n. 1, p. 161–171, 2012. Citado 2 vezes nas páginas 44 and 114.

49 ZHANG, K.; JIANG, B.; CHEN, W. An improved adaptive fault estimation design for polytopic LPV systems with application to helicopter models. In: IEEE. *Asian Control Conference, 2009. ASCC 2009. 7th.* [S.l.], 2009. p. 1108–1113. Citado 3 vezes nas páginas 44, 76, and 114.

50 ARMENI, S.; CASAVOLA, A.; MOSCA, E. Robust fault detection and isolation for LPV systems under a sensitivity constraint. *International Journal of Adaptive Control and Signal Processing*, Wiley Online Library, v. 23, n. 1, p. 55–72, 2009. Citado 2 vezes nas páginas 44 and 114.

51 LU, B.; WU, F.; KIM, S. Switching LPV control of an $f-16$ aircraft via controller state reset. *IEEE transactions on control systems technology*, IEEE, v. 14, n. 2, p. 267–277, 2006. Citado 2 vezes nas páginas 44 and 115.

52 WU, F. A generalized LPV system analysis and control synthesis framework. *International Journal of Control*, Taylor & Francis, v. 74, n. 7, p. 745–759, 2001. Citado 2 vezes nas páginas 44 and 115.

53 DO, A.-L.; SENAME, O.; DUGARD, L. An LPV control approach for semi-active suspension control with actuator constraints. In: IEEE. *American Control Conference (ACC), 2010*. [S.l.], 2010. p. 4653–4658. Citado 3 vezes nas páginas 44, 79, and 115.

54 EDWARDS, C.; SPURGEON, S. K.; PATTON, R. J. Sliding mode observers for fault detection and isolation. *Automatica*, Elsevier, v. 36, n. 4, p. 541–553, 2000. Citado 4 vezes nas páginas 44, 59, 71, and 76.

55 HROVAT, D. Survey of advanced suspension developments and related optimal control applications. *Automatica*, Elsevier, v. 33, n. 10, p. 1781–1817, 1997. Citado 3 vezes nas páginas 45, 79, and 113.

56 LU, J.; DEPOYSTER, M. Multiobjective optimal suspension control to achieve integrated ride and handling performance. *IEEE Transactions on Control Systems Technology*, IEEE, v. 10, n. 6, p. 807–821, 2002. Citado 3 vezes nas páginas 45, 79, and 113.

57 TUDÓN-MARTÍNEZ, J. C. et al. Adaptive road profile estimation in semiactive car suspensions. *IEEE Transactions on Control Systems Technology*, IEEE, v. 23, n. 6, p. 2293–2305, 2015. Citado 2 vezes nas páginas 47 and 122.

58 TÓTH, R. *Modeling and identification of linear parameter-varying systems*. [S.l.]: Springer, 2010. Citado na página 51.

59 NGUYEN, M. Q.; SENAME, O.; DUGARD, L. A switched LPV observer for actuator fault estimation. *IFAC-PapersOnLine*, Elsevier, v. 48, n. 26, p. 194–199, 2015. Citado 2 vezes nas páginas 51 and 114.

60 BRIAT, C. Convex conditions for robust stabilization of uncertain switched systems with guaranteed minimum and mode-dependent dwell-time. *Systems & Control Letters*, Elsevier, v. 78, p. 63–72, 2015. Citado 4 vezes nas páginas 51, 53, 55, and 58.

61 DAAFOUZ, J.; RIEDINGER, P.; IUNG, C. Stability analysis and control synthesis for switched systems: a switched lyapunov function approach. *IEEE transactions on automatic control*, IEEE, v. 47, n. 11, p. 1883–1887, 2002. Citado na página 51.

62 BRANICKY, M. S. Multiple lyapunov functions and other analysis tools for switched and hybrid systems. *IEEE Transactions on automatic control*, IEEE, v. 43, n. 4, p. 475–482, 1998. Citado na página 51.

63 BRIAT, C.; SEURET, A. Affine characterizations of minimal and mode-dependent dwell-times for uncertain linear switched systems. *IEEE Transactions on Automatic Control*, IEEE, v. 58, n. 5, p. 1304–1310, 2013. Citado na página 56.

64 BOYARSKI, S.; SHAKED, U. Time-convexity and time-gain-scheduling in finite-horizon robust h_∞-control. In: IEEE. *Decision and Control, 2009 held jointly with the 2009 28th Chinese Control Conference. CDC/CCC 2009. Proceedings of the 48th IEEE Conference on*. [S.l.], 2009. p. 2765–2770. Citado na página 56.

65 EDWARDS, C.; SPURGEON, S. *Sliding mode control: theory and applications*. [S.l.]: Crc Press, 1998. Citado na página 61.

66 DRAKUNOV, S.; UTKIN, V. Sliding mode observers. tutorial. In: IEEE. *Decision and Control, 1995., Proceedings of the 34th IEEE Conference on*. [S.l.], 1995. v. 4, p. 3376–3378. Citado na página 61.

67 MORENO, J. A.; OSORIO, M. A lyapunov approach to second-order sliding mode controllers and observers. In: IEEE. *Decision and Control, 2008. CDC 2008. 47th IEEE Conference on*. [S.l.], 2008. p. 2856–2861. Citado na página 63.

68 ALWI, H.; EDWARDS, C.; MARCOS, A. Fault reconstruction using a LPV sliding mode observer for a class of LPV systems. *Journal of the Franklin Institute*, Elsevier, v. 349, n. 2, p. 510–530, 2012. Citado na página 70.

69 XIAO, B.; HU, Q.; ZHANG, Y. Adaptive sliding mode fault tolerant attitude tracking control for flexible spacecraft under actuator saturation. *IEEE Transactions on Control Systems Technology*, IEEE, v. 20, n. 6, p. 1605–1612, 2012. Citado na página 71.

70 HAMAYUN, M. T.; EDWARDS, C.; ALWI, H. Design and analysis of an integral sliding mode fault tolerant control scheme. In: *Fault Tolerant Control Schemes Using Integral Sliding Modes*. [S.l.]: Springer, 2016. p. 39–61. Citado na página 71.

71 NGUYEN, M. et al. A model predictive control approach for semi-active suspension control problem of a full car. In: IEEE. *Decision and Control (CDC), 2016 IEEE 55th Conference on*. [S.l.], 2016. p. 721–726. Citado 5 vezes nas páginas 78, 79, 80, 83, and 91.

72 RUBEL, E. et al. *Semi-active suspension control*. [S.l.]: Google Patents, 1993. US Patent 5,189,615. Citado 2 vezes nas páginas 79 and 113.

73 POUSSOT-VASSAL, C. et al. Survey and performance evaluation on some automotive semi-active suspension control methods: A comparative study on a single-corner model. *Annual Reviews in Control*, Elsevier, v. 36, n. 1, p. 148–160, 2012. Citado 2 vezes nas páginas 79 and 113.

74 TSENG, H. E.; HROVAT, D. State of the art survey: active and semi-active suspension control. *Vehicle system dynamics*, Taylor & Francis, v. 53, n. 7, p. 1034–1062, 2015. Citado 2 vezes nas páginas 79 and 113.

75 UNGER, A. et al. Application of LQ-based semi-active suspension control in a vehicle. *Control Engineering Practice*, Elsevier, v. 21, n. 12, p. 1841–1850, 2013. Citado 2 vezes nas páginas 79 and 84.

76 DU, H.; SZE, K. Y.; LAM, J. Semi-active h_∞ control of vehicle suspension with magneto-rheological dampers. *Journal of Sound and Vibration*, Elsevier, v. 283, n. 3, p. 981–996, 2005. Citado na página 79.

77 POUSSOT-VASSAL, C. et al. A new semi-active suspension control strategy through LPV technique. *Control Engineering Practice*, Elsevier, v. 16, n. 12, p. 1519–1534, 2008. Citado na página 79.

78 NGUYEN, M. Q. et al. A state feedback input constrained control design for a 4-semi-active damper suspension system: a quasi-LPV approach. *IFAC-PapersOnLine*, Elsevier, v. 48, n. 14, p. 259–264, 2015. Citado 2 vezes nas páginas 79 and 114.

79 CAMACHO, E. F.; ALBA, C. B. *Model predictive control*. [S.l.]: Springer Science & Business Media, 2013. Citado 2 vezes nas páginas 79 and 95.

80 CANALE, M.; MILANESE, M.; NOVARA, C. Semi-active suspension control using "fast" model-predictive techniques. *IEEE Transactions on control systems technology*, IEEE, v. 14, n. 6, p. 1034–1046, 2006. Citado na página 79.

81 POUSSOT-VASSAL, C. et al. A methodology for optimal semi-active suspension systems performance evaluation. In: IEEE. *Decision and Control (CDC), 2010 49th IEEE Conference on*. [S.l.], 2010. p. 2892–2897. Citado na página 79.

82 GOHRLE, C. et al. Model predictive control of semi-active and active suspension systems with available road preview. In: IEEE. *Control Conference (ECC), 2013 European*. [S.l.], 2013. p. 1499–1504. Citado 2 vezes nas páginas 79 and 84.

83 PAWLOWSKI, A. et al. Predictive control with disturbance forecasting for greenhouse diurnal temperature control. *IFAC Proceedings Volumes*, Elsevier, v. 44, n. 1, p. 1779–1784, 2011. Citado na página 80.

84 MORATO, M. M. et al. Advanced control for energy management of grid-connected hybrid power systems in the sugar cane industry. In: IEEE. [S.l.], 2017. Citado na página 80.

85 POUSSOT-VASSAL, C. et al. Attitude and handling improvements through gain-scheduled suspensions and brakes control. *Control Engineering Practice*, Elsevier, v. 19, n. 3, p. 252–263, 2011. Citado 2 vezes nas páginas 81 and 117.

86 MUSKE, K. R.; RAWLINGS, J. B. Model predictive control with linear models. *AIChE Journal*, Wiley Online Library, v. 39, n. 2, p. 262–287, 1993. Citado na página 84.

87 QIN, S. J.; BADGWELL, T. A. A survey of industrial model predictive control technology. *Control engineering practice*, Elsevier, v. 11, n. 7, p. 733–764, 2003. Citado na página 84.

88 STURM, J. F. Using SeDuMi 1.02, a MATLAB toolbox for optimization over symmetric cones. *Optimization methods and software*, Taylor & Francis, v. 11, n. 1-4, p. 625–653, 1999. Citado na página 86.

89 KIENCKE, U.; NIELSEN, L. *Automotive control systems: for engine, driveline, and vehicle*. [S.l.]: IOP Publishing, 2000. Citado 2 vezes nas páginas 89 and 133.

90 MENDES, P. R. da C.; NORMEY-RICO, J. E.; ALBA, C. B. Economic energy management of a microgrid including electric vehicles. In: IEEE. *Innovative Smart Grid Technologies Latin America (ISGT LATAM), 2015 IEEE PES*. [S.l.], 2015. p. 869–874. Citado na página 91.

91 LOFBERG, J. YALMIP: A toolbox for modeling and optimization in MATLAB. *IEEE International Symposium on Computer Aided Control Systems Design*, p. 284–289, 2004. Citado 3 vezes nas páginas 94, 102, and 145.

92 OPTIMIZATION, G. et al. Gurobi optimizer reference manual. *URL: http://www. gurobi. com*, v. 2, p. 1–3, 2012. Citado na página 94.

93 WANG, Y.; BOYD, S. Fast model predictive control using online optimization. *IFAC Proceedings Volumes*, Elsevier, v. 41, n. 2, p. 6974–6979, 2008. Citado 4 vezes nas páginas 97, 98, 99, and 101.

94 BESSELMANN, T.; LOFBERG, J.; MORARI, M. Explicit MPC for LPV systems: Stability and optimality. *IEEE Transactions on Automatic Control*, IEEE, v. 57, n. 9, p. 2322–2332, 2012. Citado na página 99.

95 JANSEN, B. et al. Primal-dual algorithms for linear programming based on the logarithmic barrier method. *Journal of Optimization Theory and Applications*, Springer, v. 83, n. 1, p. 1–26, 1994. Citado na página 100.

96 BOYD, S.; VANDENBERGHE, L. *Convex optimization*. [S.l.]: Cambridge university press, 2004. Citado na página 100.

97 ZHANG, F. *The Schur complement and its applications*. [S.l.]: Springer Science & Business Media, 2006. Citado na página 100.

98 TOH, K.-C.; TODD, M. J.; TÜTÜNCÜ, R. H. SDPT3—a MATLAB software package for semidefinite programming, version 1.3. *Optimization methods and software*, Taylor & Francis, v. 11, n. 1-4, p. 545–581, 1999. Citado na página 101.

99 MORATO, M. M. *An Implementation of a Real-Time MPC Scheme for Semi-Active Suspension Control of a Full Vehicle*. [S.l.], 2017. Citado na página 113.

100 TAO, G.; JOSHI, S. M.; MA, X. Adaptive state feedback and tracking control of systems with actuator failures. *IEEE Transactions on Automatic Control*, IEEE, v. 46, n. 1, p. 78–95, 2001. Citado na página 114.

101 SCHWAGER, M.; ANNASWAMY, A. M.; LAVRETSKY, E. Adaptation-based reconfiguration in the presence of actuator failures and saturation. In: IEEE. *American Control Conference, 2005. Proceedings of the 2005*. [S.l.], 2005. p. 2640–2645. Citado na página 114.

102 CAI, X.; WU, F. Robust parameter-dependent fault-tolerant control for actuator and sensor faults. *International Journal of Control*, Taylor & Francis, v. 83, n. 7, p. 1475–1484, 2010. Citado na página 114.

103 RODRIGUES, M. et al. Fault tolerant control design for polytopic LPV systems. *International Journal of Applied Mathematics and Computer Science*, v. 17, n. 1, p. 27–37, 2007. Citado na página 114.

104 TUDON-MARTINEZ, J. C. et al. Fault tolerant strategy for semi-active suspensions with LPV accommodation? In: IEEE. *Control and Fault-Tolerant Systems (SysTol), 2013 Conference on*. [S.l.], 2013. p. 631–636. Citado na página 114.

105 SHAMMA, J. S. *Analysis and design of gain scheduled control systems*. Tese (Doutorado) — Massachusetts Institute of Technology, 1988. Citado na página 114.

106 MORATO, M. M. *Fault Estimation for Electro-Rheological Dampers: An LPV-based Extended Observer Approach*. [S.l.], 2017. Citado na página 114.

107 ZIN, A. et al. An LPV/h_∞ active suspension control for global chassis technology: Design and performance analysis. In: IEEE. *American Control Conference, 2006*. [S.l.], 2006. p. 2945–2950. Citado 2 vezes nas páginas 114 and 115.

108 ZIN, A. et al. Robust LPV-h_∞ control for active suspensions with performance adaptation in view of global chassis control. *Vehicle System Dynamics*, Taylor & Francis, v. 46, n. 10, p. 889–912, 2008. Citado na página 114.

109 ABDULLAH, A.; ZRIBI, M. Model reference control of lpv systems. *Journal of the Franklin Institute*, Elsevier, v. 346, n. 9, p. 854–871, 2009. Citado na página 114.

110 SAMMIER, D.; SENAME, O.; DUGARD, L. Skyhook and h_∞ control of semi-active suspensions: some practical aspects. *Vehicle System Dynamics*, Taylor & Francis Group, v. 39, n. 4, p. 279–308, 2003. Citado na página 115.

111 VILLA, M. M. *Fault Simulation for an Electro-Rheological Damper by the use of a Dynamic Model*. [S.l.], 2017. Citado na página 120.

112 HERNÁNDEZ-ALCÁNTARA, D. et al. Modeling, diagnosis and estimation of actuator faults in vehicle suspensions. *Control Engineering Practice*, Elsevier, v. 49, p. 173–186, 2016. Citado na página 121.

113 AUBOUET, S. *Semi-active SOBEN suspensions modeling and control*. Tese (Doutorado) — Institut National Polytechnique de Grenoble-INPG, 2010. Citado na página 127.

114 SCHERER, C.; GAHINET, P.; CHILALI, M. Multiobjective output-feedback control via LMI optimization. *IEEE Transactions on automatic control*, IEEE, v. 42, n. 7, p. 896–911, 1997. Citado na página 138.

115 BRIAT, C. *Robust control and observation of LPV time-delay systems*. Tese (Doutorado) — Institut National Polytechnique de Grenoble-INPG, 2008. Citado na página 164.

116 ZAMES, G. On the input-output stability of time-varying nonlinear feedback systems part one: Conditions derived using concepts of loop gain, conicity, and positivity. *IEEE transactions on automatic control*, IEEE, v. 11, n. 2, p. 228–238, 1966. Citado na página 164.

117 PACKARD, A.; DOYLE, J. The complex structured singular value. *Automatica*, Elsevier, v. 29, n. 1, p. 71–109, 1993. Citado na página 165.

Annex

ANNEX A – Robustness Analysis

Now, as the Fault Tolerant controller has been synthesized, this section shall be dedicated to a robustness analysis for the proposed control scheme, seen in figure 63.

For the goals of this robustness analysis we shall consider two situations: the case of sensor faults and the case of bad estimation on the loss of effectiveness actuator faults. These are, thus, detailed:

A.0.1 Badly Estimated Actuator Faults

In this work, we assume a reconfigurable fault tolerant control scheme, to be adjusted by the collected information on actuator loss of effectiveness faults. Then, for this scenario, we shall analyze the case of badly estimation of these faults.

This means, we shall analyze our control system with plausible actuator faults that are distributed as: correctly estimated multiplicative (loss of effectiveness) faults and additive (unknown to the controller) faults.

From this point, the system representation seen in (5.45) changes to:

$$\begin{aligned} \dot{x}(t) &= A.x(t) + B_1.w(t) + B_2(\alpha).u(t) + B_2.f_a(t) \\ y(t) &= C.x(t) + D_1.w(t) + D_2(\alpha).u(t) + D_2.f_a(t) \\ z(t) &= E.x(t) + F_1.w(t) + F_2(\alpha).u(t) + F_2.f_a(t) \end{aligned} \tag{A.1}$$

where the α-dependent matrices are LPV due to the well-estimated loss of effectiveness faults (by the FDI scheme) and $f_a(t)$ represents an un-estimated percentage ($\delta_a(t)$) upon the multiplicative loss of effectiveness α factors, as details equation (A.2).

$$f_a(t) = \delta_a(t).\mathbb{I}_{nu}.u(t) \tag{A.2}$$

where nu represents the number of control inputs $u(t)$ and $\delta_a(t)$ is of dimension 1.

A.0.2 Sensor Faults

In the case of sensor faults, these shall be represented by an additive signal upon the measured outputs $y(t)$. This means the LPV system representation in (5.45) changes to:

$$\begin{aligned} \dot{x}(t) &= A.x(t) + B_1.w(t) + B_2(\alpha).u(t) \\ y(t) &= C.x(t) + D_1.w(t) + D_2(\alpha).u(t) + F_y.f_s(t) \\ z(t) &= E.x(t) + F_1.w(t) + F_2(\alpha).u(t) \end{aligned} \tag{A.3}$$

where the α-dependent matrices are LPV due to the actuator loss of effectiveness faults and the signal $f_s(t)$ represents sensor faults, distributed upon the measured outputs by matrix F_y.

To simplify this analysis, we shall take $f_s(t)$ as dependent on the system states. This is:

$$f_s(t) = \delta_s(t).\mathbb{I}_{nx}.x(t) \tag{A.4}$$

where nx represents the number of system states $x(t)$ and $\delta_s(t)$ is of dimension 1.

A.0.3 Final Uncertain Representation

Then, considering the system representations presented in (A.1) and (A.3) can be coupled into a single feature. Towards an upper Linear Fractional Transformation (LFT), see [33], we can re-represent this system (A.1)-(A.3) with the use of an $P - K - \Delta$ structure, where the closed-loop system (as defined by the H_∞ Control Problem, see equation (5.52)), is given by:

$$N(\alpha^i) = \mathcal{F}_l(P(\alpha^i), C(\alpha^i)) \tag{A.5}$$

for a fixed scheduling parameter $\alpha = \alpha^i$.

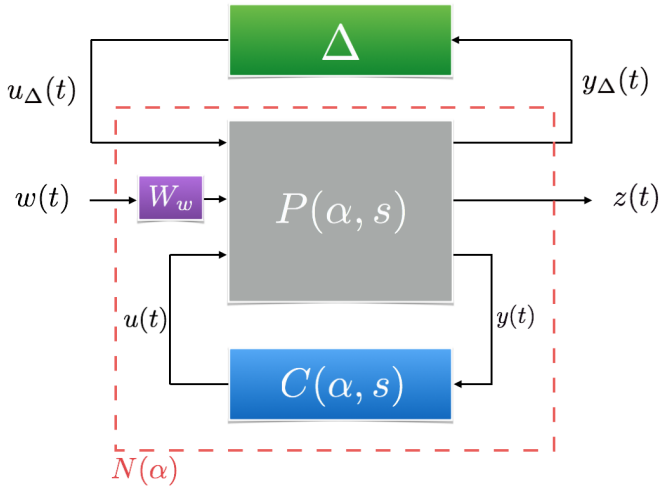

Figure 77 – $P - K - \Delta$ Representation

In this global $P - K - \Delta$ General Control Configuration, seen in figure 77, the transfer matrix (once again considering a fixed scheduling vector α) is given by:

$$T_{zw} = F_u(N, \Delta) = N_{22} + N_{21}.\Delta.(I - N_{11}.\Delta)^{-1}.N_{12} \tag{A.6}$$

Remark 17. In this representation, N is known and $\Delta(s)$ collects all the uncertainties taken into account the two detailed faults for the stability analysis of the uncertain closed-loop system. As of this, $\Delta(s)$ has the following structure:

$$\Delta(s) = \text{diag}\{ \ \delta_a.\mathbb{I}_{\text{nu}} \quad \delta_s\mathbb{I}_{\text{nx}} \ \} \tag{A.7}$$

And, in this case, we shall have $u_\Delta(t)$ as a collection of $f_a(t)$ and $f_s(t)$ and, thus of equations (A.2)-(A.4), $y_\Delta(t)$ shall be the collection of $u(t)$ and $x(t)$. The constraints upon $\Delta(s)$ are assumed to be satisfied by the chosen representation: the uncertainties are normalized, such that:

- $\|\Delta(s)\|_\infty \leq 1$
- $|\delta_a| < 1$
- $|\delta_s| < 1$

Notice that, from this point, the robustness criteria are:

- Robust Stability (RS): If $F_u(N, \Delta)$ is stable for all Δ, $\|\Delta\|_\infty < 1$ and N is internally stable;
- Robust Performance (RP) : If $\|F_u(N, \Delta)\|_\infty < 1$ for all Δ, $\|\Delta\|_\infty < 1$ and N is internally stable.

Remark 18. To relax our analysis conditions for RS and RP of LPV systems, we shall take $\alpha^i = 1_{4\times 1}$. This means, for us to evaluate robustness towards given uncertainties u_Δ, we shall assume that the system's loss of effectiveness faults are none apart from the badly estimate ones $f_a(t)$. This is adequate, for there is guarantees of nominal stability and performance for all possible values of α, due to the H_∞ problem solution. For other tools and a complete scrutinization of Robustness Analysis for LPV Systems, see [115].

Then, for RS, our analysis resides on determining wether the system remains stable for all plants inside uncertainty set. According to the definition of the upper LFT, instability may only come from the term $(I - N_{11}.\Delta)$. This is equivalent to the study of the Small Gain Theorem, [116], applied to N_{11}.

Lemma A.1. Suppose $N_{11} \in RH_\infty$. Then the closed-loop system, as presented in figure 77, for $\alpha = \alpha^i$, is well-posed and internally stable for all $\Delta \in RH_\infty$ so that:

$$\|\Delta(s)\|_\infty \leq \delta_{RS} \tag{A.8}$$

if and only if

$$\|N_{11}(s)\|_\infty < \frac{1}{\delta_{RS}} \tag{A.9}$$

Proof 1. Refer to [33].

Towards *RP*, the analysis becomes more complex: it is necessary to apply the Small Gain Theorem to the H_∞ norm of the full upper *LFT*. Let us, then, consider a structured representation of $\Delta(s)$, as seen in the following equation:

$$\Delta = \begin{bmatrix} \Delta_f & 0 \\ 0 & \Delta_r \end{bmatrix} \tag{A.10}$$

where Δ_f represent fictive full block complex uncertainty and Δ_r represents the real block diagonal matrix uncertainties.

From this point, we are cast into the following lemma:

Lemma A.2. Suppose $N = \mathcal{F}_l(P, K) \in RH_\infty$. Then the closed-loop system, as presented in figure 77, for $\alpha = \alpha^i$, is well-posed and internally stable for all $\Delta \in RH_\infty$ if and only if:

$$\mu_\Delta(N) < 1 \, \forall w \tag{A.11}$$

where the operator $\mu_\Delta(\cdot)$ stand for the structured singular value. Remark that the structured singular value cannot be determined explicitly. For this, numerical methods exist in order to compute upper and lower bounds of $\mu_\Delta(\cdot)$, as close as possible to μ_Δ.

Proof 2. Refer to [117].

A.0.4 Analysis

Finally, after background to the analysis of *RS* and *RP* has been presented, let us analyse the robustness of the proposed control scheme, considering, for now, the scheduling parameter α fixed as $1_{4\times 1}$.

In terms of (badly estimated) actuator faults, we shall take a maximal percentage $\delta_a(t)$ as 10 %. Notice that this is rather conservative for the estimation of the loss of effectiveness factors has an overall small estimation error (see section 5.4).

Then, is terms of sensor faults, we shall consider a maximal $\delta_s(t)$ as $5\,\%$, with $F_y = 1_{ny \times nx}$, being ny the number of measured outputs. This is an adequate choice for sensor faults, which usually are of small amplitude for our study case (vehicle systems with relative displacement sensors).

A.0.4.1 Robust Stability

Shall be analysed in future works.

A.0.4.2 Robust Performance

Shall be analysed in future works.

A.0.4.3 For Other α^i

Shall be analysed in future works.